DESIGN OF AN ENGINE MOUNT WITH DRY FRICTION DAMPING

A THESIS SUBMITTED TO
THE GRADUATE SCHOOL OF NATURAL AND APPLIED SCIENCES
OF
MIDDLE EAST TECHNICAL UNIVERSITY

BY

CANER BORAL

IN PARTIAL FULFILLMENT OF THE REQUIREMENTS
FOR
THE DEGREE OF MASTER OF SCIENCE
IN
MECHANICAL ENGINEERING

JULY 2010

Approval of the thesis:

DESIGN OF AN ENGINE MOUNT WITH DRY FRICTION DAMPING

Submitted by **CANER BORAL** in partial fulfillment of the requirements for the degree of **Master of Science in Mechanical Engineering Department, Middle East Technical University** by,

Prof. Dr. Canan Özgen
Dean, Graduate School of **Natural and Applied Sciences** _____

Prof. Dr. Süha Oral
Head of Department, **Mechanical Engineering** _____

Assist. Prof. Dr. Ender Ciğeroğlu
Supervisor, **Mechanical Engineering Dept., METU** _____

Dr. İbrahim Korkmaz
Co-Supervisor, **TOFAŞ A.Ş.** _____

Examining Committee Members:

Prof. Dr. Y. Samim Ünlüsoy
Mechanical Engineering Dept., METU _____

Assist. Prof. Dr. Ender Ciğeroğlu
Mechanical Engineering Dept., METU _____

Dr. İbrahim Korkmaz
TOFAŞ A.Ş _____

Assoc. Prof. Dr. Serkan Dağ
Mechanical Engineering Dept. METU _____

Inst. Dr. S. Çağlar Başlamışlı
Mechanical Engineering Dept., Hacettepe University _____

Date: 09-07-2010

I hereby declare that all information in this document has been obtained and presented in accordance with academic rules and ethical conduct. I also declare that, as required by these rules and conduct, I have fully cited and referenced all material and results that are not original to this work.

Name Surname: Caner BORAL

Signature:

ABSTRACT

DESIGN OF AN ENGINE MOUNT WITH DRY FRICTION DAMPING

Boral, Caner

M.S., Department of Mechanical Engineering

Supervisor: Asst. Prof. Dr. Ender Ciğeroğlu

Co-Supervisor: Dr. İbrahim Korkmaz

July 2010, 110 pages

Automotive engine mounts are used to support engine weight, protect engine from road inputs and isolate transmission of vibrations created by the engine, which has a drastic effect on the noise generated inside the passenger cabin. Most common types of engine mounts are elastomeric and hydraulic mounts, the former having better vibration isolation characteristics whereas the latter displays better shock isolation. Elastomeric mounts are widely used for their low initial cost, while hydraulic mounts with inertia track and decoupler are chosen for their good vibration isolation and shock excitation characteristics. However, hydraulic mounts with inertia track and decoupler are not appropriate for small segment and commercial vehicles due their high initial cost. In this thesis, the effect of the addition of a dry friction damper on the performance of elastomeric automobile engine mounts is investigated. Friction dampers are used to attenuate vibration amplitudes in many applications such as gas turbine engines, railway vehicles, space structures and civil buildings. In this study, a friction element is added to the engine mount at its axial direction and its effect is studied. Results show that, the addition of dry friction damping to the original system increases vibration

isolation performance significantly at low frequencies; whereas, due to the increased stiffness of the system, at high frequencies dry friction damper has a mitigating effect on performance. In order to overcome this problem, original system parameters are modified. In the modified system a softer mount that increase vibration isolation performance at high frequencies; but, which might cause excessive static deflection due to reduced stiffness of the system is used. On the other hand, addition of dry friction damping prevents excessive static deflections due to the increased stiffness effect and also increases the performance at high frequencies due to the soft mount. Final results showed that vibration isolation performance at low frequencies increases considerably while vibration isolation performance at high frequency is similar and even slightly better than the original system with addition of dry friction damping.

Keywords: Dry friction, dry friction damping, dry friction damper, macroslip friction, engine mount, vibration isolation

ÖZ

KURU SÜRTÜNMELİ MOTOR TAKOZU TASARIMI

Boral, Caner

Master, Makine Mühendisliği Bölümü

Tez Yöneticisi: Yrd. Doc. Dr. Ender Ciğeroğlu

Ortak Tez Yöneticisi: Dr. İbrahim Korkmaz

Temmuz 2010, 110 sayfa

Araçlarda kullanılan motor takozları, motorda yaratılan ve araç içindeki ses düzeyinde ciddi bir etkisi olan titreşimleri araç gövdesinden yalıtmak, motoru yoldan gelen girdilere karşı korumak ve motoru desteklemek için kullanılır. En sık kullanılan motor takozu çeşitleri kauçuk ve hidrolik takozlardır. Kauçuk takozların titreşim yalıtımı, hidrolik takozların ise şok girdilerine karşı yalıtımı yüksektir. Kauçuk takozlar düşük maliyeti, gelişmiş hidrolik takozlar ise iyi titreşim ve şok yalıtımı nedeniyle tercih edilmektedir. Fakat gelişmiş hidrolik takozların maliyetinin yüksek olmasından dolayı, alt segmentlerde ve hafif ticari araçlarda kullanımı uygun değildir. Bu tezde, kauçuk takozlara kuru sürtünmeli sönümleyici eklenmesinin takozun performansına etkileri incelenmiştir. Kuru sürtünmeli sönümleyiciler gaz türbinlerinde, demiryolu araçlarında, uzay yapılarında ve binalarda titreşimleri azaltmak için kullanılmaktadırlar. Bu

çalışmada, motor takozuna sürtünme elemanı eklenerek, bunun takozun performansına etkisi gözlemlenmiştir. Sonuçlar kuru sürtünmenin eklenmesinin takozun performansını orijinal sistemin rezonans frekansı civarında önemli ölçüde artırdığını, aynı zamanda da sistemin direngenliğindeki artıştan dolayı ise daha yüksek frekanslarda sistemin performansında hafif düşüşler göstermiştir. Bu sorunun üstesinden gelmek için, orijinal sistem değiştirilerek, sistemin yüksek frekanslardaki performansını artıran daha yumuşak bir takoz kullanılmıştır. Yumuşatılmış takozun statik konumlandırma ve düşük frekanslardaki girdilerle ilgili sorunları, sisteme eklenen sürtünme sayesinde aşılarak düşük ve yüksek frekanslarda iyileştirme sağlanabilir. Sonuç olarak kuru sürtünmenin eklendiği sistemde, düşük frekanslarda çok ciddi performans artışları, yüksek frekanslarda ise orijinal sistem kadar ya da daha iyi performans elde edilmiştir.

Anahtar kelimeler: Kuru sürtünme, kuru sürtünmeli sönümleme, kuru sürtünmeli sönümleyici, makro-kayma sürtünme modeli, motor takozu, titreşim izolasyonu

To my Family

ACKNOWLEDGEMENTS

I owe my deepest gratitude to Asst. Prof. Dr. Ender Ciğeroğlu for his invaluable support and guidance that created this study.

I would like to show my gratitude to Dr. İbrahim Korkmaz for his invaluable support.

I am heartily thankful to TOFAŞ for its financial support.

I would like to thank my colleague, Göksu Aydan for his friendship and technical support.

I deeply owe my family for everything they have done to encourage and support me.

TABLE OF CONTENTS

LIST OF FIGURES

FIGURES

LIST OF TABLES

TABLES

LIST OF SYMBOLS

c : Viscous damping

c_s : Suspension viscous damping

$[C]$: Viscous damping matrix

$\{f_{NL}\}$: Nonlinear force vector

$\{f_{exc}\}$: Input Force vector

F : Force

F_f : Friction force

F_s : Slip force

F_{NL} : Nonlinear force

F_{exc} : Excitation force

F_{en} : Force generated inside engine

k : Stiffness

k_f : Friction stiffness

k_s : Suspension stiffness

$[K]$: Stiffness matrix

m_e : Engine mass

m_s : Sprung mass without engine

m_{us} : Unsprung mass

$[M]$: Mass matrix

n_0 : Normal force

$\{x\}$: Displacement vector

$\{\dot{x}\}$: Velocity vector

$\{\ddot{x}\}$: Acceleration vector

X : Displacement amplitude

ε : Displacement required for slip

μ : Friction coefficient

θ : Phase angle

ω : Frequency

CHAPTER 1

INTRODUCTION

1.1. ENGINE MOUNTS

Vibrations generated by the engine cause fatigue at the chassis and vehicle components and discomfort to driver and passengers. Hence engine must be isolated from the chassis with engine mounts. Main duties of engine mounts are, supporting engine mass statically, isolating vibrations caused by engine and protecting engine components from road irregularities. Engine mounts should also be placed carefully so that engine weight is well distributed among mounts [1].

Internal combustion engine is the most widely used type of prime mover used in automobiles. Internal combustion engines may produce vibrations at various frequencies. Engine speed usually ranges from 600 rpm to 6000 rpm for standard spark ignition engines and 800 rpm to 4500 rpm for standard compression ignition engines. Moreover, engine force generated depends on the number of cylinders used in the engine. For a four cylinder spark ignition engine, engine speed of 600-6000rpm, corresponds to 20-200Hz [2]. Four cylinder engines are the most common type; however 6, 8 or even 12 cylinder engines are available.

Engine excitation is caused by gas pressure and unbalanced rotating elements in the engine. High gas pressure is generated by the combustion of fuel air mixture,

and during exhaust stage. Moreover, excitation forces are as well generated by reciprocating and rotating parts in the engine.

With today's technology lighter automobiles are manufactured with more powerful and smaller engines. Hence, vibrations exerted on chassis, driver and passengers increase [3], as a result, engine mounts should be improved.

Requirements for engine mounts change for isolation at different frequency ranges. An engine mount with high stiffness and damping shows better performance at low frequency range whereas an engine mount with low stiffness and damping has better performance at high frequency range. An ideal engine mount should have high stiffness and damping at low frequency and low stiffness and damping for high frequency [3].

Engine mounts should be robust; since they operate at harsh conditions and exposed to oil, fuel, cold and hot environments. Due to combustion, working temperature of engine is high, however engine mounts must also work at a cold day when engine is just started. So engine mounts should operate properly at both cold and hot environments. Life, reliability, initial cost and maintenance are other factors which are also considered during the design process of engine mounts.

1.1.1. Engine Mount Types

Nowadays, four types of engine mounts are used. These can be listed as: elastomeric, hydraulic, semi-active and active. Semi-active and active mounts have high initial, maintenance and operating costs, have low reliability compared to elastomeric and hydraulic mounts; hence they are not widely used. Currently, the most of the vehicles produced have elastomeric or hydraulic engine mounts.

1.1.1.1. Elastomeric Engine Mounts

Elastomeric mounts have been widely used for many years. It's one of the oldest type of engine mount. Its main advantages are simple design, reliability, low initial cost and no maintenance cost.

Elastomeric engine mounts offer good vibration isolation performance with low initial cost and nearly zero maintenance cost. Elastomeric engine mounts have compact design and high reliability. However they cannot satisfy all requirements of an ideal engine mount but sacrifice one of the requirements to satisfy the other. A simple elastomeric engine mount is shown in Figure 1.1.

A soft elastomeric engine mount with low stiffness and damping has good vibration isolation characteristics at high frequencies; however, it has problems at low frequency excitations and shock loads. On the other hand, a hard engine mount can protect engine from shocks but, it has issues with vibration isolation at high frequencies. Hence, elastomeric mounts can only satisfy requirements partially.

Figure 1.1. Elastomeric engine mount [4]

1.1.1.2. Hydraulic Engine Mounts

Hydraulic engine mounts are the solution to conflicting requirements of an ideal engine mount. Depending on the components used, they mounts can offer good protection against shock excitation and vibration isolation performance. However, hydraulic mounts with advanced components are expensive and hydraulic mounts show their best performance at their notch frequency, but passive hydraulic mounts have only one [5].

Hydraulic engine mounts have two fluid chambers. Transfer of fluid between these chambers occurs through an orifice which affects the characteristics of the mount.

Hydraulic engine mounts have three common types, hydraulic mount with simple orifice, hydraulic mount with inertia track and hydraulic mount with inertia track and decoupler. Hydraulic mounts with simple orifice offers protection from shock excitations but, has high damping at high frequency. For this reason vibration isolation performance of hydraulic mounts with simple orifice suffers at high frequency. A schematic drawing of a hydraulic mount with simple orifice is given in Figure1.2.

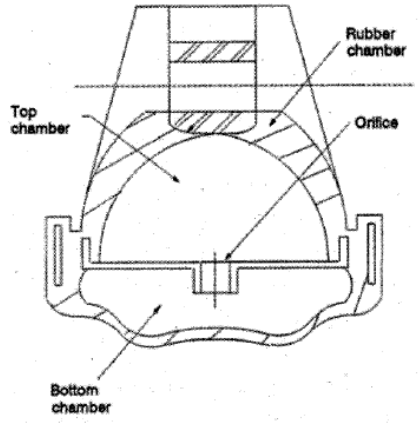

Figure1.2. Hydraulic mount with simple orifice [6]

Advanced hydraulic mounts with inertia track and decoupler offer good vibration isolation and protection from shocks and low frequency excitations. Decoupler blocks the orifice for large inputs at low frequencies hence, fluid passes through inertia track which increases damping at low frequencies. At high frequencies decoupler does not block the orifice; therefore, hydraulic engine mount has low damping [6].

1.1.2. Engine Mount Models in Literature

In the literature, engine is usually modeled as a rigid since its natural frequencies are much higher than the natural frequencies of the engine mount system. Engine is usually modeled as a 6 degree-of-freedom rigid body connected to the chassis with 3 or 4 mounts which are modeled as a spring and viscous damper. Chassis is modeled as a rigid body since displacement of the chassis is smaller than displacement of the engine. Designing of an engine mounting system occurs at early stages of a vehicle design which is not complete. Therefore chassis cannot be modeled with all components on it; as a result, it is modeled as a rigid body [3].

1.1.2.1. Elastomeric Engine Mount Models

Simplest model used is the single degree-of-freedom (SDOF) engine mount model. A sketch of the model is given in Figure 1.3.

In this model, engine is modeled as a rigid body where the engine mount is modeled as, a viscous damper and a nonlinear spring. Force generated by the viscous damper and the nonlinear spring is given as:

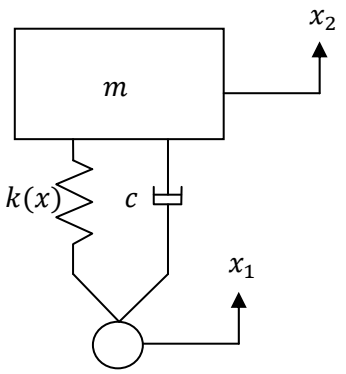

Figure 1.3. SDOF engine mount model

$$F_c = c\dot{x}\,, \tag{1.1}$$

$$F_k = k_1 x + k_2 x^2 + k_3 x^3\,. \tag{1.2}$$

In Figure 1.4 comparison of experimentally obtained spring force with the one determined from this nonlinear model is given.

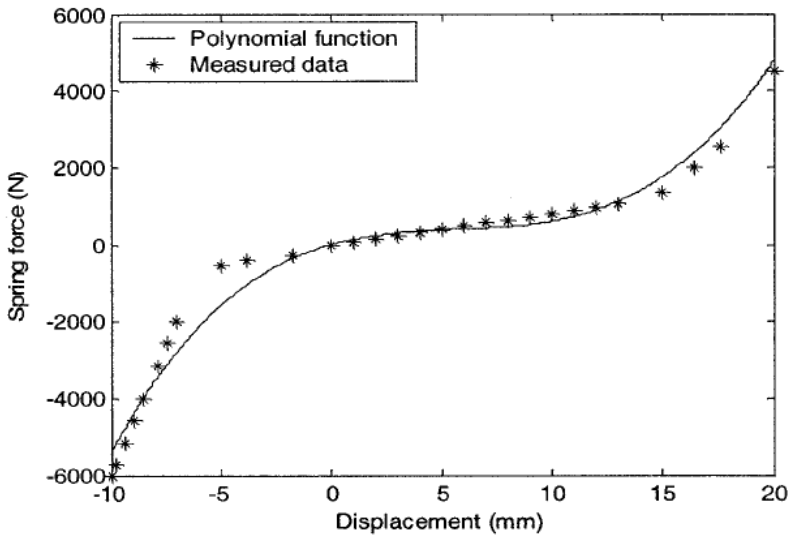

Figure 1.4. Comparison of experimental and theoretical results [7]

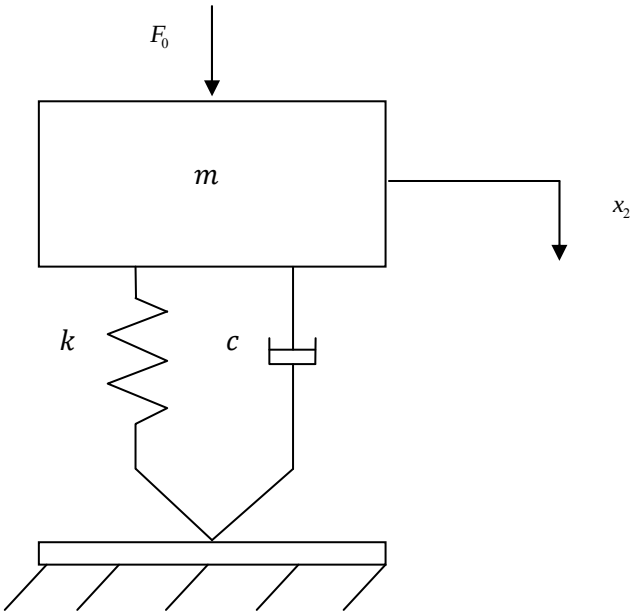

Figure 1.5. SDOF engine mount model

Another SDOF model used in the literature is given in Figure 1.5 which is used to determine the force transmitted to chassis due to the forces generated inside an engine.

Similar to the previous model engine is modeled as a rigid body. F_0 is the force generated in the engine due to pressure change and rotating unbalances.

A nonlinear spring and a viscous damper are used to represent the engine mount. This model was used by Wang [6] and the results are given in Figure1.6

The results showed that resonance frequency of the engine mount is around 210 rpm, 7Hz and, the velocity and the acceleration increases with increasing frequencies.

1.1.2.2. Hydraulic Engine Mount Models

Christopherson and Jazar [8] investigated passive hydraulic engine mounts. Hydraulic engine mount models are classified according to decoupler. They investigated linear and nonlinear models with floating and direct decoupler. Linear models neglect the decoupler closing action. A linear model with floating decoupler is given in Figure 1.7.

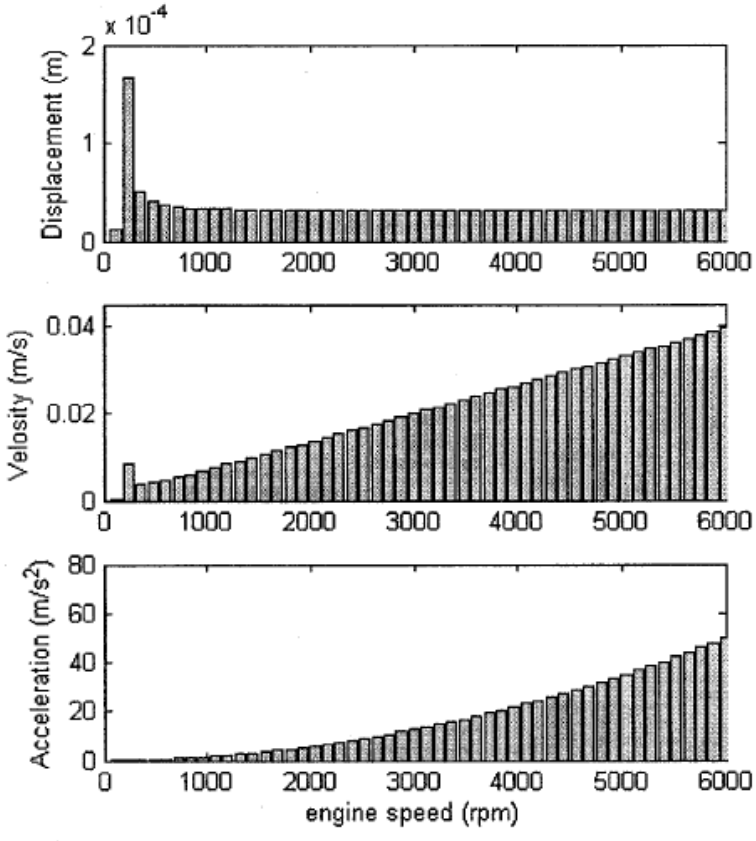

Figure1.6. Results obtained by Wang [6]

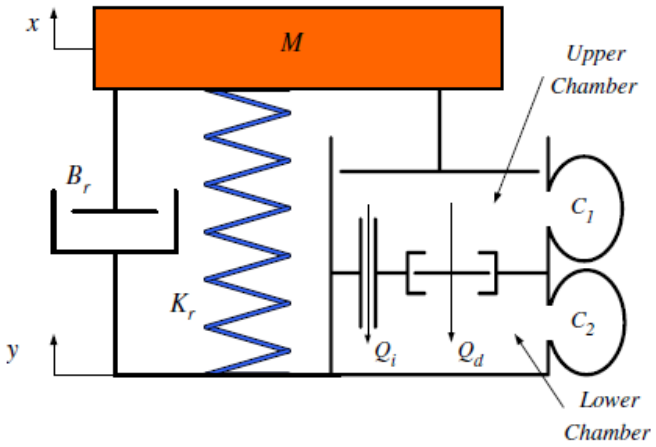

Figure 1.7. Linear hydraulic mount model with floating decoupler [8]

In this model, the system is investigated with two control volumes and the decoupler closing action is neglected.

The model with direct decoupler is given in Figure 1.8.

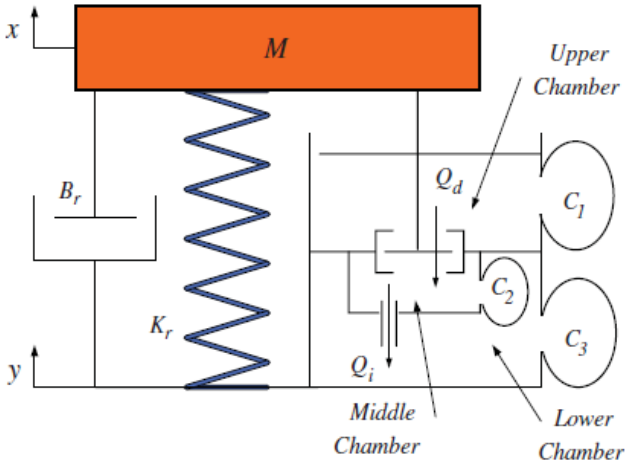

Figure 1.8. Linear hydraulic engine mount with direct decoupler [8]

In this model a third control volume s is considered as shown in Figure 1.8. In the nonlinear models closing action of decoupler is included to the solution.

Haque [9] developed nonlinear analytical models for dual-phase viscous dampers and for hydraulic dampers with flexible chambers.

1.1.3. Engine Model

Paul [10] investigated a single cylinder engine model. In this model, assuming the mass rotating at constant angular speed is balanced, only inertia forces at vertical direction and roll moment which has a rotation axis same as the crank are considered. The model is given in Figure 1.10.

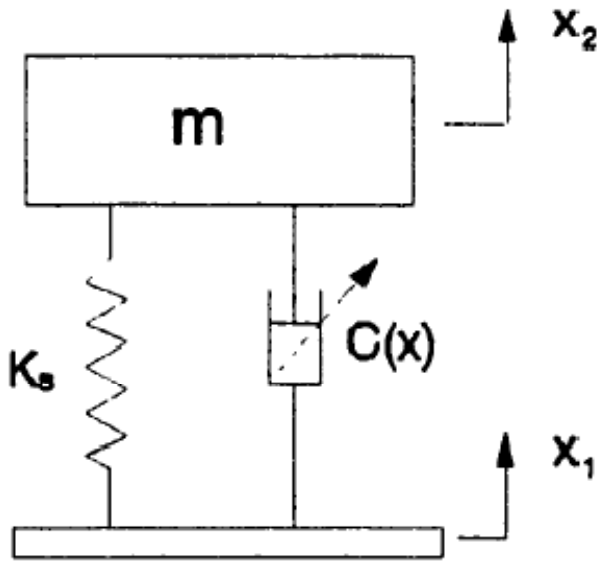

Figure 1.9. SDOF hydraulic mount model of Haque [9]

Utilizing a single cylinder model, the force and moment generated in the engine are given as:

$$F_x^{'} = \left(m_{rot} + m_{rec}\right) R\omega^2 + m_{rec} R\omega^2 \left(A_2 \cos\left(2\theta\right) - A_4 \cos\left(4\theta\right) + A_6 \cos\left(6\theta\right) - ...\right), \quad (1.3)$$

$$M_z^{'} = \left(P + m_{rec}\ddot{s}\right) s \tan\varphi \,. \quad (1.4)$$

In Equation (1.3) and (1.4), m_{rot} and m_{rec} are mass of rotating and reciprocating parts, respectively.

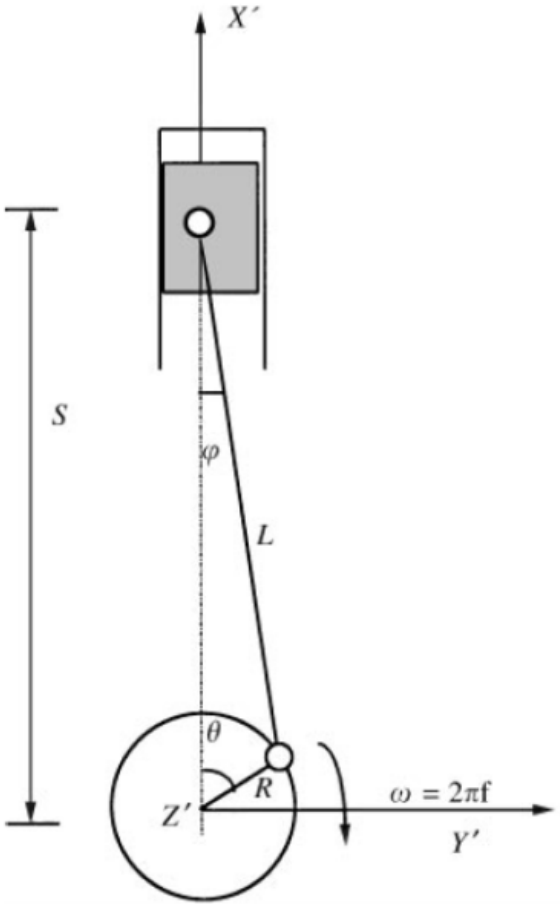

Figure 1.10. One cylinder engine model by Paul [11]

1.1.4. Modeling Engine with Engine Mounts

In the modeling of engine mount systems, engine is usually modeled as a rigid body with three degrees-of-freedom or a six degrees-of-freedom where three or four engine mounts are placed on various locations on engine or transmission. A three DOF model is used by Wang [6] is given in Figure 1.11.

This model includes vertical, roll and pitch motions of the engine. Representation of this model at pitch and roll planes are given in Figure 1.12 and Figure 1.13.

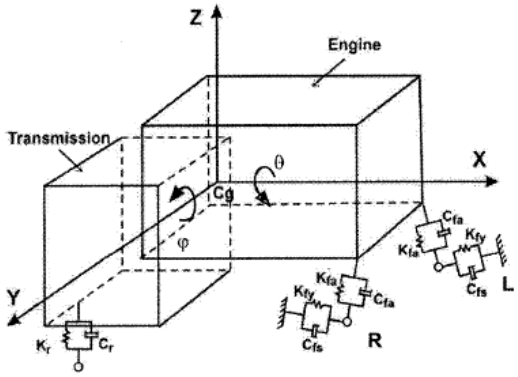

Figure 1.11. Engine mount system used by Wang [6]

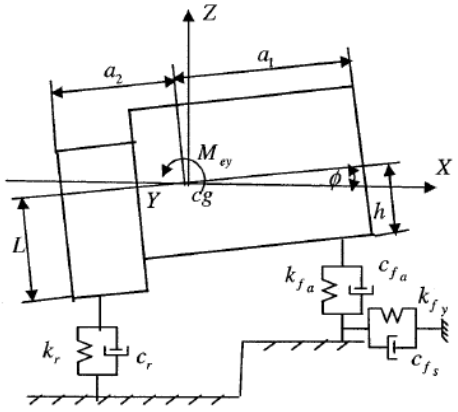

Figure 1.12. Representation of the engine on pitch plane [6]

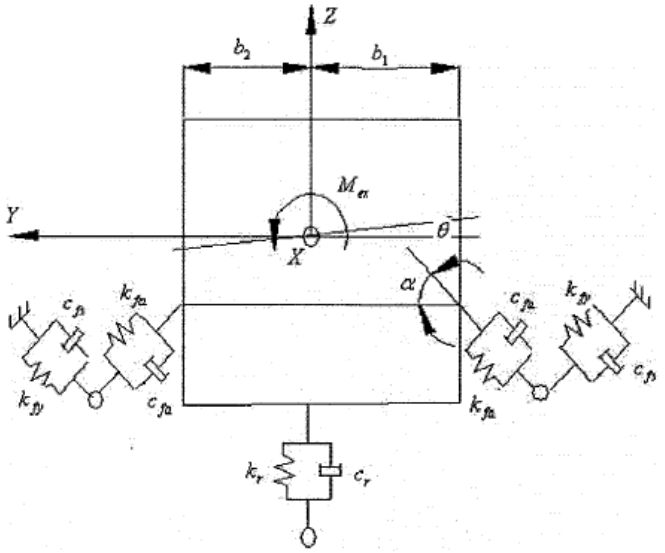

Figure 1.13. Representation of the engine on roll plane [6]

1.1.5. Modeling Motorcycle Engine with Engine Mounts

Engine mounts are also used in motorcycles. However, they have different design constraints. Several models are investigated in literature and some of them are given in the following sections.

1.1.5.1. Kaul Motorcycle Engine Mount System Model

In this model, engine modeled as a rigid body is supported by two mounts. Three translational and three rotational motions of the engine are considered [12]. Equation of motion of the system is given as follows.

$$M_{engine}\ddot{X}_e + C_e\dot{X}_e + K_eX_e = F_e e^{i\omega t}. \quad (1.5)$$

Where, F_e is the force generated in the engine due to unbalanced mass. This generated by the engine force depends on frequency.

$$F_e = \begin{bmatrix} f_{xe} & f_{ye} & f_{ze} & m_{xe} & m_{ye} & m_{ze} \end{bmatrix}^T . \tag{1.6}$$

First three terms are forces along x, y and z directions and last three terms are moments along x, y and z axes.

1.1.5.2. Kaul and Dhingra Model

Kaul and Dhingra [13] used a 6 DOF engine model and determined the optimum parameters of the engine mounts used in a motorcycle. The model used in their study is given in Figure 1.14.

In this thesis, engine mounts are modeled as springs and viscous dampers in three directions.

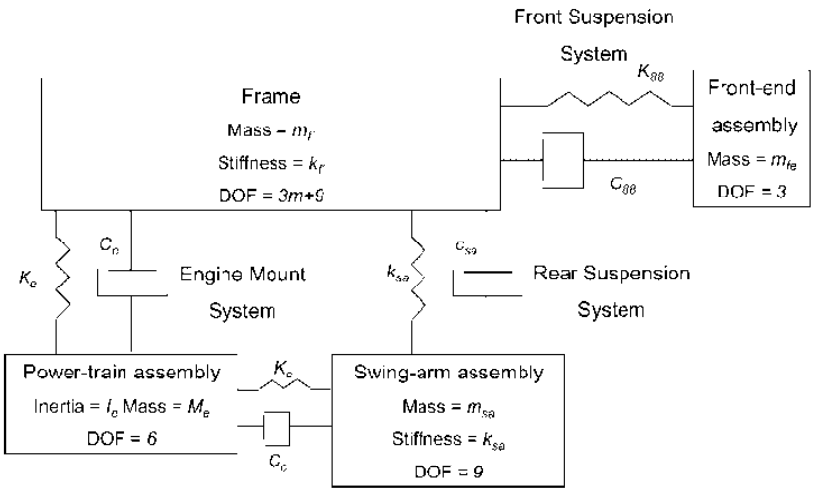

Figure 1.14. Kaul and Dhingra motorcycle engine mount system [13]

1.1.6. Engine Mount Optimization

Engine mount system is modeled as a rigid body having 6 DOF and connected to the chassis with 3 or 4 mounts. Locations and orientation of these mounts should be optimized in order to get satisfactory results. Arai, et al. [14] optimized mount position, orientation and stiffness. They improved idle/shake performance of the vehicle. Ünlüsoy [15] also worked on optimizing engine mount systems and developed software to optimize mount parameters, location and orientation. Park and Rajendra [16] considered combination of active and passive mounts. Lee and Kim [17] worked on improving life and performance of elastomeric mounts.

1.2. FRICTION DAMPING

Friction damping is used to attenuate vibrations amplitudes in many applications. In this section of the thesis, models used to represent friction at contacting surfaces and several applications which include friction damping will be discussed.

1.2.1. Friction Models in Literature

Mathematical representation of friction force has been an important topic and it is investigated by many researchers. Olsson et al. [18] investigated friction models in the literature and presented them in his study. In this section of the thesis, several friction models are presented in detail.

1.2.1.1. Dahl Model

In the friction model developed by Dahl [18], friction force increases until it reaches to the slip force. Friction force vs. displacement plot, which is also referred as hysteresis plot, is given in Figure 1.15. In Dahl's model, friction force is calculated as follows:

$$\frac{dF}{dx} = \sigma \left(1 - \frac{F}{F_c} \operatorname{sgn} \upsilon \right)^{\alpha} . \tag{1.7}$$

In Equation (1.7), x is the displacement, F is the friction force, F_c is the Coloumb friction force, σ is the stiffness coefficient, υ is the velocity and α is the parameter that defines the slope of the curve. As the friction force approaches to the Coloumb friction force, slope of the curve decreases; hence, it can never be equal to the Coloumb friction force.

In Dahl's model, friction force is independent of the amplitude of the velocity; but, depends on the direction of the velocity.

1.2.1.2. Bristle Model

According to the model developed by Haessig and Freidland [19], friction force is generated between the bristles on the surfaces of the contacting bodies that cannot be seen by eye. Bristles are shown in Figure 1.16 and a single Bristol is given in Figure 1.17. In this model, bristles act like springs when relative motion between contacting bodies occur. Total friction force is calculated by summing forces generated by all bristles. Friction force is given in Equation (1.8).

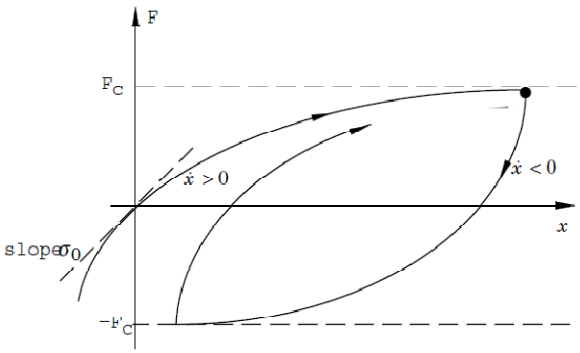

Figure 1.15. Friction force vs. displacement plot for Dahl model [18]

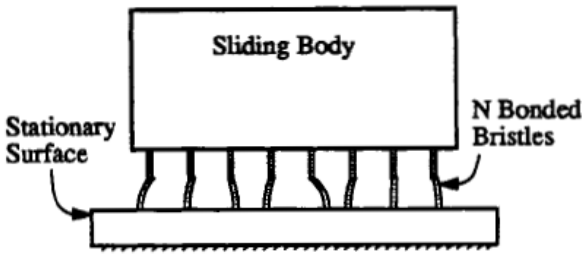

Figure 1.16. Bristle Model [19]

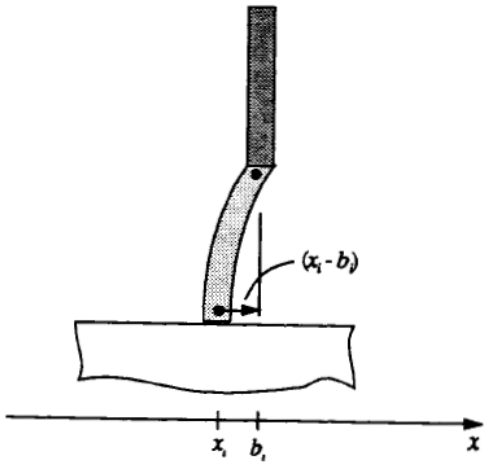

Figure 1.17. Single Bristle [19]

$$F = \sum_{i=1}^{N} \sigma_0 \left(x_i - b_i \right) \tag{1.8}$$

where, N is the number of bristles, σ_0 is stiffness of bristles, x_i is relative position and b_i is the position of the bristle.

1.2.1.3. Reset Integrator Model

Haessig and Freidland [18] developed reset integrator model to decrease calculation time of Bristle model. In this model bristles are replaced by term z which is the displacement before slip. Friction force is calculated as follows:

$$F = \left(1 + a\left(z\right)\right)\sigma_0\left(\upsilon\right)z + \sigma_1 \frac{dz}{dt}, \tag{1.9}$$

where, $\sigma_1 dz/dt$ is a damping term that is only active at stick state. When z takes its maximum value z_0, it becomes constant and friction force decreases until $a\left(z\right)$ becomes zero. $a\left(z\right)$ is a function given as:

$$a\left(z\right) = \begin{cases} a & stick \\ 0 & otherwise \end{cases}. \tag{1.10}$$

1.2.1.4. Bliman and Sorine Model

Bliman and Sorine [18] developed friction models, where the friction force only depends on the sign of the velocity and variable s , which is given as

$$s = \int_0^t \left| \upsilon(\tau) \right| d\tau \,. \tag{1.11}$$

The general form of the friction models developed by Bliman and Sorine is given in the following equations

$$\frac{dx_s}{ds} = Ax_s + B\upsilon_s \,, \tag{1.12}$$

$$F = Cx_s \,. \tag{1.13}$$

Details of these matrices can be found in reference [18].

1.2.1.5. LuGre Model

LuGre model is similar to bristle model, it uses elastic springs like bristles used in bristle model. When a force tangent to a surface is applied, springs elongate, and slip starts when displacement reaches to a certain value [18]. Friction force is calculated as follows:

$$\frac{dz}{dt} = \upsilon - \sigma_0 \frac{|\upsilon|}{g(\upsilon)} z \,, \tag{1.14}$$

$$F = \sigma_0 z + \sigma_1(\upsilon)\frac{dz}{dt} + f(\upsilon). \tag{1.15}$$

Where, z is average bristle deflection, σ_0 is stiffness of bristles and σ_1 is damping.

1.2.1.6. Leuven Model

Leuven model models presliding and sliding states with one equation. This model includes Streibeck effect, which is decrease of friction force during slip, varying break-away, stick-slip behavior and hysteretic behavior in presliding [20]. Friction force can be calculated as:

$$\frac{dz}{dt} = v\left(1 - \operatorname{sgn}\left(\frac{F_d(z)}{s(v) - F_b}\right)\left|\frac{F_d(z)}{s(v) - F_b}\right|^n\right), \tag{1.16}$$

$$F_f = F_h(z) + \sigma_1 \frac{dz}{dt} + \sigma_2 v, \tag{1.17}$$

where, v is velocity, n is a parameter used to shape transition curves and $s(v)$ is the function that determines behavior at constant velocity and given as follows

$$s(v) = \operatorname{sgn}(v)\left(F_c + (F_s - F_c)e^{-\left(\frac{|v|}{V_s}\right)^{\delta}}\right). \tag{1.18}$$

$F_h(z)$ is hysteresis force, which has nonlocal memory and shows nonlinear behavior.

$$F_h(z) = F_b + F_d(z) \tag{1.19}$$

where, F_b is the start of sign change of the velocity and $F_d(z)$ is the transition curve [20]. Leuven model models friction force more accurately than LuGre model.

1.2.1.7. Macro-Slip Model

Macro-slip model is composed of a linear spring and a Coloumb friction element as shown in Figure 1.18 [21]. Force generated on the linear spring is due to relative motion between contacting bodies. When this force is lower than the slip force, friction element sticks and friction force is equal to the multiplication of stiffness coefficient of the spring and relative displacement between contracting bodies. When the force on the spring exceeds the slip force, friction element slips and friction force is equal to the slip force. For single harmonic relative motion the hysteresis curve generated is given in Figure 1.18. Details of the model can be found in reference [21].

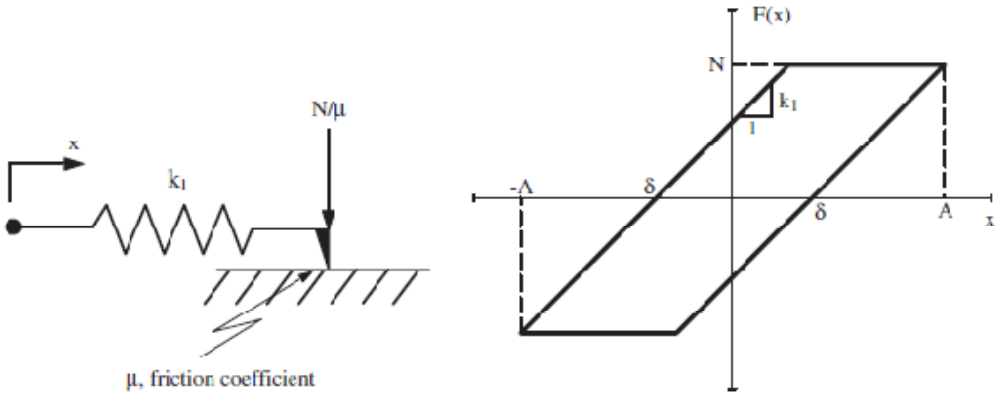

Figure 1.18. Macro-slip model and hysteresis curve [21]

1.2.1.8. Micro-Slip Model

In micro-slip model, friction contact is modeled as an elastic body as a result partial slip of the friction contact is possible [24]. In this model, damping can be obtained without having gross-slip. It was observed that this model gives more

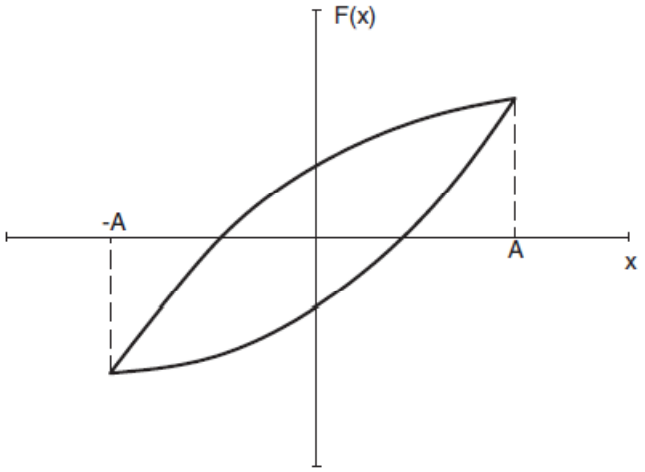

Figure 1.19. Hysteresis curve of micro-slip model [21]

realistic results than macro-slip model. A typical hysteresis curve for micro-slip model is shown in Figure 1.19.

1.2.1.9. Two-slope Friction Model

Ciğeroğlu and Özgüven developed a new two-slope friction model where the advantages of macro-slip and micro-slip models are combined. This model gives better results than macro-slip since micro-slip effects are included; on the contrary, it requires less computation time compared to the micro-slip friction model. Analytical solution of the two-slope model is available whereas the solution of the micro-slip model should be obtained by numerical methods [21]. A typical hysteresis curve for the two-slip friction model is given in Figure 1.20.

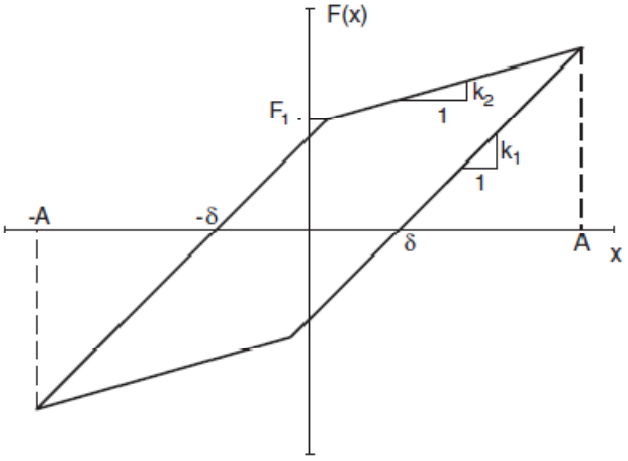

Figure 1.20. Hysteresis curve of two-slope friction model [21]

Hysteresis curves of micro-slip friction model and macro-slip friction model are compared in Figure 1.21.

1.2.2. Applications of Friction Damping

Friction damping is used at various applications for many reasons. One of them is dissipation of energy in order to stop motion of a system. Automobile brakes are an example of this. Another use of friction is at clutches. In automobiles, torque should be transferred from engine to wheels; however, this transmission should stop when the driver changes gear. Therefore friction clutches are used to separate these shafts whenever necessary.

Friction damping is also used for vibration attenuation. Several applications for vibration attenuation are given in the following sections.

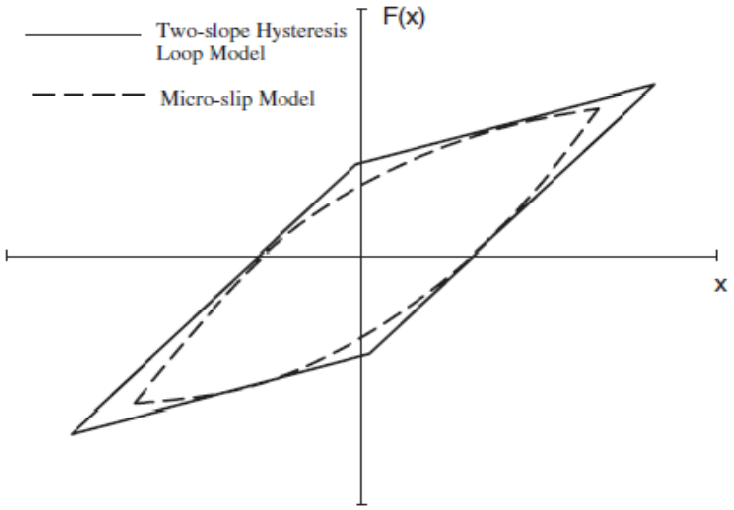

Figure 1.21. Comparison of hysteresis curves [21]

1.2.2.1. Gas Turbine Engines

An important component of gas turbine engines is the blades used in turbines and compressors. These engines run at very high speeds and blades are subjected to vibrations due to flowing air; therefore they are viable to high cycle fatigue. In order to reduce vibrations friction dampers are placed between the blades or the blades and cover plates [21]. Friction dampers are widely used for HCF prevention in gas turbine engines, Firrone and Zucca [22] and Şanlıtürk et al. [23] are several researchers who worked on vibration attenuation with friction dampers.

1.2.2.2. Belt Drives

At internal combustion engines, dry friction tensioners are used in belt pulley system in order to have enough tension on the belt all the time. An example of this system is shown in Figure 1.22.

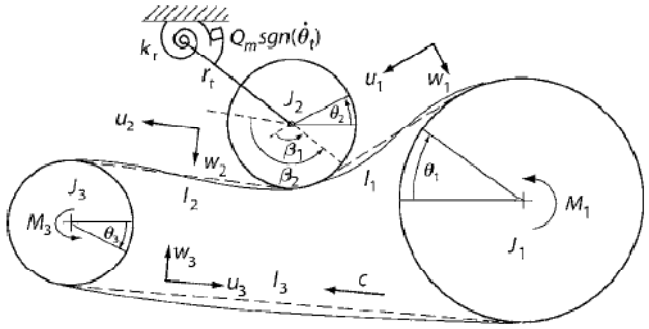

Figure 1.22. Dry friction tensioner [25]

1.2.2.3. Tuned Mass Damper

Another usage of friction damping is observed at tuned mass dampers (TMD). TMD are used at commercial buildings, automobiles and many other applications. TMD is composed of a mass placed on the vibrating structure in order to take energy of the structure on itself hence reduce vibrations on the original structure. Usage of dry friction damping at TMD increases performance of TMD. Ricciardelli investigated this topic [26]. Wang, Zan, Yang and Fei used friction damping at TMD to improve machining stability [27].

1.2.2.4. Semi-Active Friction Dampers

Usage of Semi-active friction dampers on automobiles are investigated by Lorenz et al. [28]. Authors designed a semi-active friction damper for automotive industry. Another example for usage of semi-active friction dampers is the work done by Stammers and Sireteanu [29]. In their study, authors reduced vibrations transmitted to driver using friction dampers.

Friction damping is used on space structures. Gaul, et al. [30] worked on semi-active friction dampers. They controlled normal force with various control strategies.

CHAPTER 2

MODELLING OF ENGINE WITH ENGINE MOUNTS

2.1. ENGINE MOUNT MODELS

Investigating performance of engine mounts requires a mathematical engine model which represents engine and engine mounts accurately. In this study, engine mount systems are represented with three models that have varying complexity. First model is a single degree-of-freedom model which the represents engine with a concentrated mass and connects it to the chassis with stiffness, viscous damping and friction damping elements. Second model is a combination of a quarter car model with the previous engine model added on top of it, which represents engine, sprung mass and unsprung mass with concentrated masses and connects these elements with stiffness and damping elements. The final model is a 6 degree-of-freedom engine model which models the engine as a six degree-of-freedom rigid body and includes 3 translational and 3 rotational motions of the engine. In the 6-DOF model, engine is supported by 3 engine mounts which are represented by stiffness, viscous and friction damping elements in three directions.

2.1.1. SDOF Engine Mount Model

SDOF model is the simplest model used in this study. SDOF model is used to investigate the effect of addition of dry friction damping to a simple system. It should be noted that even though a simple model is used, the nonlinear nature of dry friction complicated the analysis and therefore, it is a good starting point for this study. In the SDOF engine and engine mount model, engine is represented with a concentrated mass. Depending on the input, chassis is either taken as fixed or vibrating with sinusoidal motion. If input is taken as the force generated in the engine, chassis is assumed to be fixed. Otherwise if input is chassis deflection, chassis is vibrating with sinusoidal motion. The connection between engine and chassis is represented by stiffness and damping elements. Stiffness of the spring is modeled as linear, cubic or piecewise linear while damping element includes viscous and friction damping. A sketch of the SDOF model is shown in Figure 2.1.

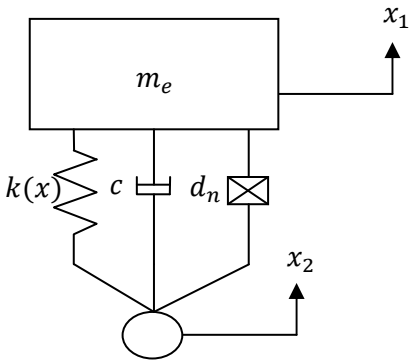

Figure 2.1. SDOF engine mount

In the figure, the input is taken as the chassis displacement. Equation of motion for this system can be written as follows,

$$m_e\ddot{x}_1 + c\dot{x}_1 + kx + f_{NL} = f_{exc}, \tag{2.1}$$

where,

$$f_{exc} = \begin{cases} f_{en} & for\ engine\ excitation \\ c\dot{x}_2 + kx & for\ chassis\ excitation \end{cases}. \tag{2.2}$$

In Equation (2.1), m_e represents the mass of the engine carried by one engine mount, c is the viscous damping coefficient, $k(x)$ is the stiffness coefficient, x_1 and x_2 are the engine and chassis displacements, respectively. f_{exc} is the excitation force and f_{NL} represents the nonlinear forces generated by friction damping and cubic or piecewise stiffness.

2.1.2. Engine on Quarter Car Model

Vehicle and engine model includes SDOF model and a quarter car model where SDOF engine model is placed on top of the sprung mass of the quarter car model. In this model, vehicle suspension characteristics affect engine displacement hence engine mount system can be analyzed for different vehicles and displacement input is due to the road irregularities. This model is used for investigating the effect of dry friction damping on the engine due to the input coming from the road. A sketch of vehicle and engine model is given in Figure 2.2.

In the figure, input of the system is the displacement coming from road irregularities. Equation of motion of the system can be given as follows:

$$[M]\{\ddot{x}\} + [C]\{\dot{x}\} + [K]\{x\} + \{f_{NL}\} = \{f_{exc}\} \tag{2.3}$$

In this equation, $[M]$, $[C]$ and $[K]$ represents mass, damping and stiffness matrices, respectively, and $\{x\}$ is the displacement vector, $\{f_{NL}\}$ and $\{f_{exc}\}$ are nonlinear and excitation vectors. These matrices are,

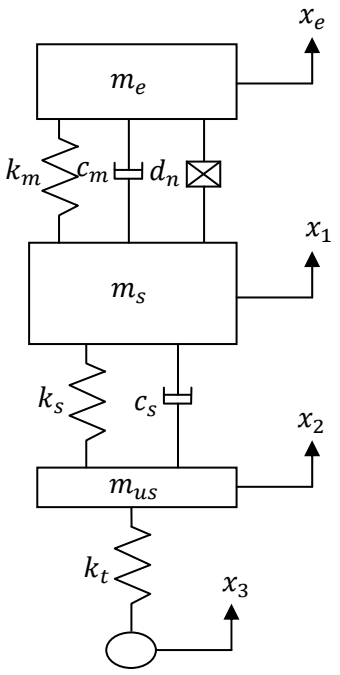

Figure 2.2. Vehicle and engine model

$$[M]=\begin{bmatrix} m_e & 0 & 0 \\ 0 & m_s & 0 \\ 0 & 0 & m_{us} \end{bmatrix}, \tag{1.4}$$

$$[C]=\begin{bmatrix} c_t & -c_t & 0 \\ -c_t & c_s+c_t & -c_s \\ 0 & -c_s & c_s \end{bmatrix}, \tag{1.5}$$

$$[K]=\begin{bmatrix} k_t & -k_t & 0 \\ -k_t & k_s+k_t & -k_s \\ 0 & -k_s & k_s+k_t \end{bmatrix}. \tag{1.6}$$

In this model suspension parameters are selected for a mid-sized vehicle. Stiffness coefficient of the suspension is $k_s = 15000N/m$, viscous coefficient is $c_s = 1000Ns/m$, sprung mass is $m_s = 230kg$, engine mass is $m_e = 70kg$ and unsprung mass is taken as $m_{us} = 30kg$. In this study sprung mass does not include engine mass since engine is represented by another concentrated mass.

2.1.3. 6-DOF Engine Model

In 6-DOF engine model, engine is modeled as a rigid body with 3 translational and 3 rotational motions. In general, engine mounting systems have 3 or 4 engine mounts placed at various locations of the engine. In this study, 3 engine mounts are used to connect the engine to the chassis. These mounts can be placed at any location and they can have friction damping in three directions. The engine is modeled as a rectangular prism. A sketch showing 6-DOF engine model is given in Figure 2.3.

Equation of motion of this system is given as follows [31]:

$$[M]\{\ddot{x}\} + [C]\{\dot{x}\} + [K]\{x\} + \{f_{NL}\} = \{f_{exc}\}, \tag{2.7}$$

where, $[K], [M]$ and $[C]$ are stiffness, mass and viscous damping matrices of the system, which are expressed in Equations (2.8) and (2.9). Moreover, $\{x\}$ is the displacement vector, $\{f_{NL}\}$ and $\{f_{exc}\}$ are the nonlinear force and input force vectors.

$$[M]=\begin{bmatrix} m_{en} & 0 & 0 & 0 & 0 & 0 \\ 0 & m_{en} & 0 & 0 & 0 & 0 \\ 0 & 0 & m_{en} & 0 & 0 & 0 \\ 0 & 0 & 0 & I_{xx} & 0 & 0 \\ 0 & 0 & 0 & 0 & I_{yy} & 0 \\ 0 & 0 & 0 & 0 & 0 & I_{zz} \end{bmatrix} \tag{2.8}$$

$$[K]=\begin{bmatrix} \sum_i k_{x_i} & 0 & 0 & 0 & \sum_i k_{x_i} a_{z_i} & -\sum_i k_{x_i} a_{y_i} \\ & \sum_i k_{y_i} & 0 & -\sum_i k_{y_i} a_{z_i} & 0 & \sum_i k_{y_i} a_{x_i} \\ & & \sum_i k_{z_i} & \sum_i k_{z_i} a_{y_i} & -\sum_i k_{z_i} a_{x_i} & 0 \\ & & & \sum_i k_{y_i} \left(a_{z_i}\right)^2 + k_{z_i} \left(a_{y_i}\right)^2 & -\sum_i k_{z_i} a_{x_i} a_{y_i} & -\sum_i k_{y_i} a_{x_i} a_{z_i} \\ & & & & \sum_i k_{x_i} \left(a_{z_i}\right)^2 + k_{z_i} \left(a_{x_i}\right)^2 & -\sum_i k_{x_i} a_{y_i} a_{z_i} \\ & & & & & \sum_i k_{x_i} \left(a_{y_i}\right)^2 + k_{y_i} \left(a_{x_i}\right)^2 \end{bmatrix} \tag{2.9}$$

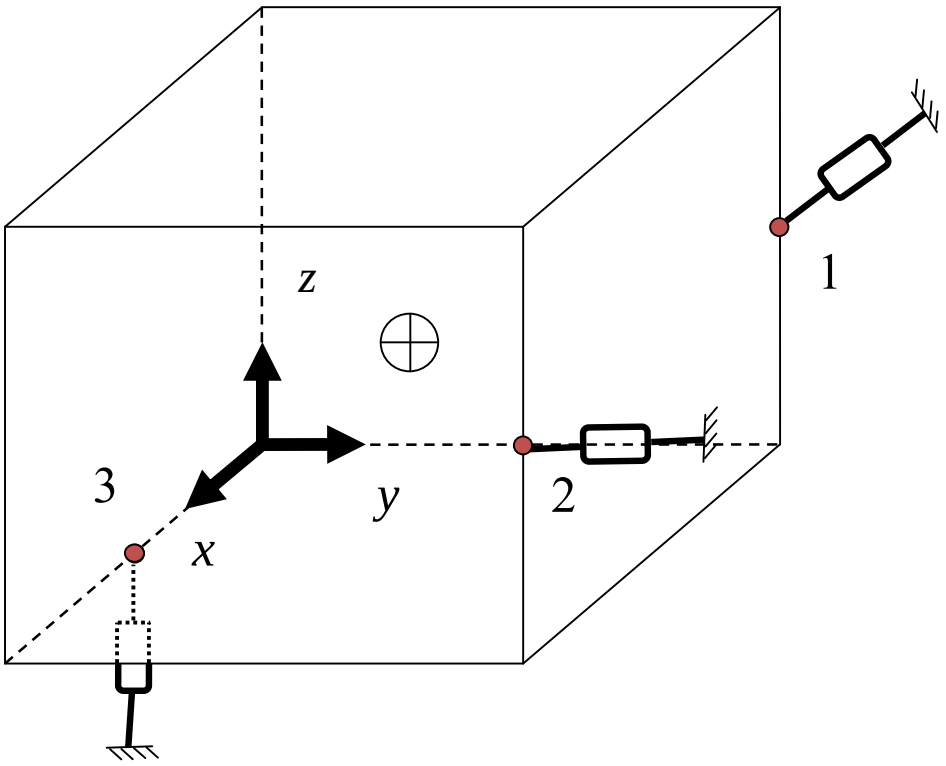

Figure 2.3 6-DOF engine model

Where, i represents the mount to which the element belongs to, x, y and z represents the direction in which the stiffness or damping element is oriented and a is the distance of the i^{th} mount to the origin in different directions. The viscous damping matrix is similar to the stiffness matrix.

During the derivation of the equation of motion, several simplifications are made. These simplifications are given in [31] as:

1"The reference axes X, Y, Z are selected to coincide with the principal inertial axes of the body."

2. The principal elastic axes of all isolators are orthogonal with the reference axes of the body.

2.2. MACRO-SLIP FRICTION MODEL

Macro-slip friction model is composed of a linear spring and a friction element as shown in Figure 2.4

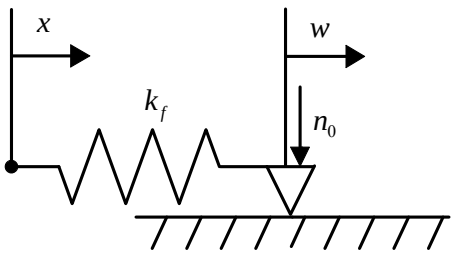

Figure 2.4. Macro-slip friction model

If x increases, linear spring compresses and friction force is generated at the fight end as follows:

$$F_f = k_f (x - w), \tag{2.10}$$

Where w is constant at this stage. Friction force increases until it reaches to the slip force and friction element starts to slip, where w is no longer constant. Slip force is the maximum force that the spring element can hold before slip motion starts and given as,

$$F_s = \mu n_0 . \tag{2.11}$$

Where F_s is the slip force and μ and n_0 are coefficient of friction and normal force, respectively. During slip state friction force obtained from Equation (2.10) and Equation (2.11) is equal to each other, resulting in:

$$k_f (x - w) = \mu n_0 , \tag{2.12}$$

$$\varepsilon = (x - w) = \frac{\mu n_0}{k_f} . \tag{2.13}$$

In Equation (2.13), ε is the relative displacement which is necessary to start slip motion. When slip occurs, both bodies move with the same velocity, and the relative distance between the two bodies is constant; hence, friction force remains constant. Slip will continue until the relative motion between the two bodies, x , reverses its direction in this case, the load on the linear spring will decrease and friction element will stick. When the relative displacement is ε in the reverse direction, the spring force will be zero, and when the relative displacement reaches 2ε , friction element will start to slip in the reverse direction.

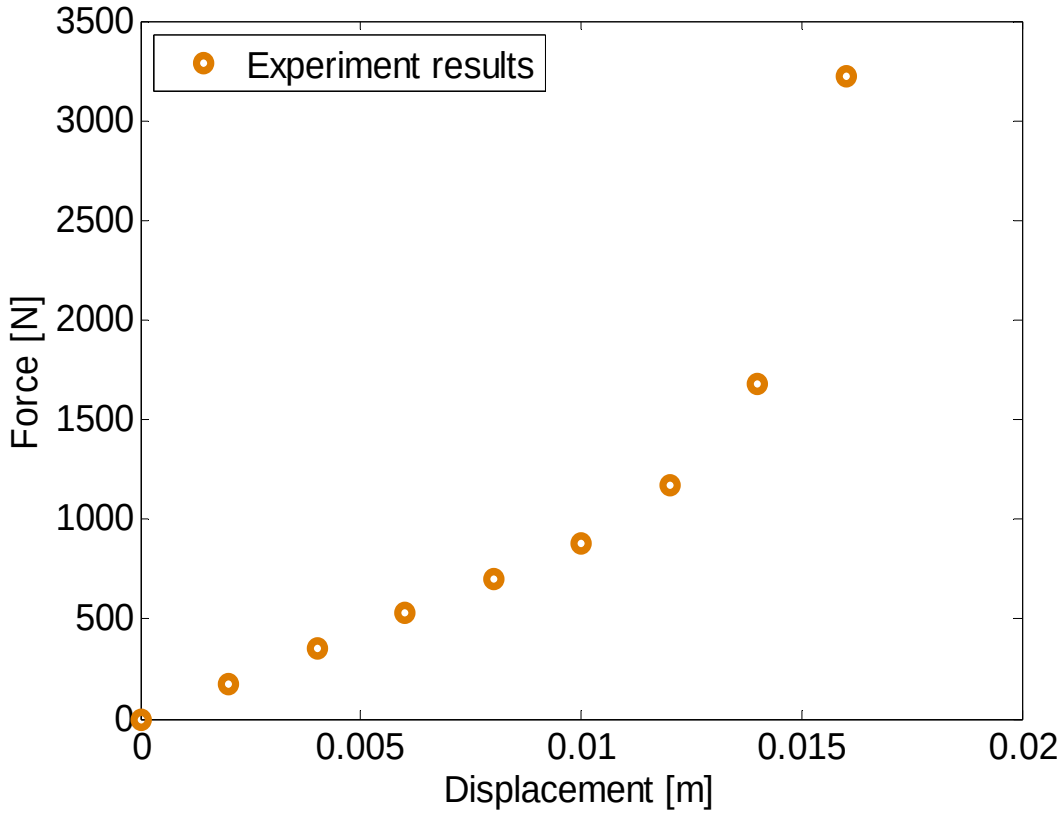

Figure 2.5. Experiment results from TOFAŞ

2.3. STIFFNESS MODELS

Elastomeric engine mounts have complex shapes that cannot always be represented by a linear stiffness. Hence, more sophisticated models should be used to represent stiffness of an elastomeric engine mount. In this study, elastomeric mount considered is the one whose test data has been sent by TOFAŞ. Data taken from the experiment is shown in the Force vs. displacement plot given in Figure 2.5.

The test data given in Figure 2.5 can be represented with three models: linear stiffness model, cubic stiffness model and piecewise linear stiffness model.

Linear stiffness is the simplest model used for elastomeric engine mount. In this model, mount acts like a simple linear spring. The force on the mount is related to the relative motion between the two ends as follows:

$$F_m = k_1 x . \tag{2.14}$$

Due to the complex shape of elastomeric engine mounts, cubic stiffness may be used as well. The force on the mount is related to the relative motion between the two ends as follows:

$$F_m = k_1 x + k_c x^3 . \tag{2.15}$$

It is observed that, the force-displacement data available for this study has an increase in stiffness when the relative displacement is larger than a specific value. In addition to modeling force-displacement characteristics as a cubic stiffness it can as well be modeled as a piecewise linear stiffness. The spring force for this case is given as follows:

$$F_m = \begin{cases} k_1 x, & x < \delta \\ k_2 x + b, & x \geq \delta \end{cases} . \tag{2.16}$$

where,

$$b = \left(k_1 - k_2\right)\delta . \tag{2.17}$$

2.4. COMPARISON OF STIFFNESS MODELS

Three stiffness models are used in this study to represent the elastomeric mount used. Curve fit tool of MATLAB is used for each model and the results obtained are compared with the experimental data in Figure 2.6.

The force on the mount of linear stiffness model is given as:

$$F_m = k_1 x, \tag{2.18}$$

where, $k_1 = 133000 N/m$.

For cubic stiffness model, the force on the mount is calculated as follows:

$$F_m = k_1 x + k_c x^3, \tag{2.19}$$

where, $k_1 = 34770\, N/m$ and $k_c = 5.708 \times 10^8\, N/m^3$.

Finally for piecewise stiffness model, the force on the mount is given as:

$$F_m = \begin{cases} k_1 x, & x < \delta \\ k_2 x + b, & x \geq \delta \end{cases}, \tag{2.20}$$

where, $k_1 = 91870\, N/m, k_2 = 513800\, N/m$, $\delta = 0.01225$ and $b = -5169\, N$.

The results obtained with cubic and piecewise stiffness models shows similarity at high displacements, whereas cubic stiffness model calculates force less at small deflections. The force on the mount calculated by linear model is more than other models for small displacements, on the other hand the force calculated is less for high displacements. Piecewise linear stiffness represents test data the closest. This is due to the designed shape of the elastomeric mount. After a specific displacement, another elastic part of the mount starts contacting with the base platform hence stiffness of the mount increases after that displacement. This situation can be modeled with piecewise stiffness accurately.

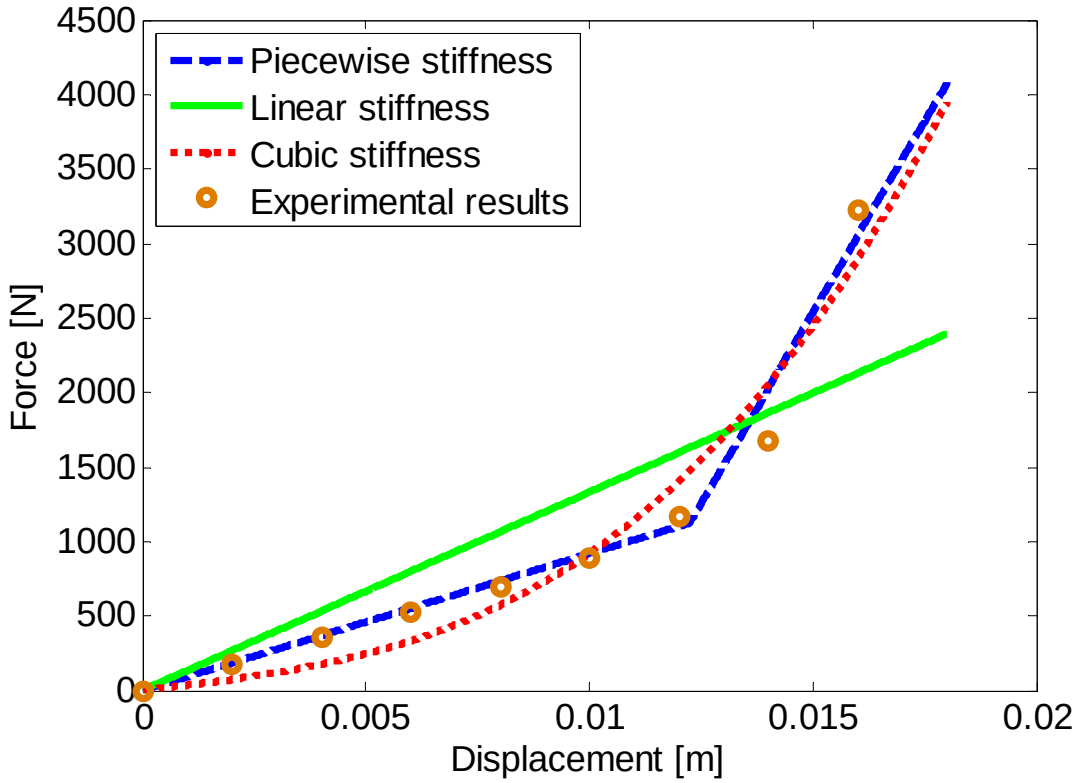

Figure 2.6. Comparison of stiffness models

CHAPTER 3

SOLUTION METHOD

3.1. SOLUTION OF EQUATIONS OF MOTION

Equation of motion of the system without nonlinearities is given as follows:

$$[M]\{\ddot{x}\}+[C]\{\dot{x}\}+[K]\{x\}=\{f_{exc}\}, \tag{3.1}$$

where $[M]$, $[C]$ and $[K]$ are the mass, viscous damping and stiffness matrices, $\{\ddot{x}\}$, $\{\dot{x}\}$ and $\{x\}$ are the acceleration, velocity and displacement vectors, respectively. Excitation force vector is denoted by $\{f_{exc}\}$.

The system with harmonic excitation can be solved in two ways, frequency domain and time domain analysis, that can be obtained using different methods. Frequency domain solution for a broad frequency interval of the excitation force is obtained within a reasonable time. On the other hand, in time marching the equation of motion has to be integrated till the solution reaches the steady state at each frequency of the excitation force. In order to obtain solution for many frequencies, analysis must be conducted many times; hence time domain solution requires excessive time. Frequency domain solution is obtained by assuming a simple harmonic solution as

$$\{x\} = \mathrm{Im}\left(\{X\} e^{i\omega t}\right). \tag{3.2}$$

Substituting this into the equation of motion (3.1), a set of algebraic equations is obtained.

$$\left[[K] - \omega^2 [M] + i\omega [C]\right]\{X\} = \{F_{exc}\}. \tag{3.3}$$

Now, the set of linear algebraic equations obtained, can be solved by using matrix inversion or modal analysis methods.

In this thesis, due to the elastomeric stiffness and dry friction damping there are nonlinear terms in the equations of motion. If these terms are included, the equations of motion becomes as follows:

$$[M]\{\ddot{x}\} + [C]\{\dot{x}\} + [K]\{x\} + \{f_{NL}\} = \{f_{exc}\}, \tag{3.4}$$

where $\{f_{NL}\}$ is the nonlinear forcing vector. Since nonlinear force is added to the equation of motion, the method shown above cannot be applied directly due to the nonlinear force vector, which is a function of $\{x\}$ and $\{\dot{x}\}$. In order to overcome this problem, Harmonic Balance Method is utilized.

3.2 HARMONIC BALANCE METHOD

Nonlinear forces in the equation of motion create problems while converting the differential equations into algebraic equations. Harmonic Balance Method (HBM) can be used to model nonlinear elements periodically in the equation of motion using Fourier integrals. Hence, using HBM nonlinear differential equations of motion are transferred into a set of nonlinear algebraic equations. For simple harmonic excitation,

$$\{f_{exc}\} = \mathrm{Im}\left(\{F_{exc}\} e^{i\omega t}\right), \tag{3.5}$$

Where $\{F_{exc}\}$ is the complex amplitude vector of external excitations. Since the excitation is harmonic a simple harmonic solution can be assumed as shown:

$$\{x\} = \{X_s\}\sin(\theta) + \{X_c\}\cos(\theta) = \mathrm{Im}\left(\{X\} e^{i\omega t}\right), \tag{3.6}$$

where, $\{X\}$ is the complex displacement vector and it is given as:

$$\{X\} = \{X_c\} i + \{X_s\}, \tag{3.7}$$

and θ is defined as:

$$\theta = \omega t. \tag{3.8}$$

Using Fourier series, a nonlinear force can be represented in terms of sine and cosine components with N harmonics as follows:

$$\{f_{NL}(x,\theta)\} \cong \sum_{m=1}^{N} \left\{F^s_{NL_m}\right\}\sin(m\theta) + \left\{F^c_{NL_m}\right\}\cos(m\theta), \tag{3.9}$$

where, N is the number of harmonics that is used in calculations. For this study, only the fundamental harmonic is considered; hence, resulting in a simpler force equation as shown:

$$\{f_{NL}(x,\theta)\} = \left\{F^s_{NL}\right\}\sin(\theta) + \left\{F^c_{NL}\right\}\cos(\theta). \tag{3.10}$$

However, in order to apply this, sine and cosine components of the nonlinear forces needs to be calculated. These components of the nonlinear forces F^s_{NL} and F^c_{NL}, are obtained by Fourier integrals as follows [31]:

$$F_{NL}^{c} = \frac{1}{\pi}\int_{0}^{2\pi} F\cos(\theta)d\theta\,, \tag{3.11}$$

$$F_{NL}^{s} = \frac{1}{\pi}\int_{0}^{2\pi} F\sin(\theta)d\theta\,. \tag{3.12}$$

Similar to Equation (3.6) the nonlinear force can also be expressed in complex form as:

$$\left\{ f_{NL}\left(x,\theta\right)\right\} = \mathrm{Im}\left(\left\{F_{NL}\right\}e^{i\omega t}\right), \tag{3.13}$$

where,

$$\left\{F_{NL}\right\} = \left\{F_{NL}^{c}\right\}i + \left\{F_{NL}^{s}\right\}, \tag{3.14}$$

Inserting Equations (3.5), (3.6) and (3.13) into Equation (3.4) , the following set of nonlinear algebraic equation is obtained

$$\left[\left[K\right]-\omega^{2}\left[M\right]+i\omega\left[C\right]\right]\left\{X\right\}+\left\{F_{NL}\right\}=\left\{F_{exc}\right\}. \tag{3.15}$$

This set of nonlinear algebraic equations can be solved by a nonlinear equation solver such as Newton's method. In this study Newton's method with arc-length continuation method is used to obtain the solution of Equation (3.15).

In this study, 3 types of nonlinearities are used. They will be discussed in the following sections.

3.2.1. Cubic Stiffness

Elastomeric engine mounts have complex shapes hence modeling it with a linear stiffness element may not give realistic results. So a cubic coefficient is used to

model elastomeric mount. Force displacement relationship for this model is given as follows:

$$F = k_1 x + k_c x^3 . \tag{3.16}$$

Assuming a solution in the form given in Equation (3.10) sine and cosine components of the Fourier expansion are calculated as follows:

$$F_{NLc}^{c} = \frac{1}{\pi}\int_0^{2\pi} k_c \left(X_s \sin(\theta) + X_c \cos(\theta)\right)^3 \cos(\theta) = \frac{3X_c k_c \left(X_c^2 + X_s^2\right)}{4}, \tag{3.17}$$

$$F_{NLc}^{s} = \frac{1}{\pi}\int_0^{2\pi} k_c \left(X_s \sin(\theta) + X_c \cos(\theta)\right)^3 \sin(\theta) = \frac{3X_s k_c \left(X_c^2 + X_s^2\right)}{4}. \tag{3.18}$$

Results of these integrals are added to the equation of motion in order to include the effect of cubic stiffness nonlinearity.

3.2.2. Piecewise Stiffness

Another way of modeling the elastomeric mount is piecewise stiffness which is shown in Figure 3.1. Due to its nonlinear behavior, force generated by piecewise stiffness element can be approximated by Fourier series.

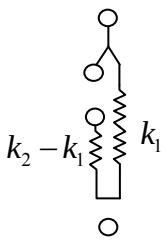

Figure 3.1. Piecewise stiffness element

A simple harmonic input similar to the input given in Equation (3.6), can be simplified by changing its phase angle as shown:

$$\{x(t)\} = X_s' \sin(\alpha), \tag{3.19}$$

$$\alpha = \theta + \phi. \tag{3.20}$$

X_s' and ϕ are calculated using the following equations,

$$X_c \cos(\theta) + X_s \sin(\theta) = X_s' \sin(\theta + \phi), \tag{3.21}$$

$$X_s' \sin(\theta + \phi) = X_s' \sin(\theta)\cos(\phi) + X_s' \cos(\theta)\sin(\phi). \tag{3.22}$$

From Equation (3.22),

$$X_s = X_s' \cos(\phi), \tag{3.23}$$

$$X_c = X_s' \sin(\phi), \tag{3.24}$$

where,

$$X_s' = \sqrt{X_s^2 + X_c'}. \tag{3.25}$$

From Equation (3.23) and(3.24), ϕ can be calculated as:

$$\phi = \arctan\left(\frac{X_c}{X_s}\right), \tag{3.26}$$

Which has two solutions; therefore, in order to obtain a single solution, ATAN2 function can be used as:

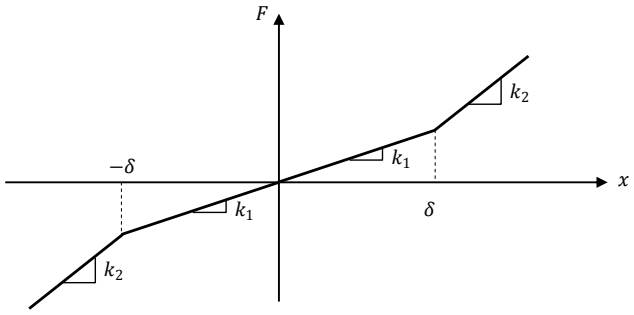

Figure 3.2. Total Force vs. displacement

$$\phi = ATAN2(X_c, X_s), \tag{3.27}$$

With this change of variables, Fourier integrals can be simplified. For piecewise linear stiffness element, force displacement relationship is given in Figure 3.2

Piecewise stiffness can be represented by summation of a linear spring and a sprint element with a gap. Force displacement relationships for these two elements are given in Figure 3.3. Total force can be calculated by adding linear and nonlinear force components. Hence, linear portion of the stiffness element is added to the stiffness matrix of the system and nonlinear portion is calculated with Fourier integrals and added to nonlinear force vector in set of nonlinear algebraic equations [21].

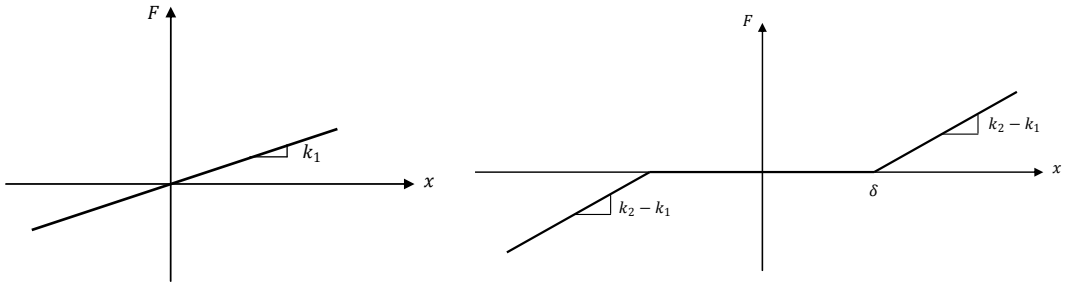

a) Linear Force b) Non-linear For

Figure 3.3. Force vs. displacement

Components of Fourier series for $X_s^{'} > \delta$:

$$F_{NLp}^{s'} = \frac{1}{\pi}\int_0^{2\pi} F(\alpha)\sin(\alpha)\,, \tag{3.28}$$

$$F_{NLp}^{c'} = \frac{1}{\pi}\int_0^{2\pi} F(\alpha)\cos(\alpha)\,, \tag{3.29}$$

$$F(\alpha) = \begin{cases} 0 & 0 < \alpha < \alpha_1 \\ \left(k_2 - k_1\right)\left(X_s^{'}\sin(\alpha) - \delta\right) & \alpha_1 < \alpha < \pi - \alpha_1 \\ 0 & \pi - \alpha_1 < \alpha < \pi + \alpha_1 \\ \left(k_2 - k_1\right)\left(X_s^{'}\sin(\alpha) + \delta\right) & \pi + \alpha_1 < \alpha < 2\pi - \alpha_1 \\ 0 & 2\pi - \alpha_1 < \alpha < 2\pi \end{cases}, \tag{3.30}$$

$$\alpha_1 = \arcsin\left(\frac{\delta}{\sqrt{X_s^2 + X_c^2}}\right). \tag{3.31}$$

Therefore, the results of the integrals are:

$$F_{NLp}^{s'} = \left(k_2 - k_1\right)\left(X_s^{'}\sin(2\alpha_1) + X_s^{'}\pi - 4\delta\cos(\alpha_1) - 2X_s^{'}\alpha_1\right), \tag{3.32}$$

$$F_{NLp}^{c'} = 0\,. \tag{3.33}$$

Phase angle used in the equations should be changed so that angle θ is used in the solution.

$$F_{NLp}^{s} = \frac{F_{NLp}^{s'}X_s - F_{NLp}^{c'}X_c}{\sqrt{X_s^2 + X_c^2}} \tag{3.34}$$

$$F_{NLp}^{c} = \frac{F_{NLp}^{s'}X_c + F_{NLp}^{c'}X_s}{\sqrt{X_s^2 + X_c^2}} \tag{3.35}$$

Finally, F_{NLp}^{s} and F_{NLp}^{c} can be added to the vector of nonlinear forces.

3.2.3. Dry Friction

Fourier integrals are also used for calculating the friction force. The friction model used in this study is a simplified version of the model used by Ciğeroğlu et al. [33]. In that study a friction element for two dimensional motion with varying normal force is considered. However in this thesis, a simpler friction model with constant normal force is used. For a simple harmonic input given in Equation (3.6), friction force is calculated using Fourier integrals.

Phase angle of the simple harmonic input given in (3.6) is also changed for friction force in order to simplify Fourier integrals. The formulation is similar with the formulation used for piecewise stiffness.

In order to calculate Fourier integrals, the angles where friction element changes its state from stick to slip or slip to stick should be known. These angles are given at Ciğeroğlu et al.'s [33] study. For simplified case, the angle from slip to stick case is calculated as:

$$F_f = k_f (x - w) = \pm \mu n_0 . \tag{3.36}$$

The angle from stick to positive slip state can be obtained from:

$$k_f (x - w_0) + f_0 - \mu n_0 = 0 , \tag{3.37}$$

where,

$$f_0 = -\mu n_0 . \tag{3.38}$$

w_0 and f_0 are the position of friction element and the friction force at the start of slip state. In order to guarantee this state change the following condition should also be satisfied:

$$k_f \frac{\partial x}{\partial t} > 0 . \tag{3.39}$$

The angle from stick to negative slip state can be obtained from:

$$k_f (x - w_0) + f_0 + \mu n_0 = 0 , \tag{3.40}$$

where,

$$f_0 = \mu n_0 . \tag{3.41}$$

w_0 and f_0 are position of friction element and friction force at the start of slip state. In order to guarantee this state change, the condition given below should also be satisfied:

$$k_f \frac{\partial x}{\partial t} < 0 . \tag{3.42}$$

Assuming a single harmonic motion as given in Equation (3.6) the friction state changes occur at the angles calculated using Equations (3.43) and (3.44)

Slip to stick state change occurs at $\pi / 2$ and $3\pi / 2$, stick to positive slip state change occurs at:

$$\alpha_2 = \arcsin\left(1 - \frac{2\mu n_0}{k_f X_s^{'}} \right). \tag{3.43}$$

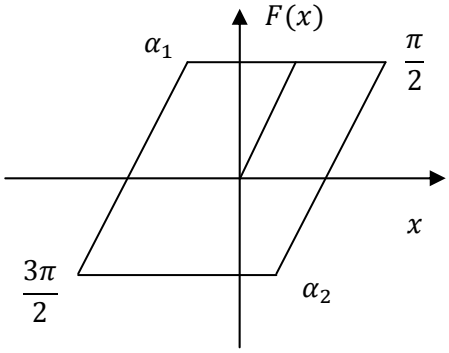

Figure 3.4. Hysteresis curve for friction force

Stick to negative slip state change occurs at:

$$\alpha_1 = \alpha_2 + \pi\,. \tag{3.44}$$

These angles, where state changes occur, can be seen clearly at the hysteresis curve given in Figure 3.4.

Friction force given in Figure 3.4 is expressed in Equation (3.45).

$$F(\alpha) = \begin{cases} k_f\left(x(\alpha) - x\left(\dfrac{3\pi}{2}\right)\right) - \mu n_0 & \dfrac{3\pi}{2} < \alpha < \alpha_1 \\ \mu n_0 & \alpha_1 < \alpha < \dfrac{\pi}{2} \\ k_f\left(x(\alpha) - x\left(\dfrac{\pi}{2}\right)\right) + \mu n_0 & \dfrac{\pi}{2} < \alpha < \alpha_2 \\ -\mu n_0 & \alpha_2 < \alpha < \dfrac{3\pi}{2} \end{cases} \tag{3.45}$$

Sine and cosine components of Fourier series representation of the friction force are calculated using Equations (3.11) and (3.12)

$$F_{NLf}^{s'} = \frac{2n_0\mu}{\pi}\left[\cos(\alpha_1)-\cos(\alpha_2)\right]+\frac{2X_s^{'}k_f}{\pi}\left[\cos(\alpha_2)-\frac{\pi}{4}+\frac{\alpha_2}{2}-\frac{\sin(2\alpha_2)}{4}\right], \quad (3.46)$$

$$F_{NLf}^{c'} = \frac{2n_0\mu}{\pi}\left[\sin(\alpha_2)-\sin(\alpha_1)\right]+\frac{X_s^{'}k_f}{\pi}\left[1-2\sin(\alpha_2)+\left(\sin(\alpha_2)\right)^2\right]. \quad (3.47)$$

Then, phase angle is changed back to θ as shown in Equations (3.48) and (3.49).

$$F_{NLf}^{s} = \frac{F_{NLp}^{s'}X_s - F_{NLp}^{c'}X_c}{\sqrt{X_s^2+X_c^2}}, \quad (3.48)$$

$$F_{NLf}^{c} = \frac{F_{NLp}^{s'}X_c + F_{NLp}^{c'}X_s}{\sqrt{X_s^2+X_c^2}}. \quad (3.49)$$

3.3. SOLUTION OF NONLINEAR EQUATIONS

An equation of motion of the form given in Equation (3.50) should be solved in this study to observe affect of addition of friction damping to engine mount performance.

$$\left[\left[K\right]-\omega^2\left[M\right]+i\omega\left[C\right]\right]\left\{X\right\}+\left\{F_{NL}\right\}=\left\{F_{exc}\right\} \quad (3.50)$$

In Equation (3.50), $\left\{F_{NL}\right\}$ stands for the nonlinear force vector which is the summation of all nonlinear forces calculated by Fourier series approximation.
In this thesis, Newton's method with arc-length continuation is used to solve the resulting set of nonlinear equations.

3.3.1. Newton's Method for Solving Nonlinear Systems of Equations

For the set of nonlinear algebraic equations given in Equation (3.15), a residual vector is defined as:

$$\left\{R\left(\{X\},\omega\right)\right\}=\left[-\omega^2\left[M\right]+i\omega\left[C\right]+\left[K\right]\right]\{X\}+\{F_{NL}\}-\{F_{exc}\}. \qquad (3.51)$$

Solution will be at the points where the residual is equals to zero.

$$\left\{R\left(\{X\},\omega\right)\right\}=0 \qquad (3.52)$$

An iteration step for Newton's method is given as follows [34], [35]:

$$\{X\}_{k+1}=\{X\}_k-\left[\frac{\partial\left\{R(\{X\},\omega)\right\}}{\partial\{X\}}\right]^{-1}\left\{R(\{X\},\omega)\right\}, \qquad (3.53)$$

where, $\left[\partial\left\{R(\{X\},\omega)\right\}/\partial\{X\}\right]$ is denoted as the Jacobian and given as follows:

$$\left[\frac{\partial\left\{R\left(\{X\},\omega\right)\right\}}{\partial\{X\}}\right]=\left[[K]-\omega^2[M]+i\omega[C]\right]+\left[\frac{\partial\{F_{NL}\}}{\partial\{X\}}\right]. \qquad (3.54)$$

Accuracy of Newton's method depends on the initial estimate. An initial estimate can be calculated using partial derivative of the residual with respect to the excitation frequency. The initial estimate is calculated as follows [36]:

$$\{X\}_k^i=\{X\}_k+\left(\frac{\partial\{X\}}{\partial\omega}\bigg|_{\{X\}_k}\right)\Delta\omega, \qquad (3.55)$$

where,

$$\frac{\partial\{X\}}{\partial\omega} = -\left[\frac{\partial\left\{R\left(\{X\},\omega\right)\right\}}{\partial\{X\}}\right]^{-1}\frac{\partial\left\{R\left(\{X\},\omega\right)\right\}}{\partial\omega}. \tag{3.56}$$

3.3.2. Arc-Length Continuation Method

Newton's method may encounter some problems during the solution of nonlinear equations. An example can be taken as cubic stiffness. During the solution of the system with cubic stiffness element, Newton's method always searches the solution at the next frequency value; however, the solution curve turns back for the system with cubic stiffness element. This situation can be observed in Figure 3.5.

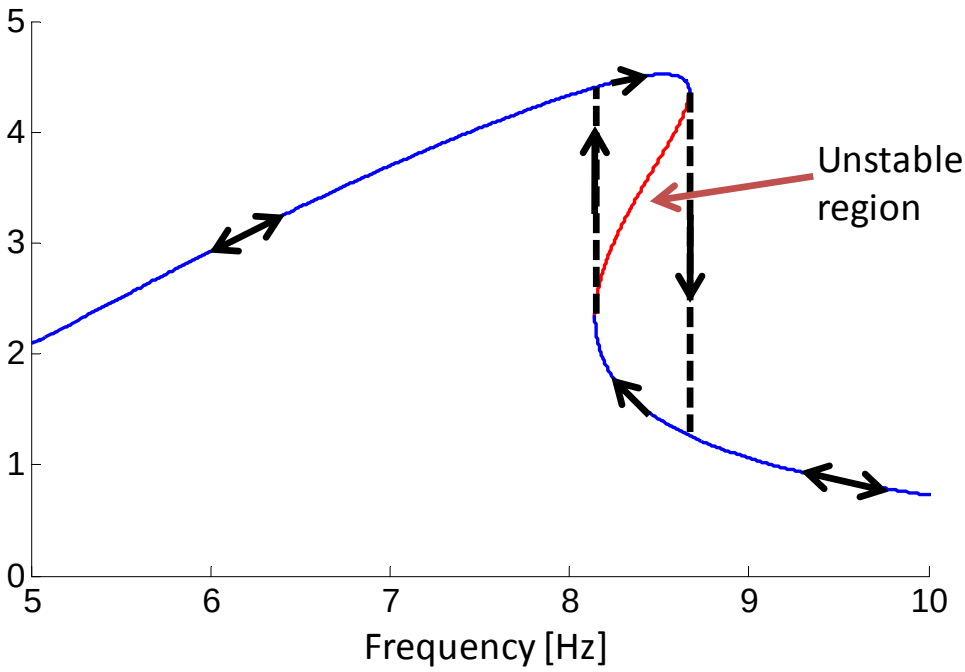

Figure 3.5. Unstable region

At the unstable regions there are more than one solution for a single frequency, hence solution curve must turn back. At the turning point, slope will be infinity hence Jacobian will be singular. Inverse of Jacobian cannot be taken; therefore, Newton's method fails. In Newton's method does not fail, then it will jump up or down to the next frequency point for the solution and misses the turning point and the solution at the unstable region cannot be traced. This situation is shown with dashed lines in Figure 3.5. Time domain analysis also confirms the solution with Newton's method and jump phenomenon can also be observed in the time domain solution given in Figure 3.7.

In the arc-length continuation method, a new parameter, the arc-length, is added to the nonlinear equations which makes the Jacobian non-singular at the turning points. Moreover, instead of frequency in this case the path following parameter will be the arc-length; hence, Newton's method can trace the solution even it is turning back. As a result, the solution at the unstable region can be found. The new path following parameter arc-length is denoted with s which is the radius of the hypothetical sphere in which the next solution point will be searched. Frequency will be an unknown in the new system of nonlinear equations. With the addition of the arc-length parameter to the system, the vector of unknowns for the new system of nonlinear equations is:

$$\{q\} = \begin{Bmatrix} \{X\} \\ \omega \end{Bmatrix}. \tag{3.57}$$

Since the frequency becomes an unknown, a new equation is needed. This new equation is the equation of the hypothetical sphere which has a radius s and centered at the previous solution point. This situation is explained in Figure 3.6.
In the figure, a turning point is given, where the next solution happens to be at a lower frequency than the previous one; thus, solution with Newton's method

cannot detect the next solution. Newton's method would rather jump to the next frequency value resulting in a jump down as shown in Figure 3.5.

Equation of the sphere centered at the previous solution point is given as follows:

$$\left(\{X\}_k - \{X\}_{k-1}\right)^2 + \left(\omega_k - \omega_{k-1}\right)^2 = s^2, \tag{3.58}$$

where, $\{X\}$ is the displacement vector, ω is the frequency and s is the arc-length.

$$\Delta\{X\} = \{X\}_k - \{X\}_{k-1}, \tag{3.59}$$

$$\Delta\omega = \omega_k - \omega_{k-1}. \tag{3.60}$$

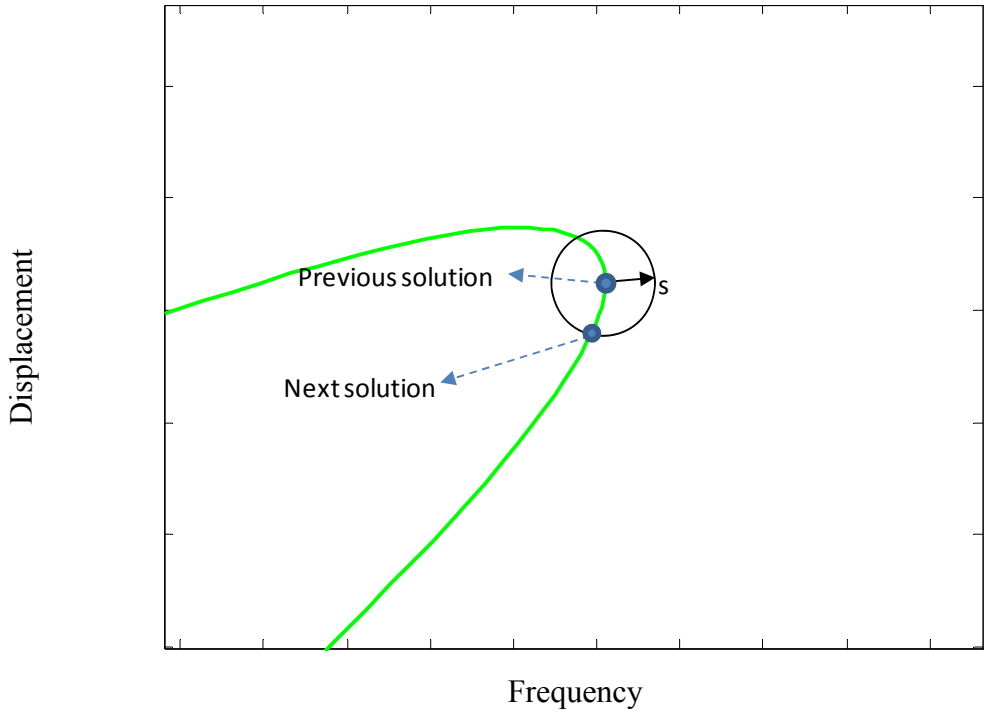

Figure 3.6. Turning point

Using Equation (3.57), (3.59) and (3.60),

$$\{\Delta q\}_k = \begin{Bmatrix} \Delta\{X\} \\ \Delta\omega \end{Bmatrix}, \tag{3.61}$$

$$\{\Delta q\}_k = \left\{\{q\}_k - \{q\}_{k-1}\right\}. \tag{3.62}$$

Finally $\{\Delta q\}_k$ is substituted into the Equation the of sphere which results in the extra equation needed as

$$h\left(\{X\}_k, \omega_k\right) = \{\Delta q\}_k^T \{\Delta q\}_k - s^2 = \{0\}. \tag{3.63}$$

An iteration step is given in Equation (3.64):

$$\{q\}_{k+1} = \{q\}_k - \left[\begin{matrix} \dfrac{\partial\{R(\{X\},\omega)\}}{\partial\{X\}} & \dfrac{\partial\{R(\{X\},\omega)\}}{\partial\omega} \\ \dfrac{\partial h(\{X\},\omega)}{\partial\{X\}} & \dfrac{\partial h(\{X\},\omega)}{\partial\omega} \end{matrix}\right]^{-1}\Bigg|_{\{X\}_k,\omega_k} \begin{Bmatrix} \{R(\{X\},\omega)\} \\ h(\{X\},\omega) \end{Bmatrix}, \tag{3.64}$$

where,

$$\left[\begin{matrix} \dfrac{\partial h(\{X\},\omega)}{\partial\{X\}} & \dfrac{\partial h(\{X\},\omega)}{\partial\omega} \end{matrix}\right] = \left[2\{\Delta q\}_k^T\right]. \tag{3.65}$$

While using the arc-length continuation method, the value of the arc-length parameter is vital for convergence of the solution. If the selected arc-length value is too large, convergence may not be obtained or it may back trace the solution curve [37]. Therefore, the number of iterations are always monitored and if necessary arc-length is modified as follows:

$$s_k = s_{k-1}\sqrt{\frac{n_{norm}}{n_{k-1}^{iter}}}\,. \tag{3.66}$$

3.3. TIME DOMAIN SOLUTION

In this thesis, time domain solution of the system is used for the verification of the frequency domain results. The equation of motion is solved by "ode45" function of MATLAB. Time domain analyses are conducted with an excitation at a certain frequency. Therefore, in order to compare the results with frequency domain analysis, the solution needs to be obtained for every frequency value separately. Hence, time domain solution takes too much time.

In time domain analysis it is also possible to change the excitation frequency after a specific time in order to observe the frequency sweep characteristics which results in the identification of the so-called jump phenomenon which has been observed in the Newton's method. In Figure 3.7, excitation frequency is changed from 8.8 Hz to 8.9Hz at $t = 1s$ while keeping the excitation amplitude constant. Similar to the prediction obtained by the frequency domain solution, a slight increase in frequency resulted in a decrease in the vibration amplitude which I referred as a jump down in the frequency domain analysis. Comparisons of time domain and frequency domain analyses are given in the results chapter.

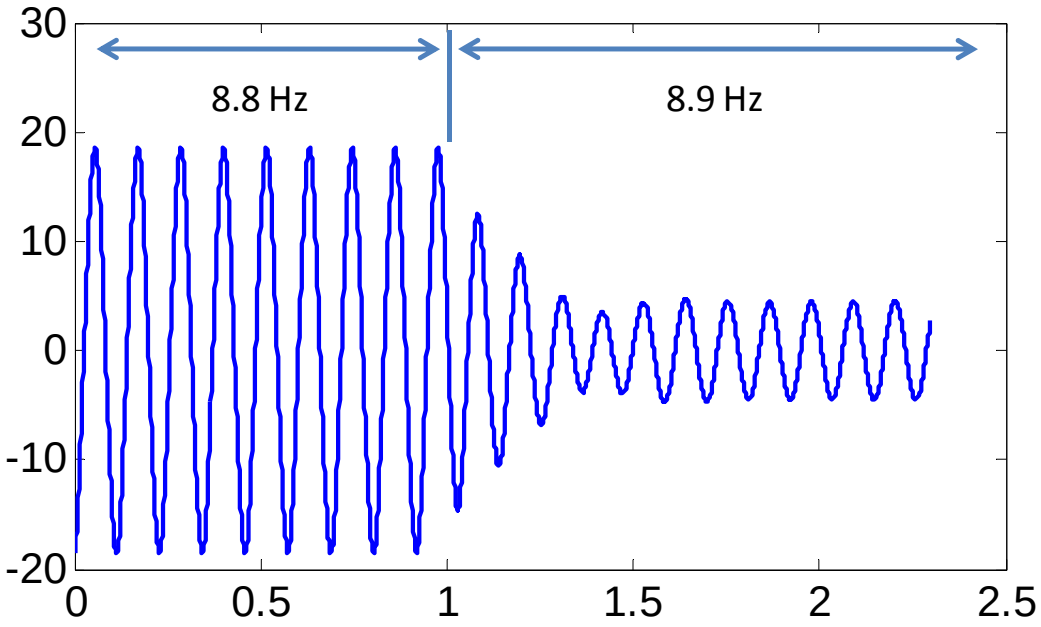

Figure 3.7. Jump at time domain solution

CHAPTER 4

RESULTS

4.1. RESULTS OF THE ANALYSIS

In this section, results of three engine mount models are presented. Initially, SODF engine mount model is considered, and then vehicle and engine model is used. Finally 6-DOF engine model is investigated. Piecewise linear stiffness model is used in the solutions given throughout the chapter. Results are presented at the following sections.

4.2. RESULTS OF SDOF ENGINE MOUNT MODEL

SDOF engine mount model is the simplest model and it is investigated to observe the addition of dry friction damping to a system. Hence a general idea about how dry friction damping affects a system is revealed in this analysis.

Force generated in the engine is the input excitation considered in this part of this study. In order to observe the affect of dry friction damping, force transmissibility curves are obtained. Force transmissibility is calculated as follows:

$$\mu_f = \frac{f_{exc}}{f_{en}}. \tag{4.1}$$

Where μ_f is the force transmissibility, f and f_{en} are force transmitted to the chassis and force generated in the engine respectively. The excitation force generated inside the engine is defined as:

$$f_{exc} = f_0 \omega^2 \sin(\omega t). \tag{4.2}$$

where, ω is the excitation frequency and f_0 is a constant which is used to adjust the amplitude of the excitation.

An important parameter of friction damping is the normal force between the contacting bodies. As the normal force increases, the sliding force increases; hence, system behavior changes. For very large normal forces, friction element may stick all the time and system acts as if a parallel stiffness element is added. Magnitude of the input also affects the system behavior and has similar relationship like normal force. For small inputs, normal force might be high and system cannot slip; therefore, normal force should be adjusted according to expected input. Forced response results are obtained for various values of the normal force and given in Figure 4.1. In Figure 4.1, friction damper with various normal force values is added to SDOF engine mount. It is observed that, as the normal force increases, transmissibility around resonance frequency of the original system decreases; however, at higher frequency values, friction damping has mitigating effect on the performance of the mount. This situation might cause problems for an automobile engine mount, thus a solution is proposed.

The problem observed at high frequency in Figure 4.1 is due to the high normal force applied to the system. In order to decrease the transmissibility around the resonance frequency, high normal force is required; however, this increases response at higher frequencies. This is because the system slips less and sticks more thus it acts like a stiffer system. In order to overcome this problem, the stiffness of the original mount is decreased. Since adding dry friction makes the

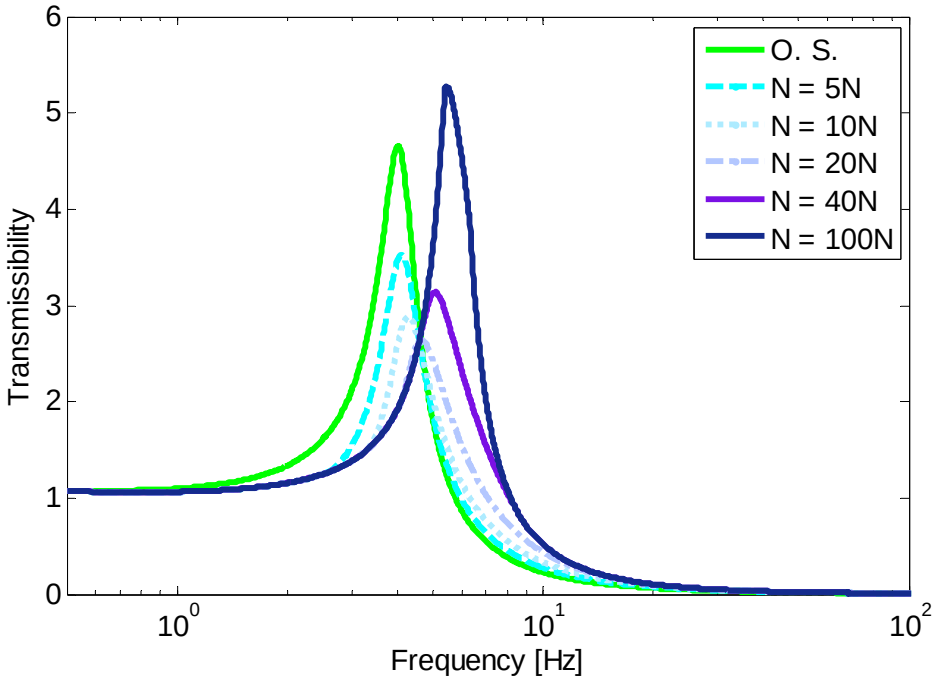

Figure 4.1. Results for SDOF system without modification

system act like a stiffer system, if the stiffness of the engine mount is decreased, overall stiffening effect can be limited. The forced response of the modified system, which has half of the stiffness of the original system, for various normal force values together with the response of the original system are given in Figure 4.2.

In Figure 4.2 the results show that modifying the system solves the problem at high frequency values. A properly selected value for normal force gives performance increase at all frequencies. 10N normal force curve drawn in red can be considered as a good example to the properly selected normal force value. Comparison of this curve and the force transmissibility of the original system are given in Figure 4.3.

The force transmissibility of the system is reduced more than 60% at the resonance frequency and significant improvement around resonance frequency of the original system is observed in Figure 4.3.

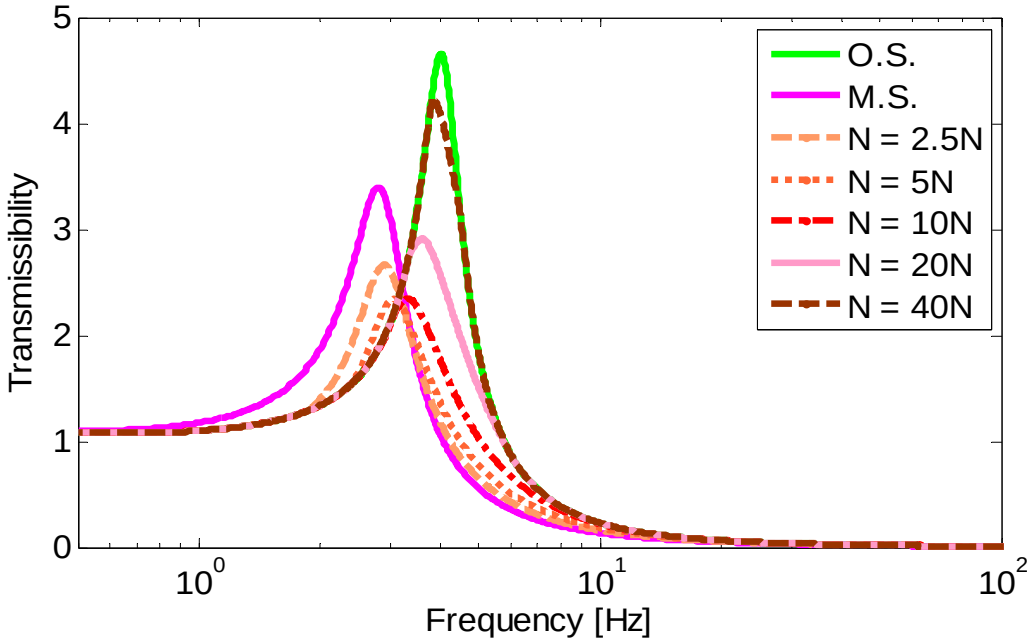

Figure 4.2. Results for SDOF system without modification

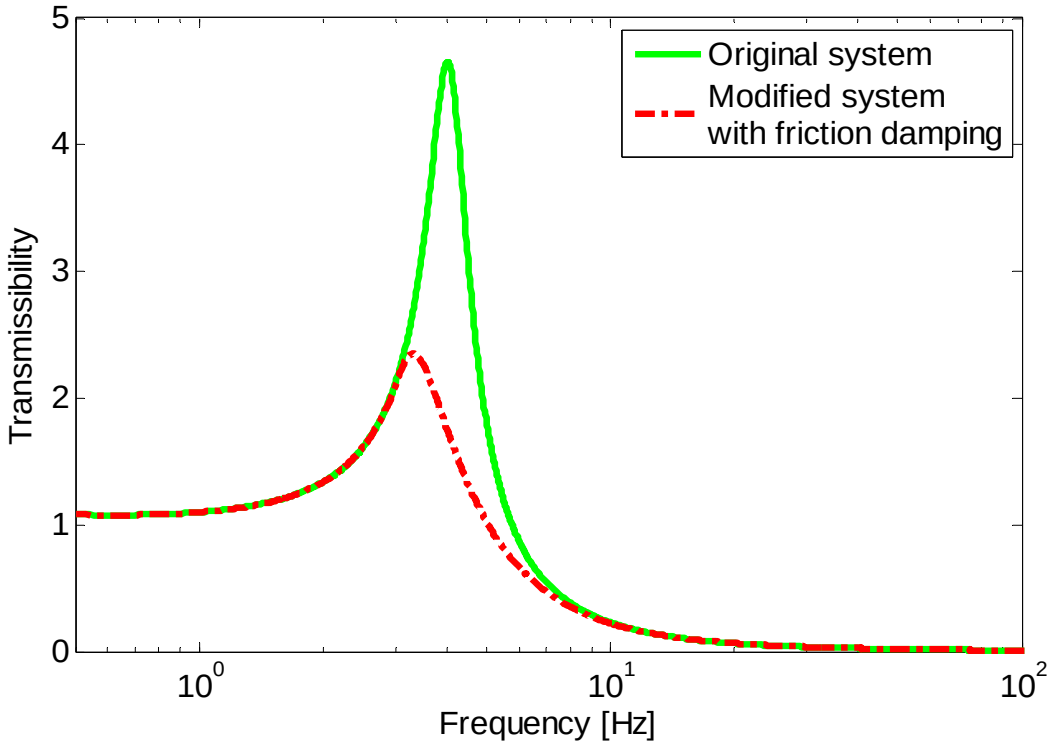

Figure 4.3. Comparison of original system and modified system with friction damping

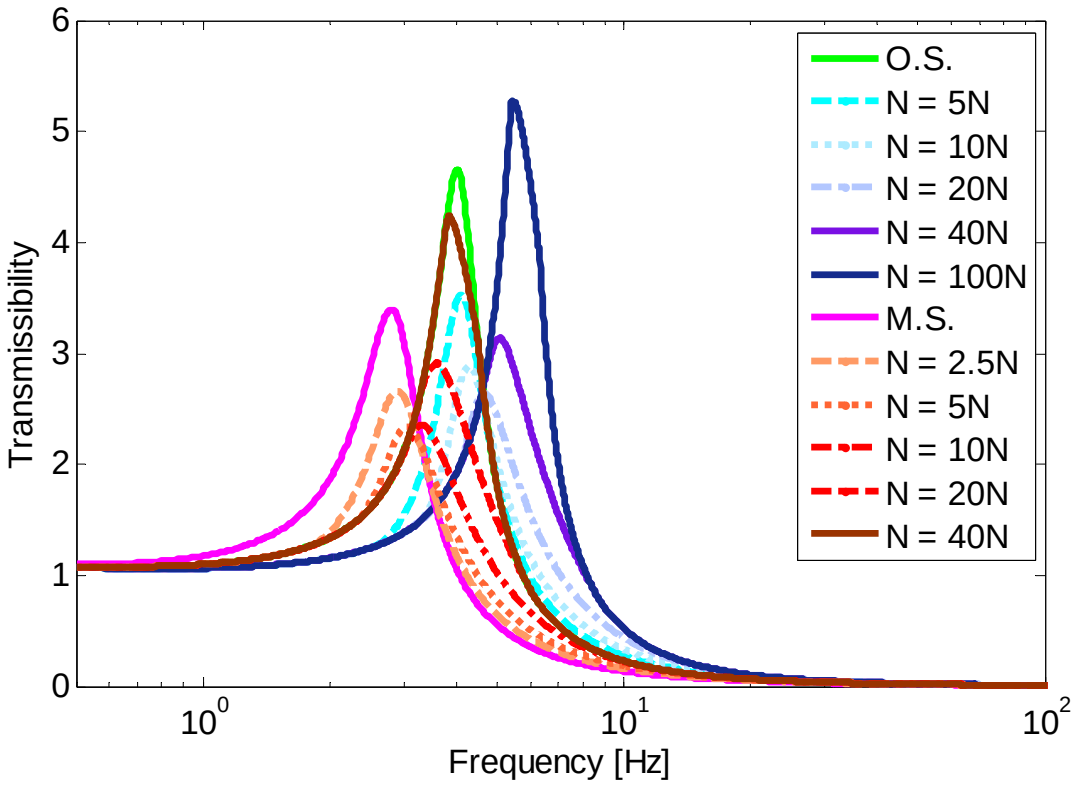

Figure 4.4. Response of SDOF engine mount with dry friction damping

Optimization of the normal force also resulted in a close value of 9N.

All of the results obtained with SDOF engine mount model are given in Figure 4.4 for comparison.

Another analysis with SDOF model was conducted to compare the stiffness models mentioned in chapter 2. Parameters for three models were determined using curve fit tool of MATLAB, and then responses of the system with these parameters are obtained for the same excitation amplitude. In Figure 4.5, results obtained with three models are compared.

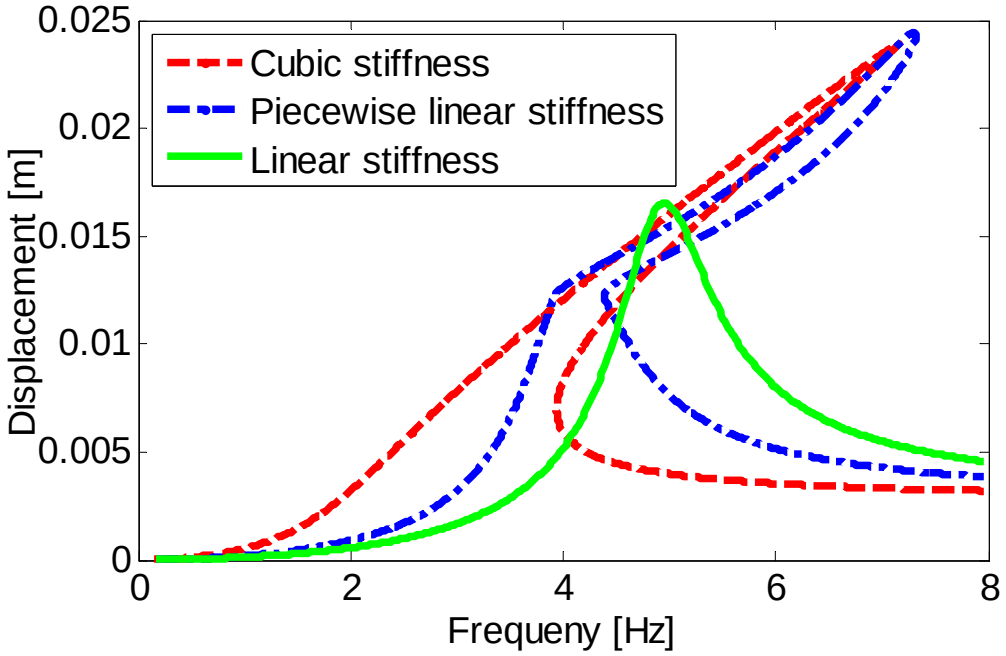

Figure 4.5. Displacement of engine for different stiffness models

4.3. RESULTS OF ENGINE ON QUARTER CAR MODEL

Engine on quarter car model is used to add the effect of suspension system to the SDOF engine with engine mount model. Since suspension is added to the system, input can as well be taken as road irregularities. Therefore protection of engine from road irregularities can be investigated with this model.

In this case, transmissibility is defined as the ratio of the displacement of the sprung mass to the displacement of the engine. This definition of transmissibility focuses on performance of engine mount rather than vehicle suspension system while suspension system is still isolating the vehicle from road input.

$$\mu_d = \frac{x_{en}}{x_1}. \tag{4.3}$$

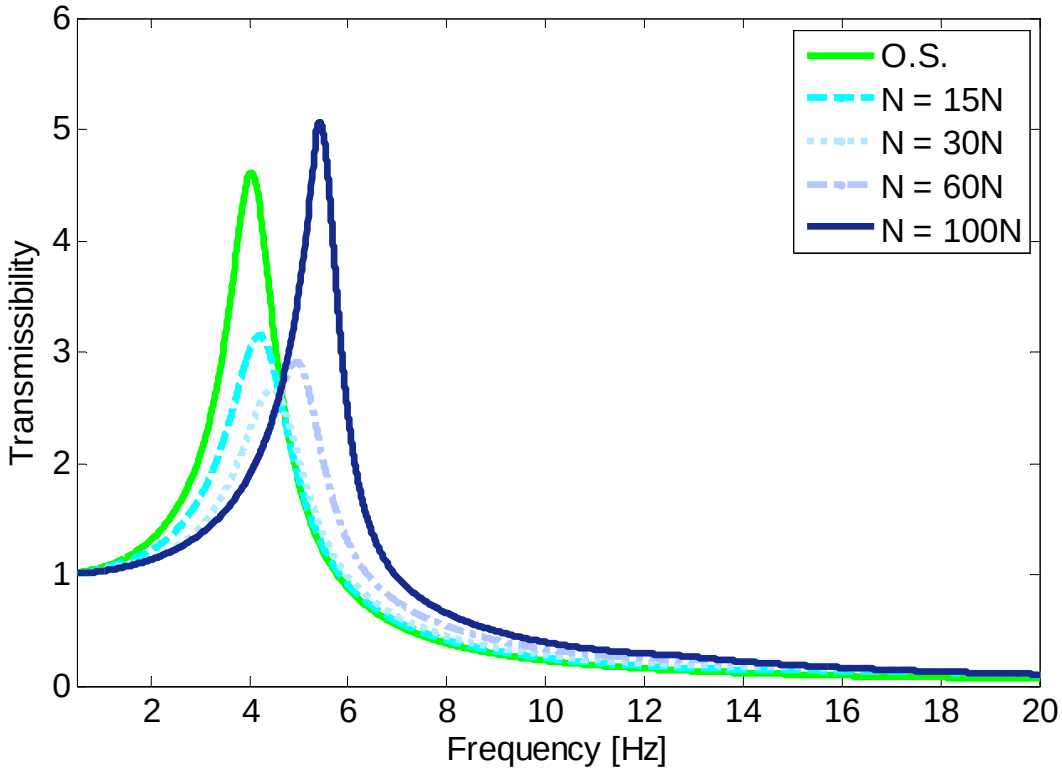

Figure 4.6. Results of engine on quarter car model without modification

Where μ_d is the displacement transmissibility, x_{en} and x_1 are the displacements of the engine and the chassis, respectively.

Transmissibility curves for the 3-DOF model are given in Figure 4.6 for various normal force values.

The results are similar to the results of the SDOF engine mount model. Increasing normal force reduces the transmissibility around resonance frequency of the original system but increases transmissibility at higher frequencies. In order to overcome this problem, engine mount is modified and a mount stiffness is decreased to half of the original mount. Transmissibility curves for various normal force values together with the modified system without dry friction damping are given in Figure 4.7.

Modifying the system and selecting a proper value for normal force improves performance of the mount over a wide frequency range. The system with 30N normal force and the original system are given in Figure 4.8.

All of the results obtained using the 3-DOF model are given in Figure 4.9 for comparison.

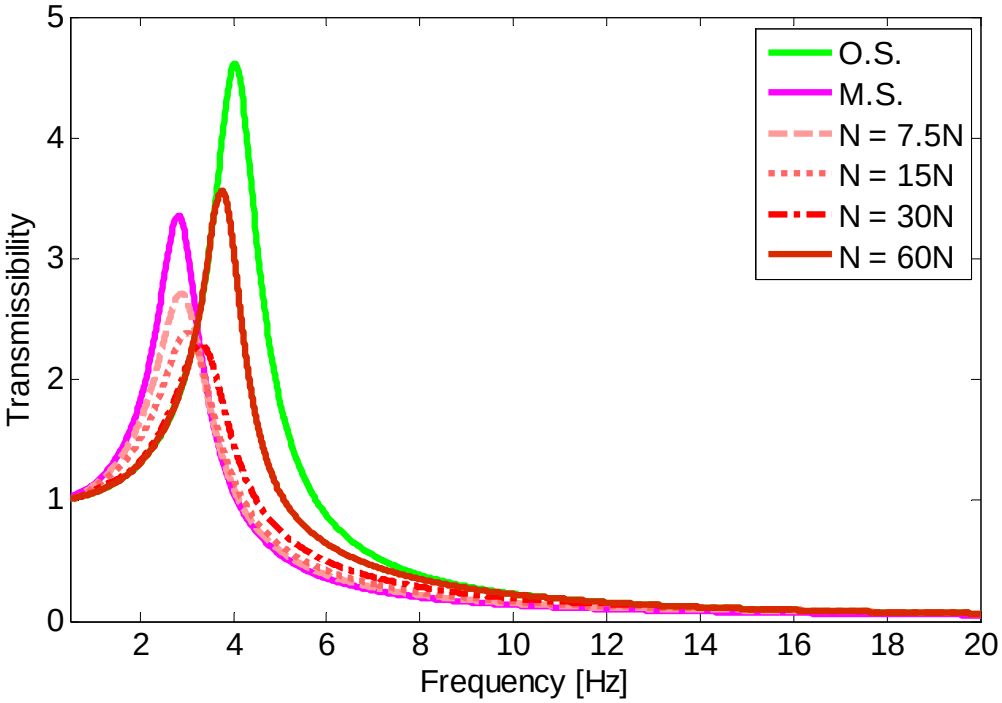

Figure 4.7. Results of vehicle and engine model with modified system

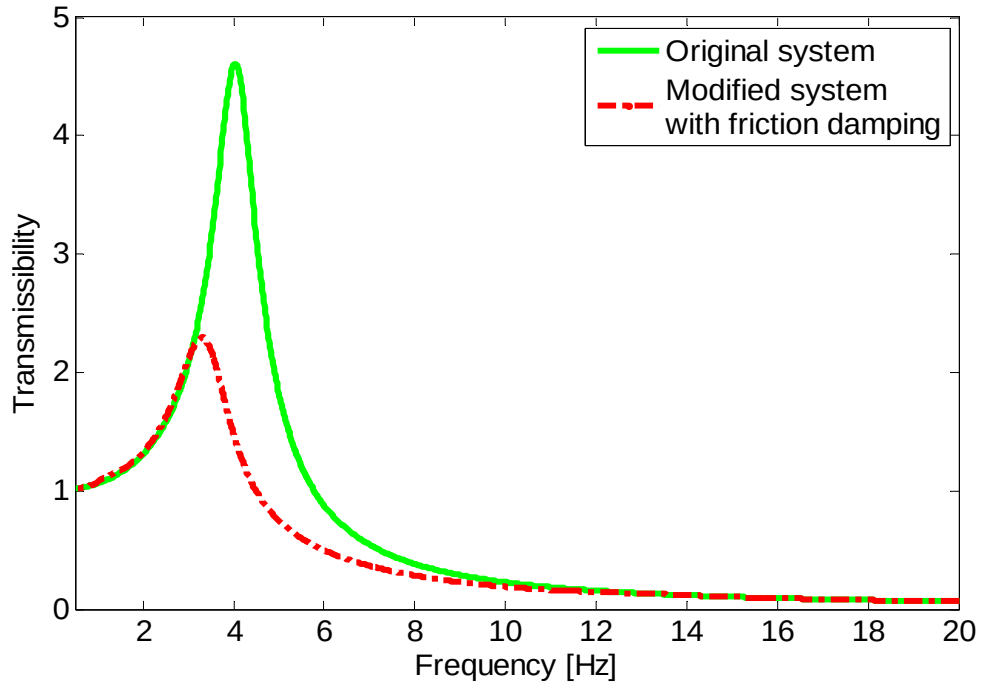

Figure 4.8. Comparison of original system and modified system with friction damping

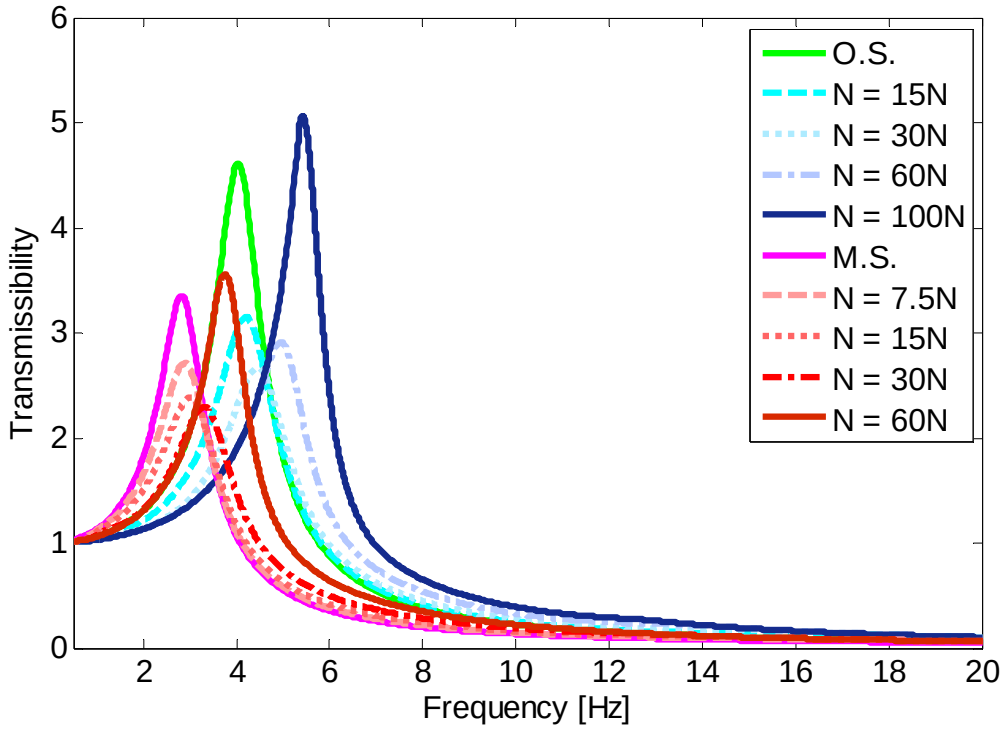

Figure 4.9. Response of 3-DOF model with dry friction damping

4.4. VERIFICATION OF THE NONLINEAR SOLUTION METHOD

Results of frequency domain analysis are also verified with time domain solution. Time domain solution can be obtained by solving the differential equation. In this thesis, "ode45" solver of MATLAB is used to obtain time domain solution Transmissibility of the original system computed with both methods for 50N normal force is plotted in Figure 4.10. It is observed that, the frequency domain solution method works without having any problems. Moreover, it can be seen that, for this system single harmonic solution captures then nonlinear characteristic of the system very accurately. The only small difference between the two methods occur around the resonance frequency and approximately two times the resonance frequency and this is an expected results, since the effect of nonlinearities increases as the displacement increase.

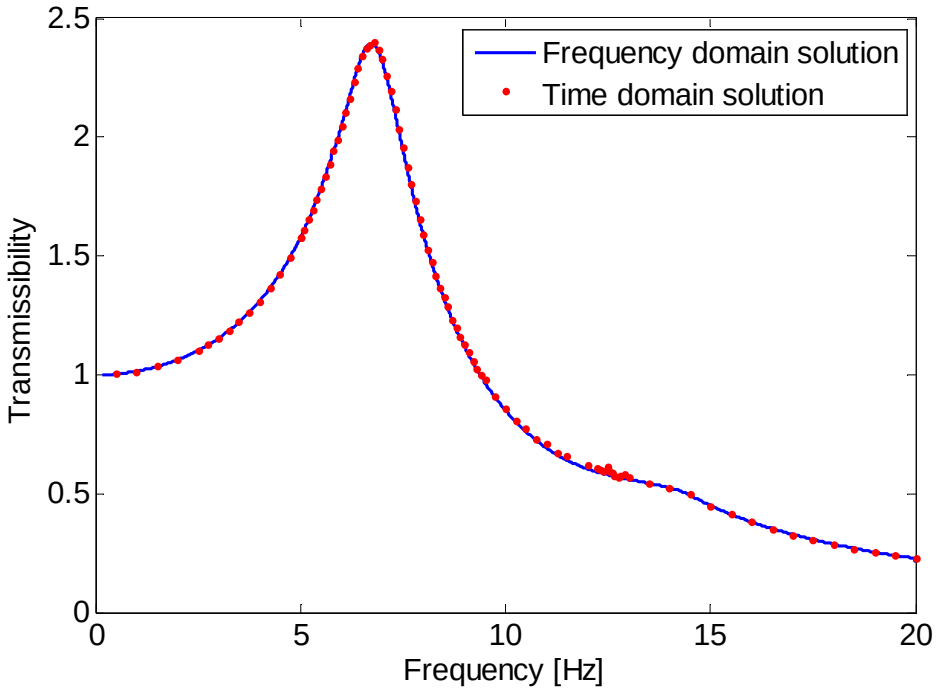

Figure 4.10. Comparison of frequency domain and time domain solution

4.5. RESULTS OF 6-DOF ENGINE MODEL

6-DOF engine model is used to observe motion of the engine inside a limited space available and determine displacements of the engine due to the excitations coming from the chassis. This is a more realistic model and it can be used for optimization purposes to determine the mounting locations as well as the engine mount properties. This model includes 3 translational and 3 rotational degrees of freedom. In following analyses, input is given from the 3 engine mounts as displacements. Considering the design which will be covered in Chapter 5 in the engine mounts used friction elements are present in only one direction. Friction elements are oriented perpendicular to each other. Stiffness values of mounts in the axial direction are taken same as the SDOF model and stiffness in the radial direction is calculated as follows:

$$k_r = \lambda k_a . \tag{4.4}$$

Where, k_r is the stiffness in the radial directions, k_a is the stiffness in the axial direction and λ is the parameter that defines the ratio of the radial stiffness to the axial stiffness. In this study, λ is taken as 1 and 1.2.

In this part of the thesis, displacements of the engine in 3 translational and 3 rotational directions are potted against frequency. The input for this part of the study is deflection of mounts and input is a sine wave with amplitude $0.0035m$. Here, ratio of the radial stiffness to the axial stiffness is 1. Locations of mounts are given in Table 4.1. Undamped natural frequencies of the system are given in Table 4.2. Forced response results for varying normal force values are given in Figure 4.11 to Figure 4.16.

Table 4.1. Locations of the mounts.

	x position [m]	y position [m]	z position [m]
First mount	-0.5	0.25	0
Second Mount	0.5	0.25	0
Third Mount	0	-0.25	-0.5

Table 4.2 Undamped Natural Frequencies of the system

	x	y	z	α	β	γ
Frequency [Hz]	6.10	5.82	7.07	12.03	11.59	14.05

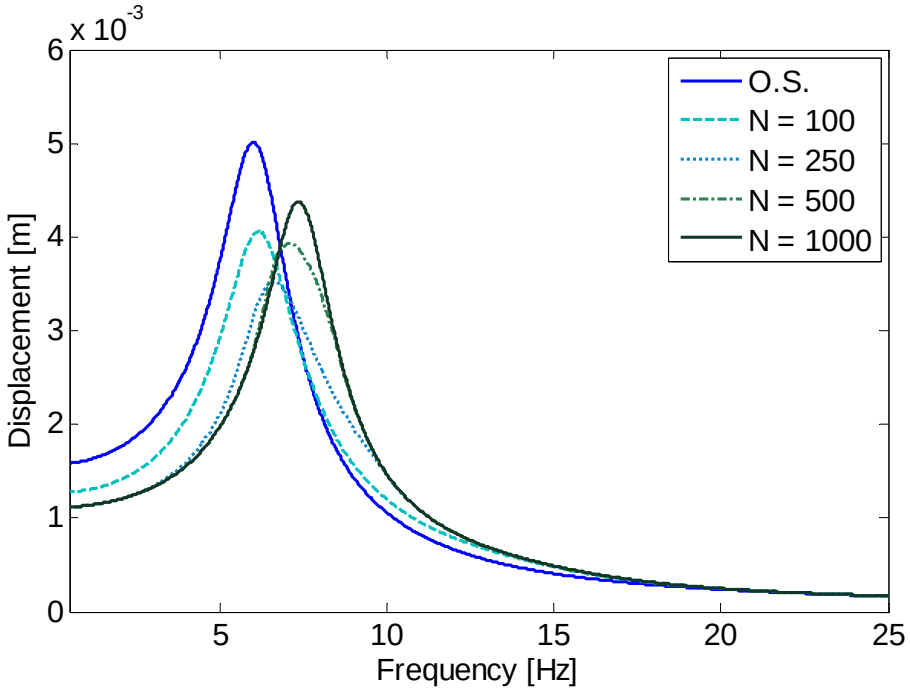

Figure 4.11. Displacement in x direction vs. frequency

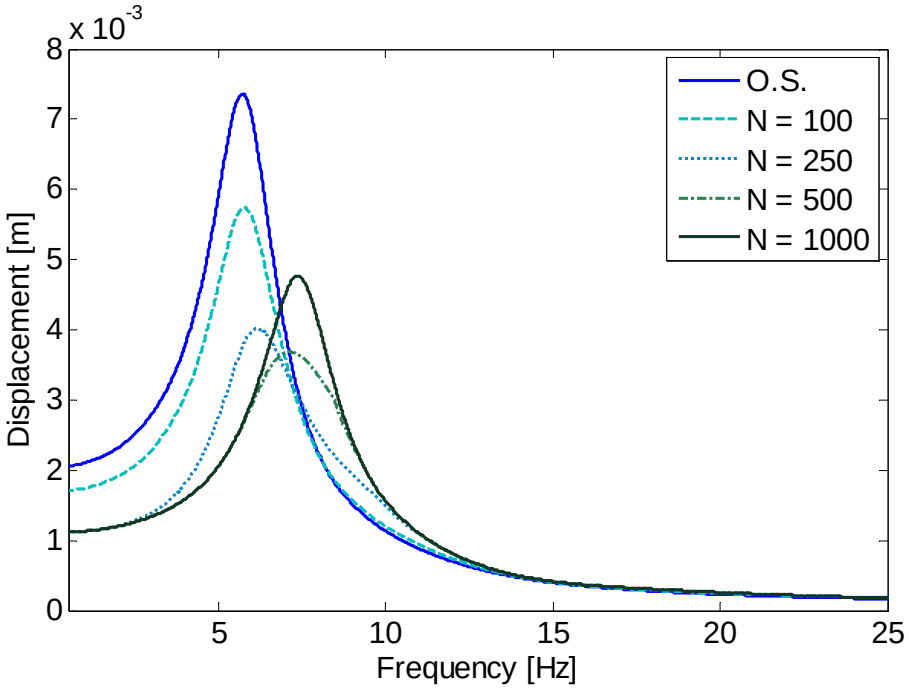

Figure 4.12. Displacement in y direction vs. frequency

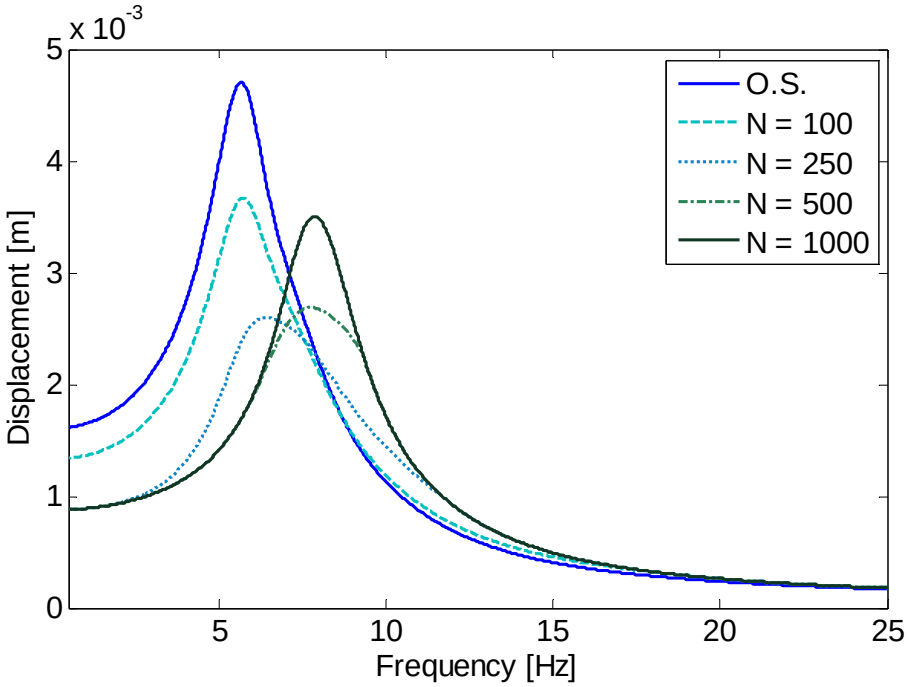

Figure 4.13. Displacement in z direction vs. frequency

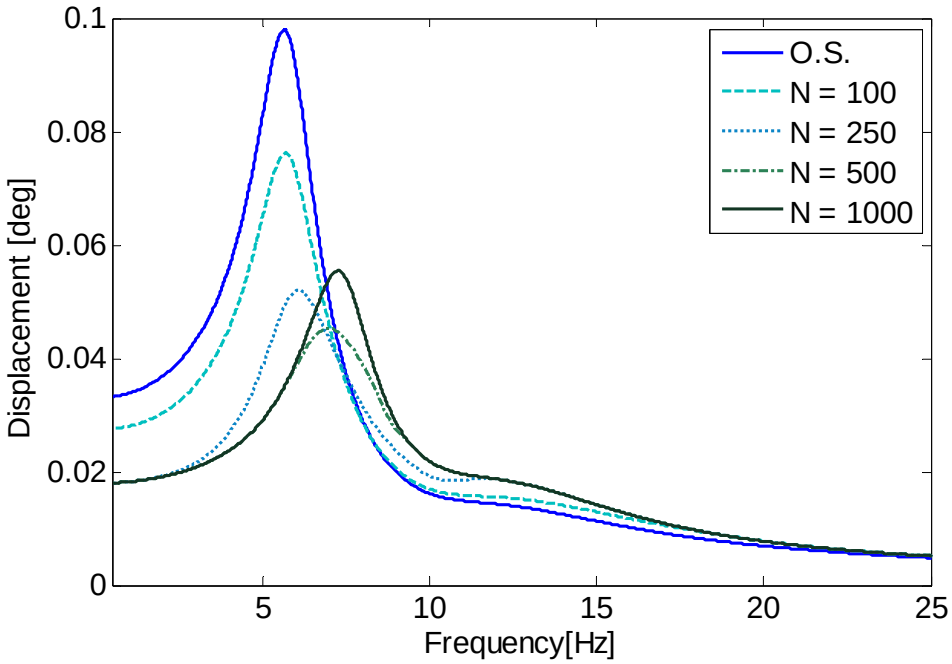

Figure 4.14. Rotation in α direction vs. frequency

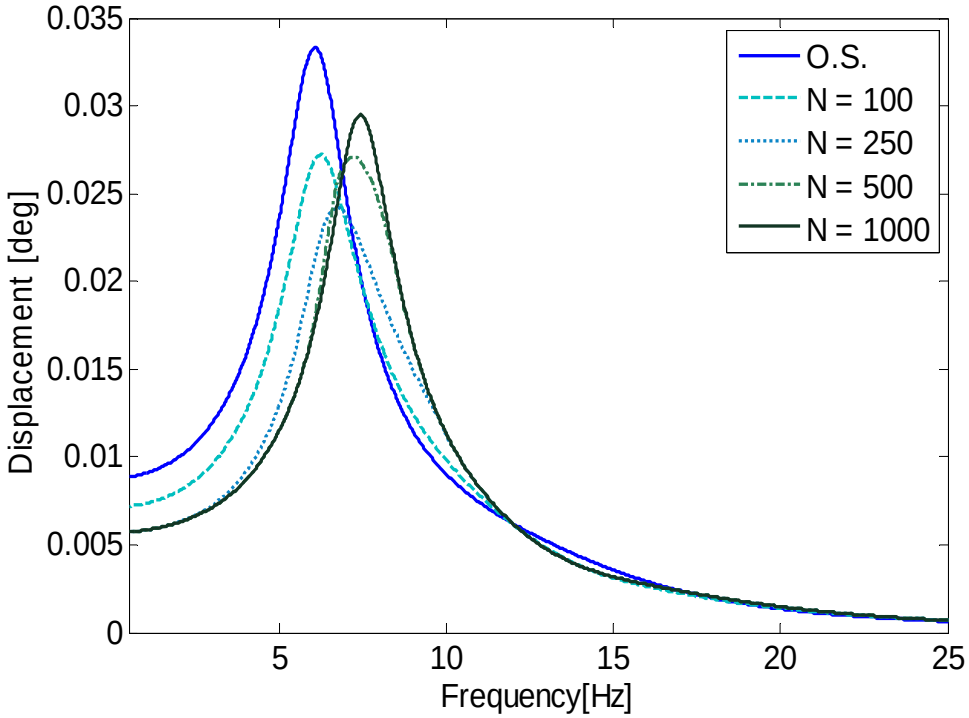

Figure 4.15. Rotation in β direction vs. frequency

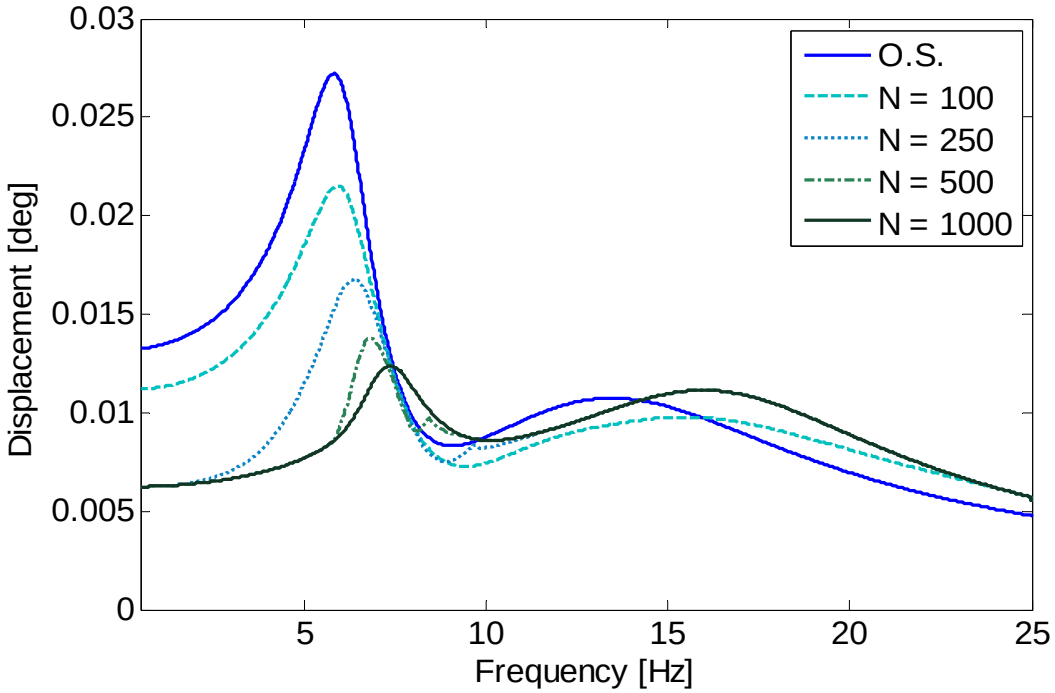

Figure 4.16. Rotation in γ direction vs. frequency

Typical behavior observed in the SDOF model is obtained in these analyses, where displacements around the resonance frequency decreased; however, displacements increased at higher frequencies increased. In order to overcome this problem, stiffness of the mount is decreased to half. Results with softer mounts are given in Figure 4.17 to Figure 4.22.

Softer mounts resulted in decreased displacements for all degrees of freedom. A normal force value of 250N gives quite good results for all cases. Effect of friction damping on the same system for $\lambda = 1.2$ is investigated in Figure 4.23 -Figure 4.28.

Same problems arise as seen in this analysis; therefore, stiffness of mounts is decreased to half in order to obtain better results at high frequencies. Using softened mounts, forced response results obtained are given in Figure 4.29 to Figure 4.34.

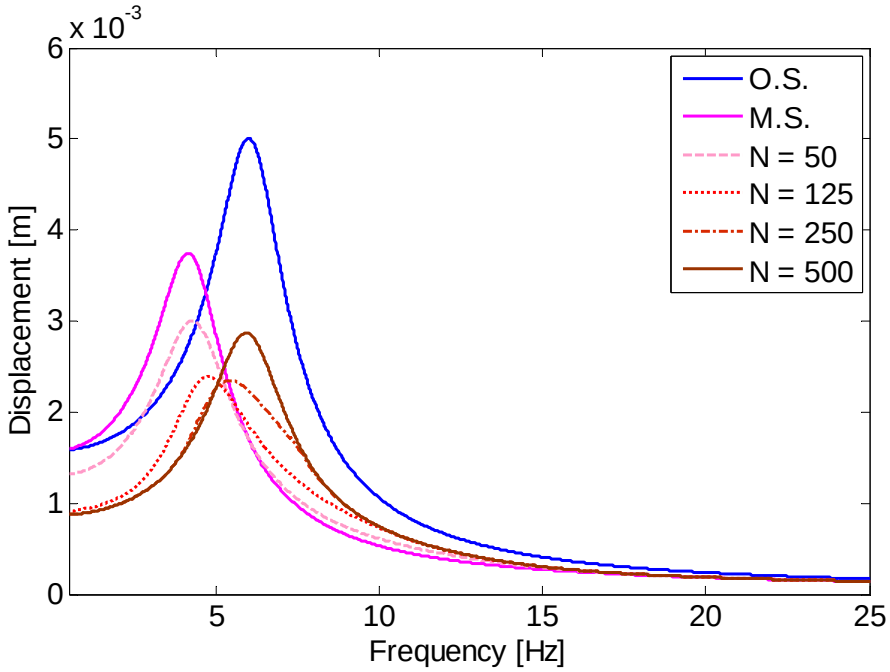

Figure 4.17. Displacement in x direction vs. frequency

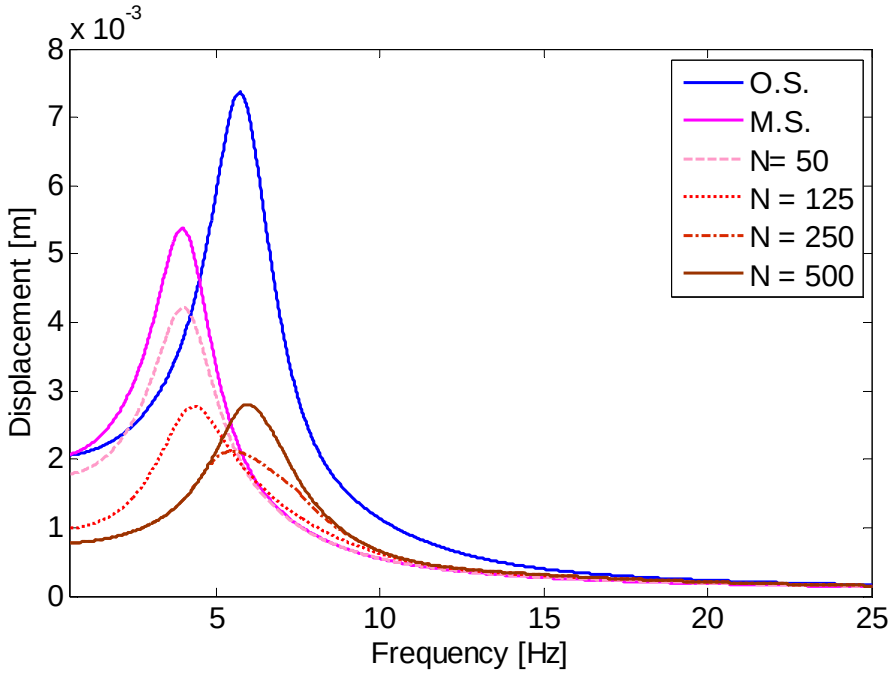

Figure 4.18. Displacement in y direction vs. frequency

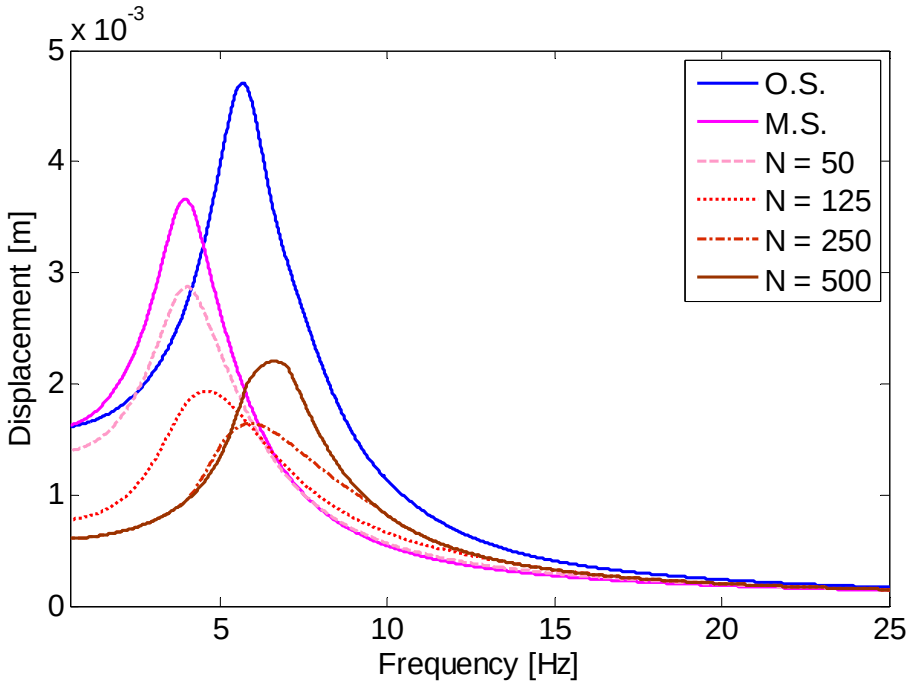

Figure 4.19. Displacement in z direction vs. frequency

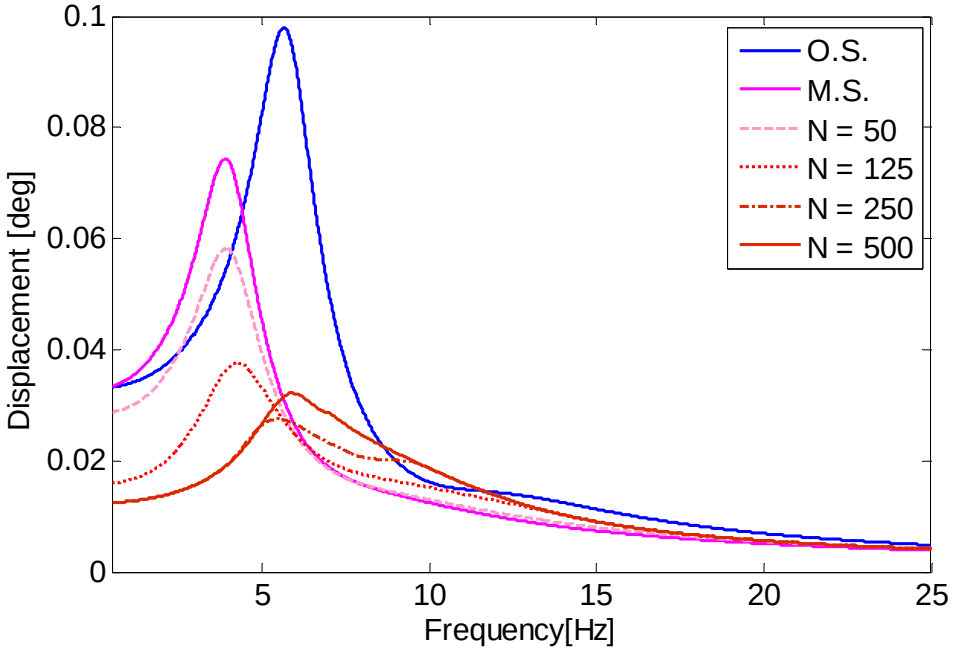

Figure 4.20. Rotation in α direction vs. frequency

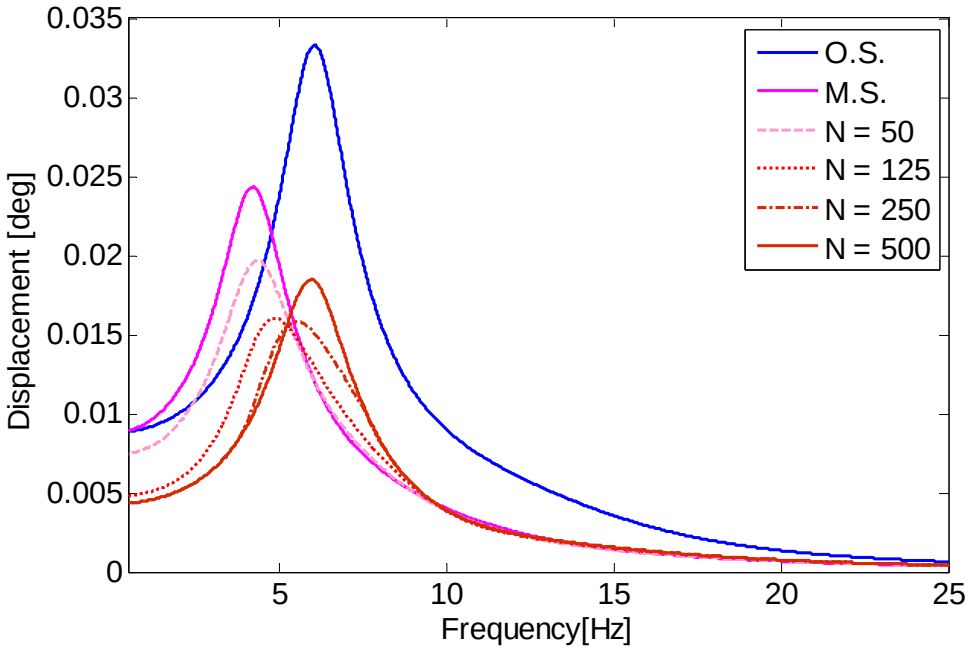

Figure 4.21. Rotation in β direction vs. frequency

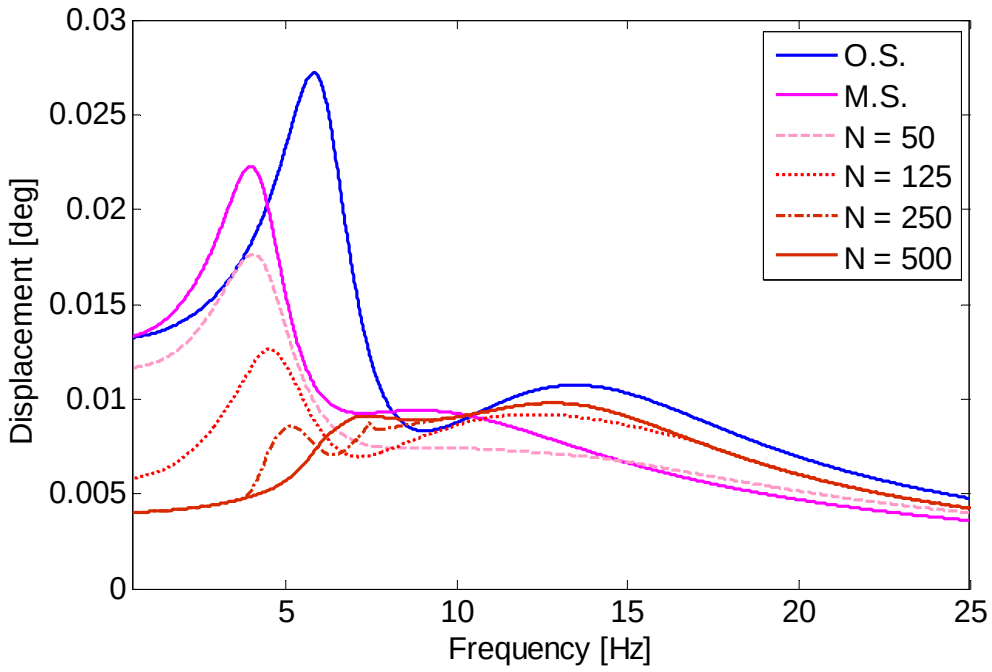

Figure 4.22. Rotation in γ direction vs. frequency

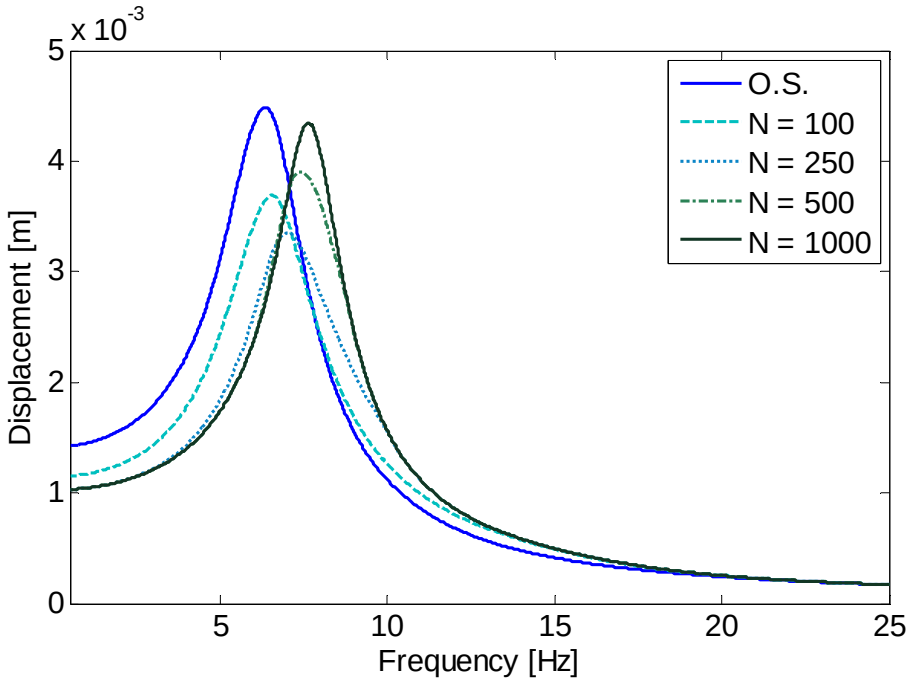

Figure 4.23. Displacement in x direction vs. frequency

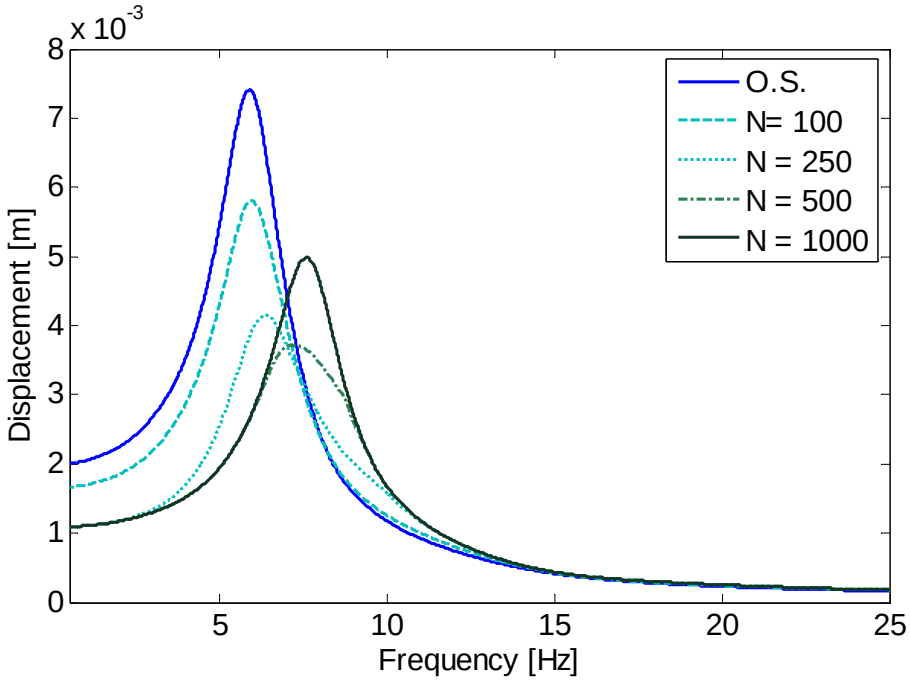

Figure 4.24. Displacement in y direction vs. frequency

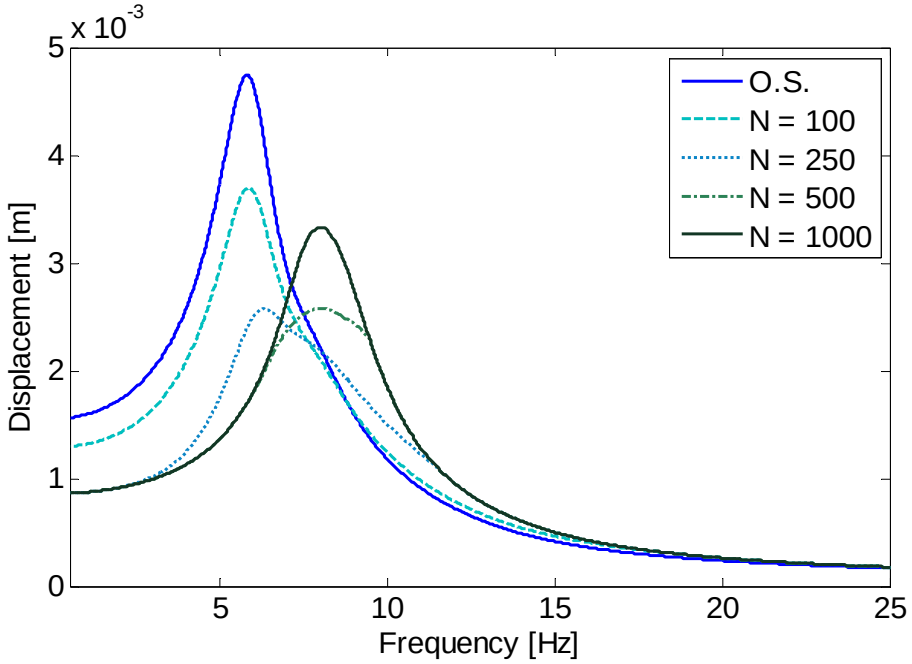

Figure 4.25. Displacement in z direction vs. frequency

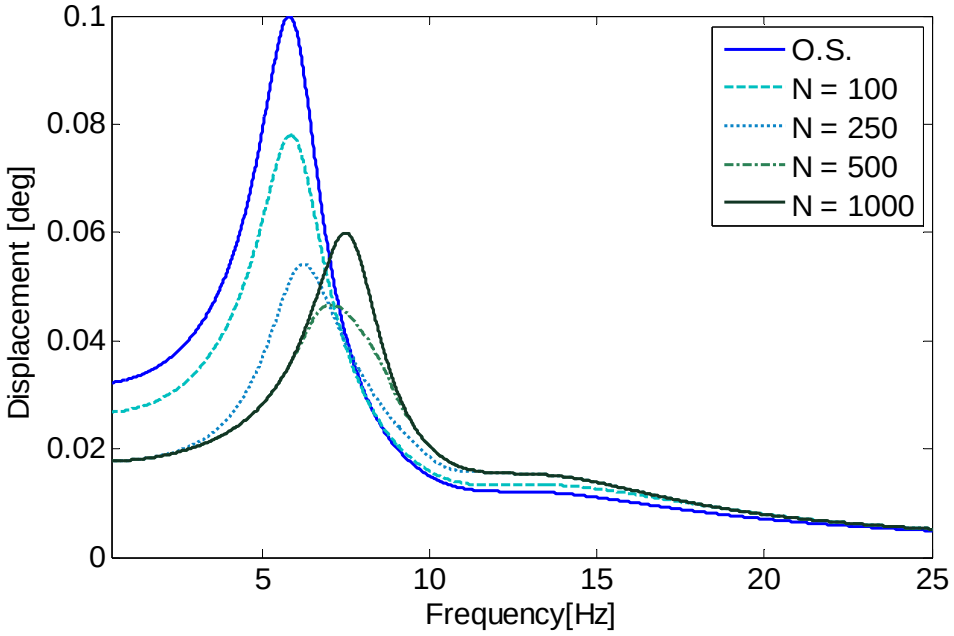

Figure 4.26. Rotation in α direction vs. frequency

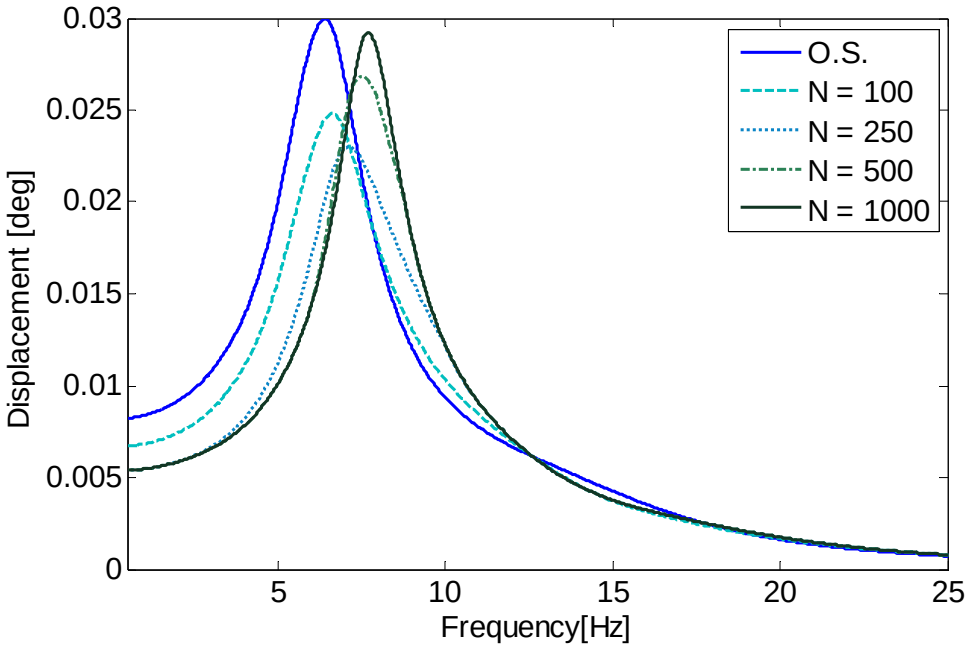

Figure 4.27. Rotation in β direction vs. frequency

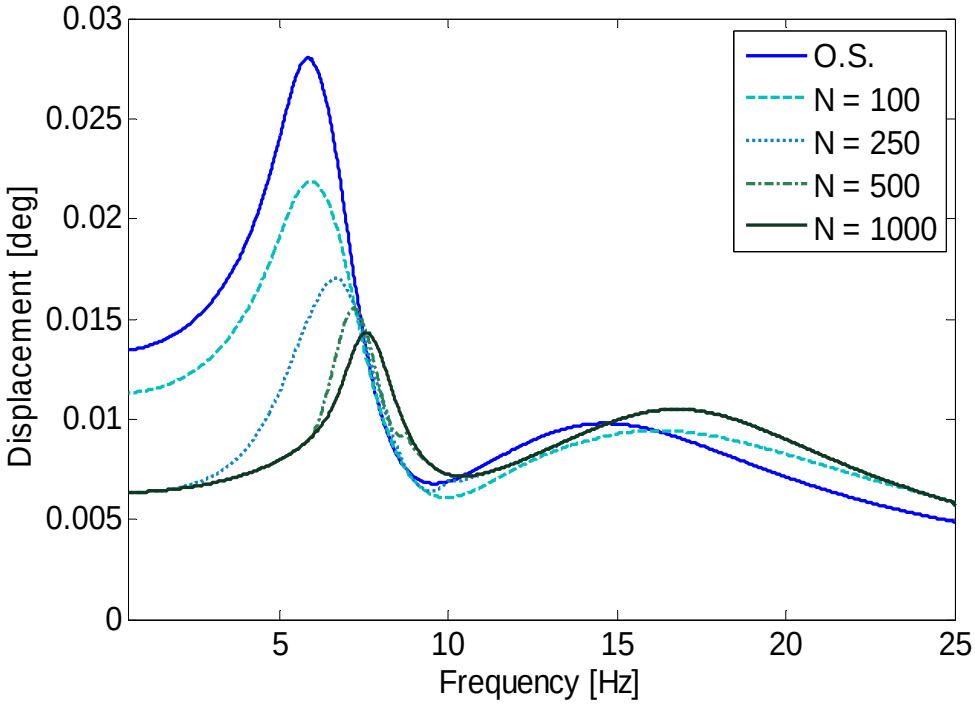

Figure 4.28. Rotation in γ direction vs. frequency

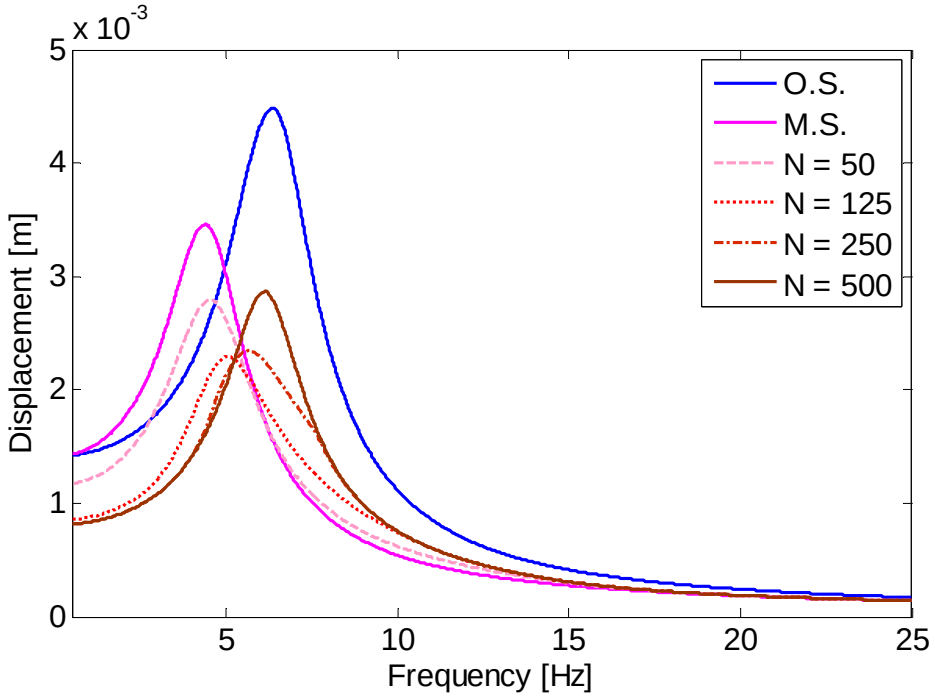

Figure 4.29. Displacement in x direction vs. frequency

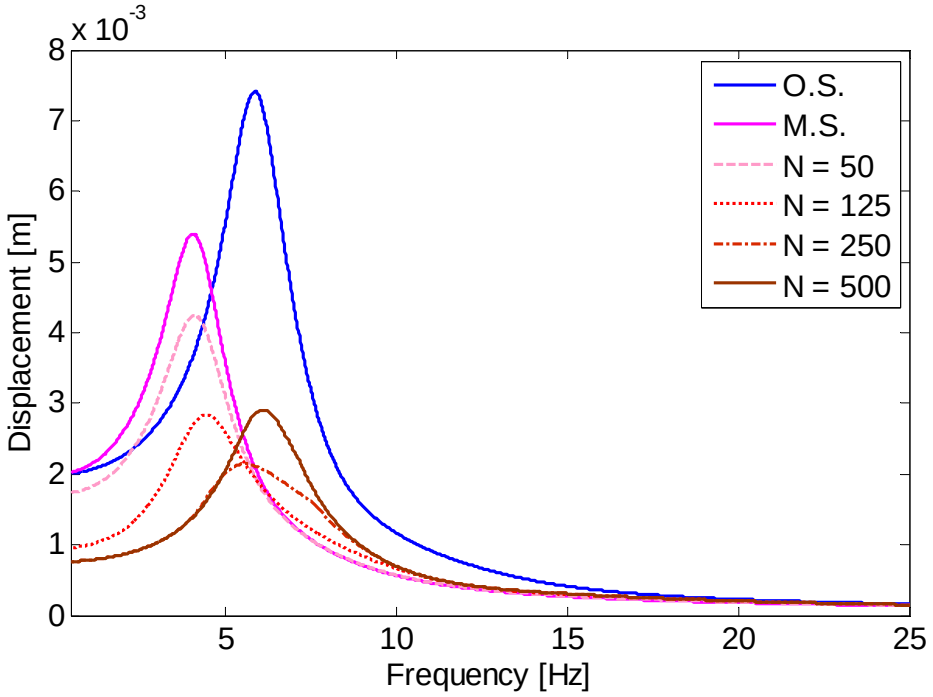

Figure 4.30. Displacement in y direction vs. frequency

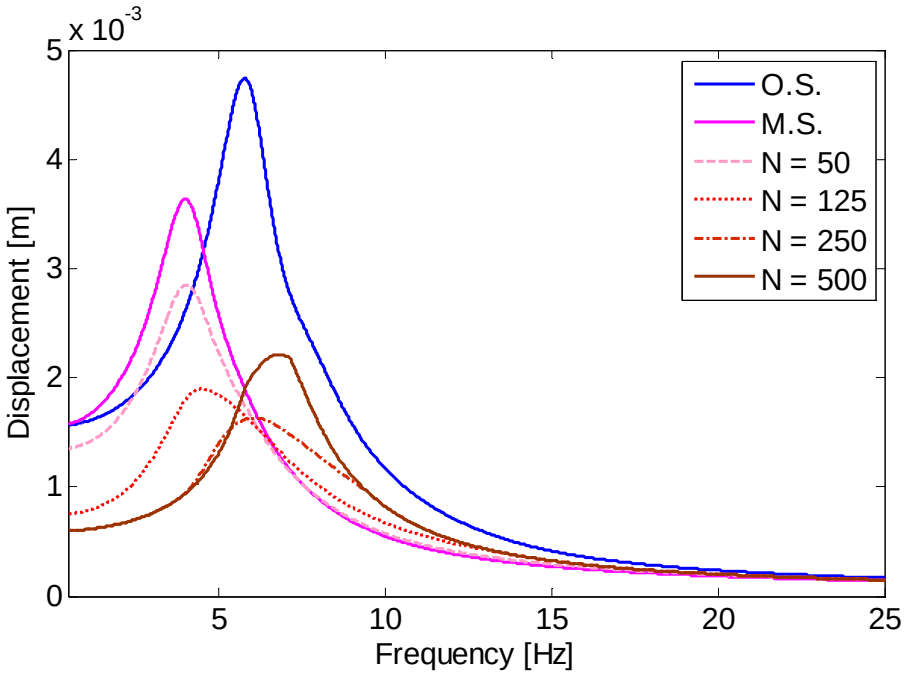

Figure 4.31. Displacement in z direction vs. frequency

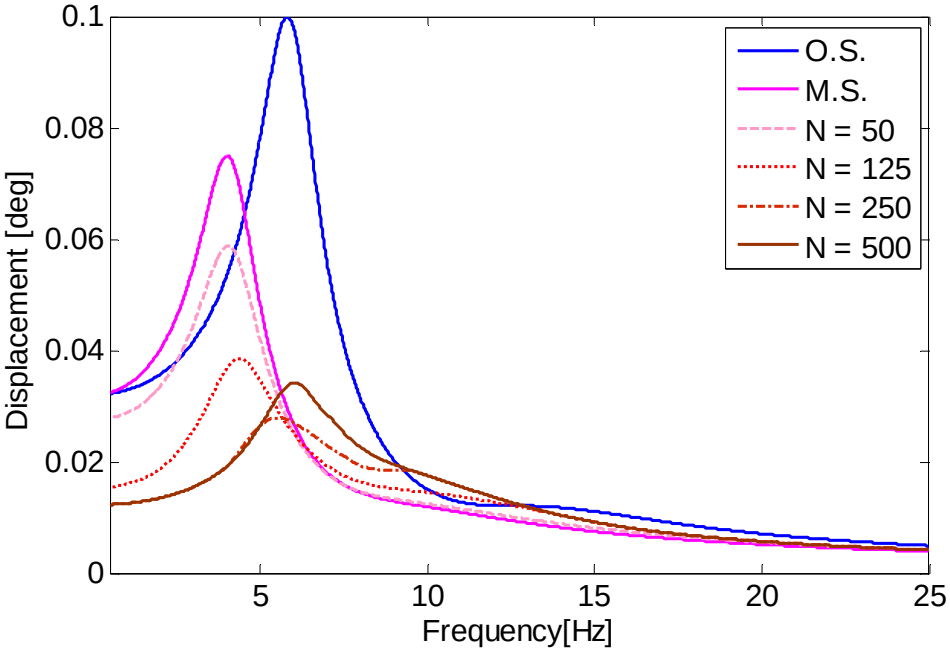

Figure 4.32. Rotation in α direction vs. frequency

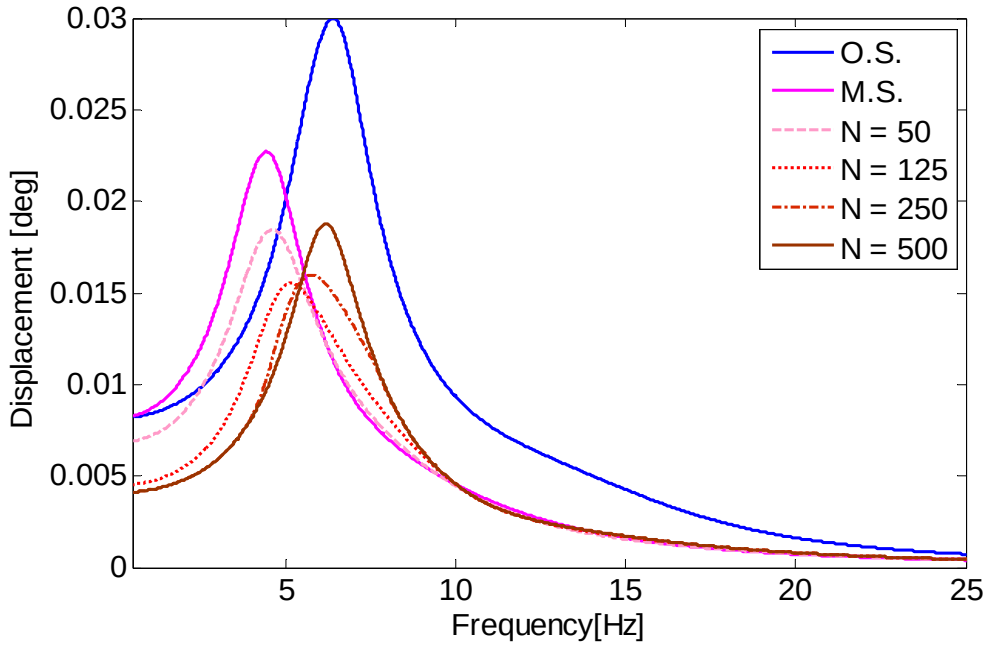

Figure 4.33. Rotation in β direction vs. frequency

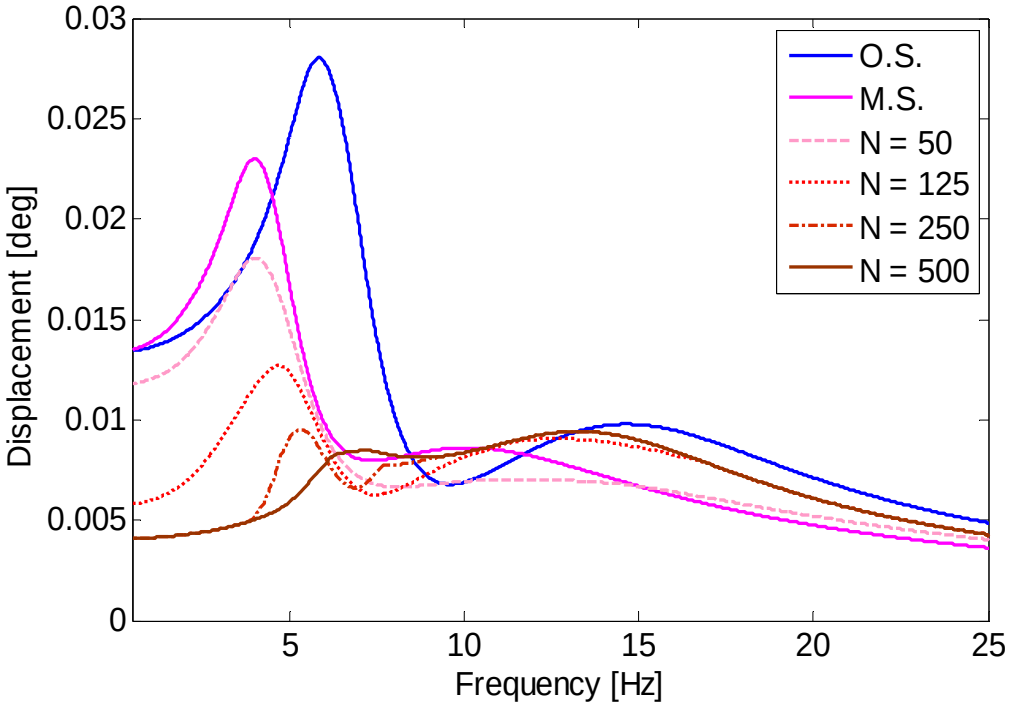

Figure 4.34. Rotation in γ direction vs. frequency

Using softened mounts, displacements in the 3 translational and 3 rotational directions decrease. However, displacements increase in a narrow frequency range for α and γ rotations. This can be prevented by applying lower normal force. These analyses showed that λ does not have an important affect on how friction damping affects the system.

Another source of vibration is the force and torque generated inside the engine due to rotating and reciprocating parts. These sources of vibrations are represented by an inertia force in z direction and a rolling moment about y axis [10]. Motion of the engine under this excitation is investigated. Forced response results in the 3 translational and 3 rotational directions are given in Figure 4.35to Figure 4.40.

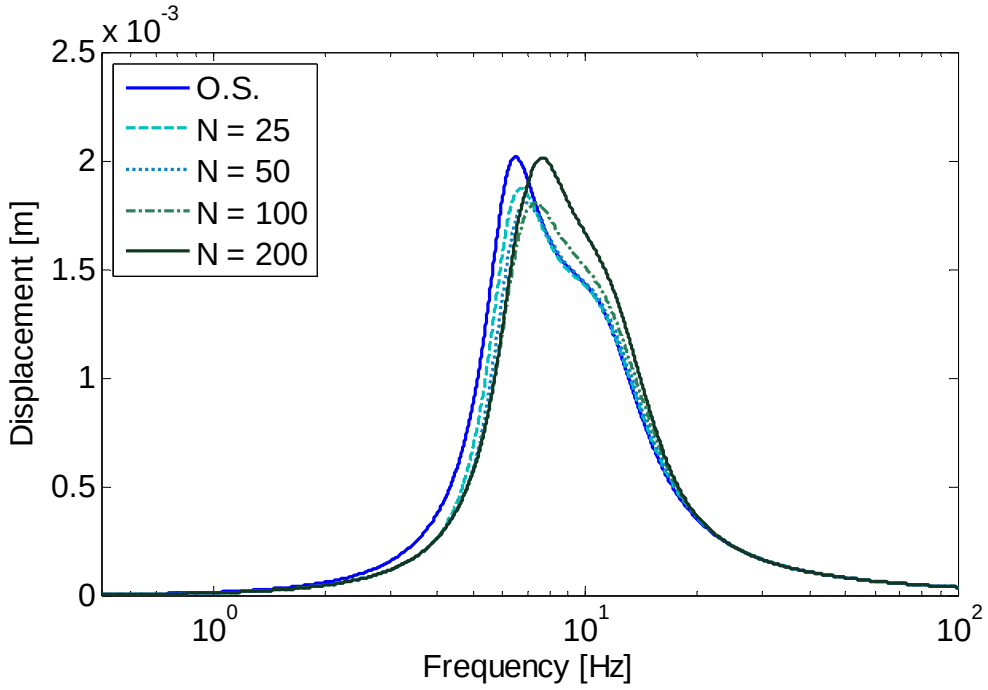

Figure 4.35. Displacement in x direction vs. frequency

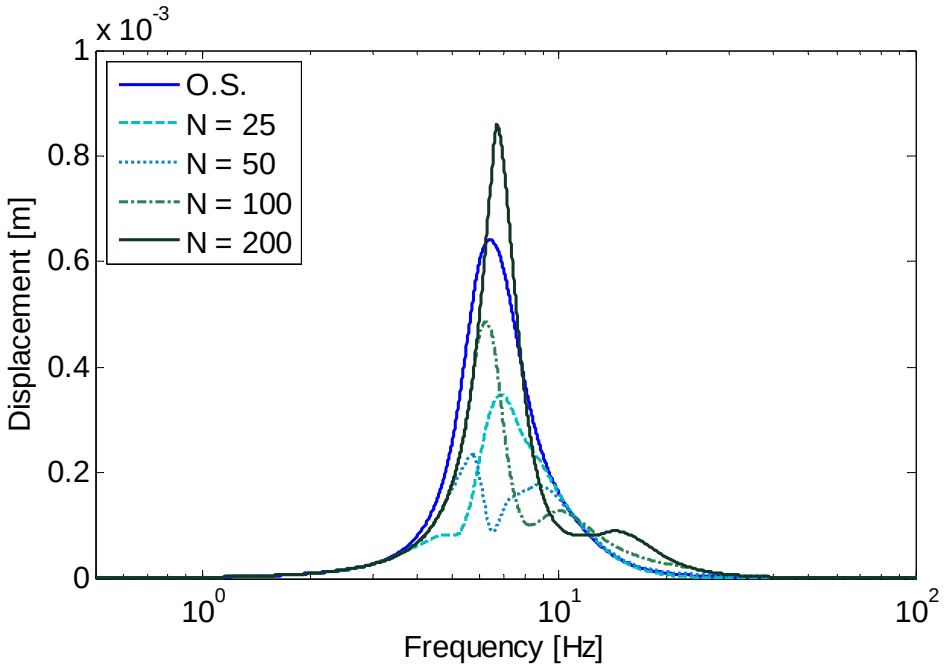

Figure 4.36. Displacement in y direction vs. frequency

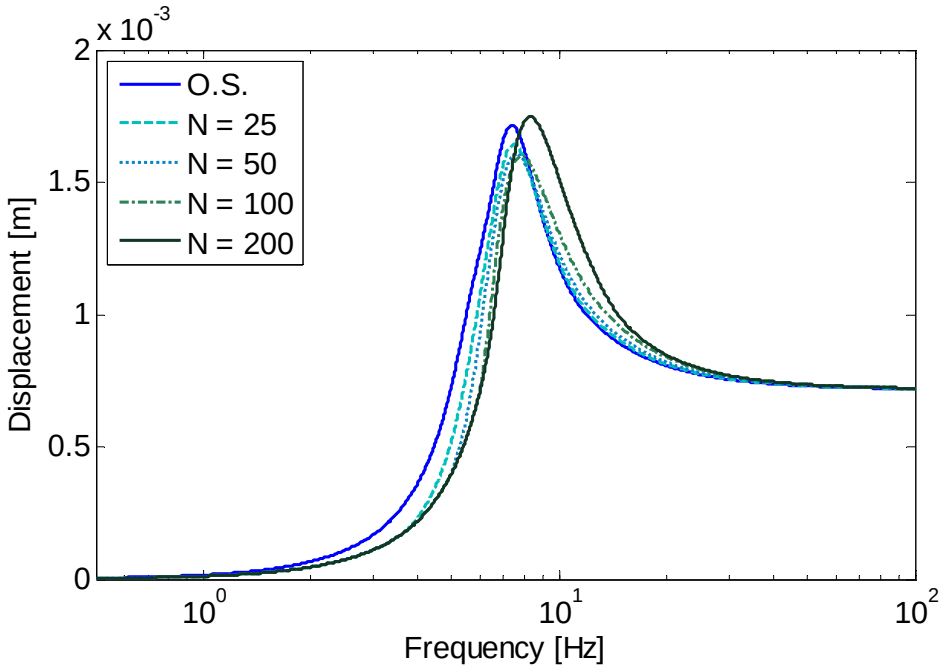

Figure 4.37. Displacement in z direction vs. frequency

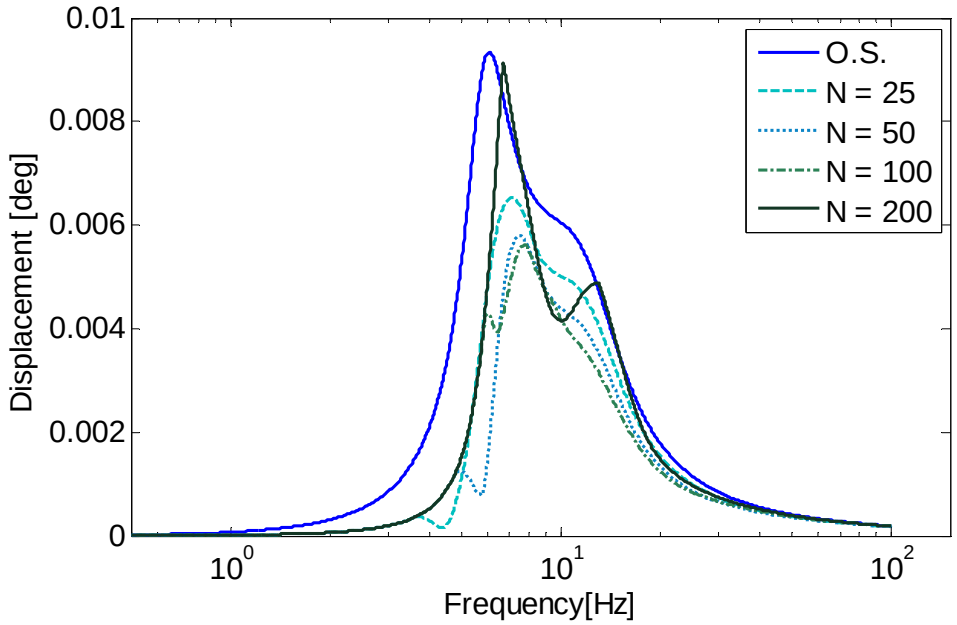

Figure 4.38. Rotation in α direction vs. frequency

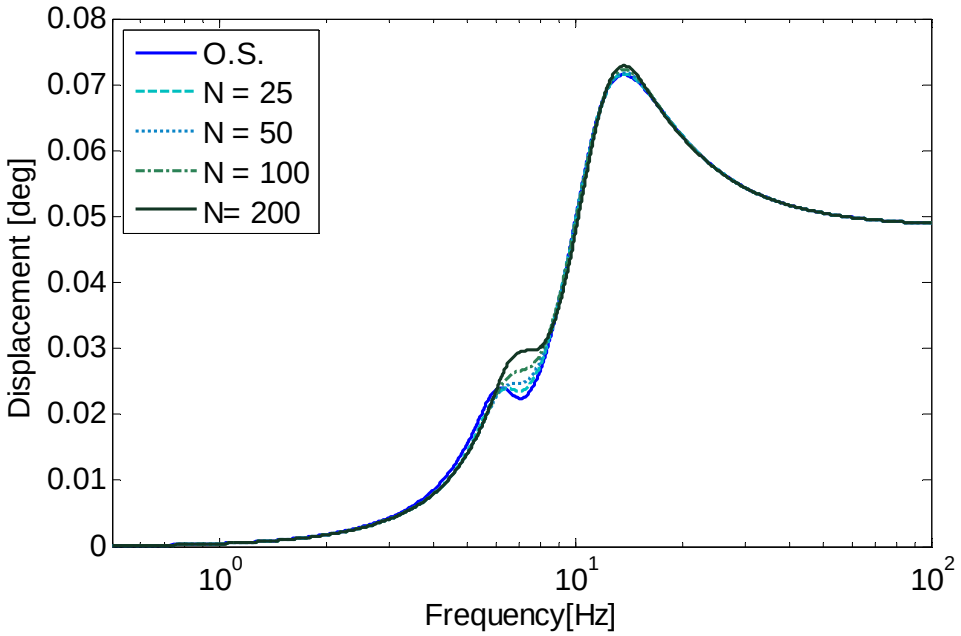

Figure 4.39. Rotation in β direction vs. frequency

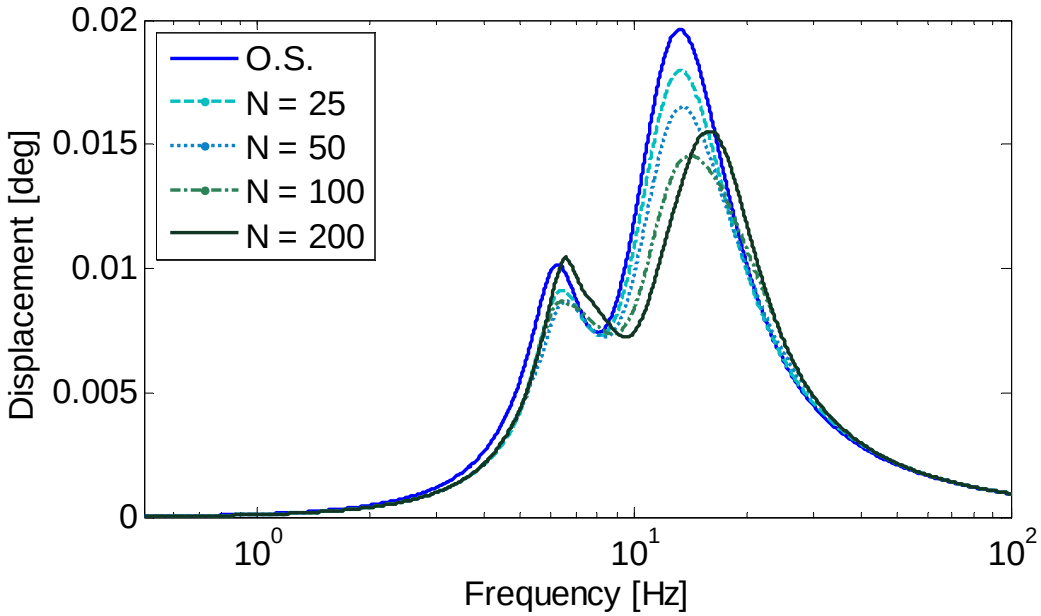

Figure 4.40. Rotation in γ direction vs. frequency

Investigating the results, it can be concluded that addition of dry friction shows similar behavior with results of SDOF model. However, rotation around y axis is not affected significantly. The reason behind this is the positions and orientations of mounts. To explain this, orientation and position of each mount should be considered separately.

Place of the first mount is shown in Figure 4.41. Friction element of this mount is placed parallel with x axis. Considering the rotation of the engine about y axis, displacement of first mount in x direction is very small for small rotations, hence effect of friction damping is limited.

Second mount is placed at position 2 shown in Figure 4.41. Friction element in the second mount is placed parallel to y axis. For the rotation of the engine about y axis, displacement of the second mount in y direction is nearly zero, so friction element in the second mount cannot dissipate energy.

Location of third mount is shown in Figure 4.41 and friction element is placed parallel with z axis. Considering the rotation of the engine about y axis, the displacement of the third mount in z direction is very small for small rotations, so friction element on this mount cannot dissipate significant amount of energy. Since all three engine mounts cannot dissipate much energy with the friction elements, rotation of the engine about y axis is not affected much by addition of friction damping at this arrangement of mounts.

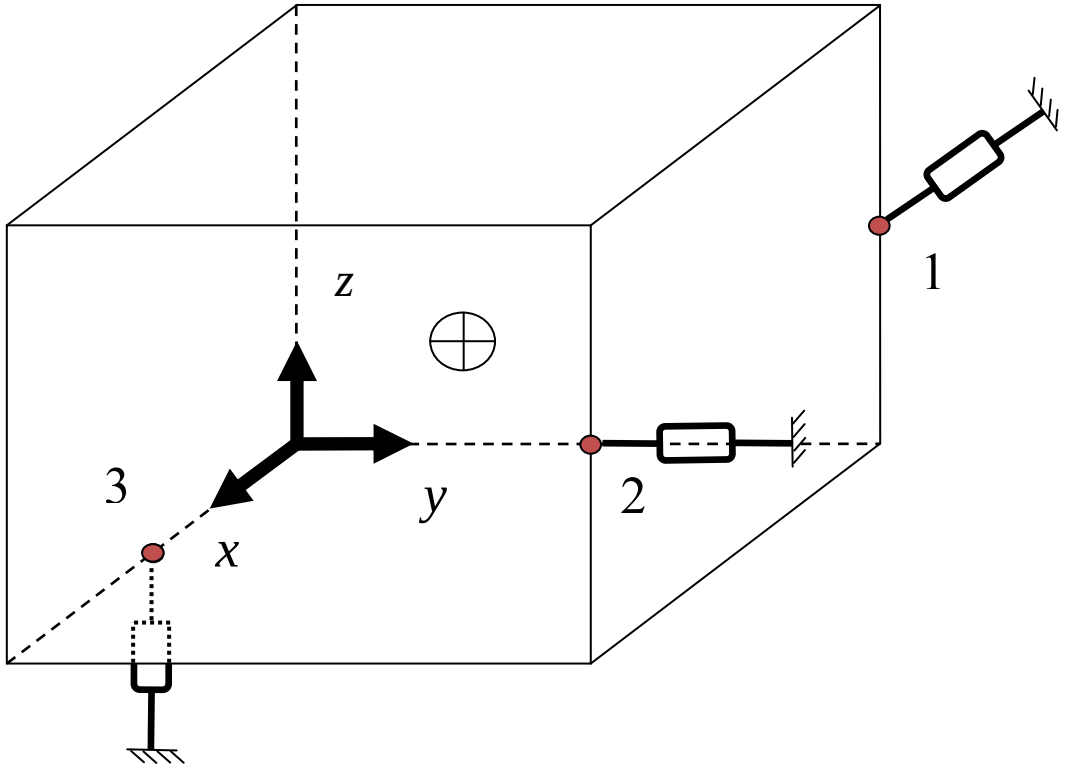

Figure 4.41. 6-DOF engine model

This situation can be eliminated by changing the position of one of the mounts. Placing third mount to the position shown in Figure 4.42 increases the displacement of the third mount in z direction in case a rotation about y axis

occurs. Therefore friction element of the third mount can dissipate more energy. This situation is also observed when Figure 4.39 is compared with Figure 4.43. In Figure 4.43, where the solution for the second engine mount configuration is given, friction damping affected the system much more than Figure 4.39. Dissipation of energy in third mount can also be observed from the state of friction element. The blue and the red dots in Figure 4.44 show if the friction element at third mount slips or sticks. Zero value means the friction element is always sticking else it changes state. The blue dots are representing the stick-slip condition for the original position of the third mount whereas; the red dots are representing the stick-slip condition for new position of the third mount. It can be observed that friction element at the third mount slips more at its new position.

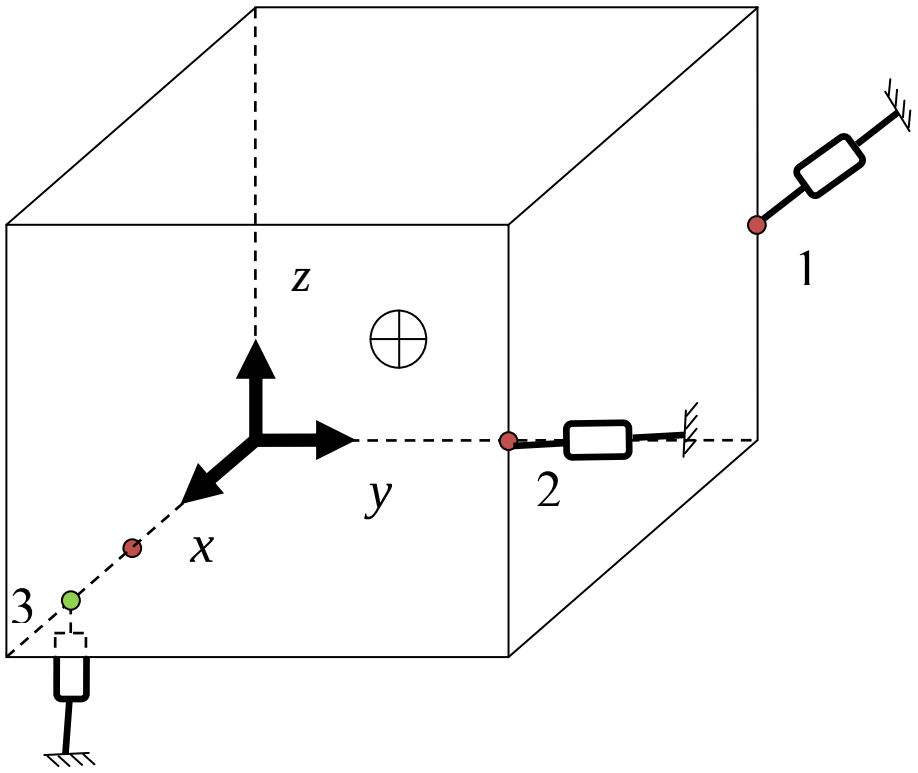

Figure 4.42. New position of the third mount.

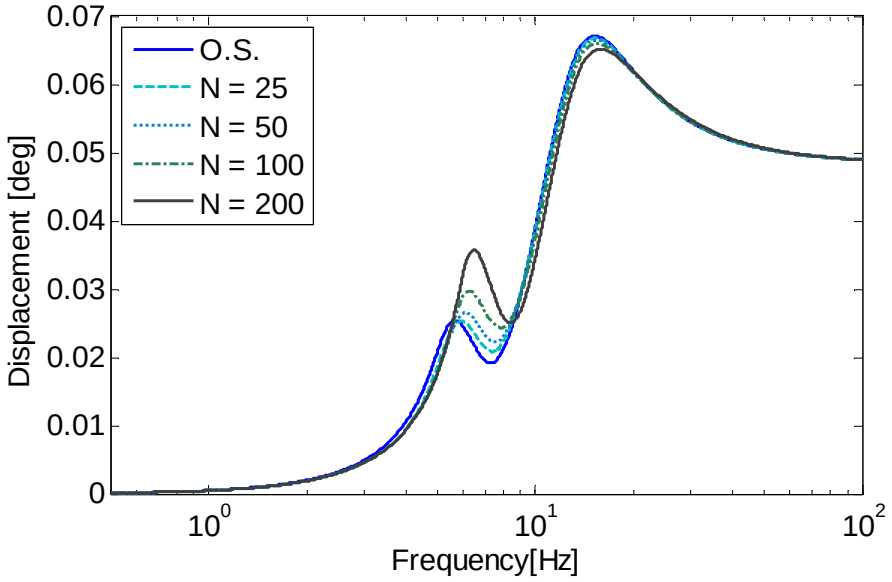

Figure 4.43. Rotation in β direction for new position of third mount

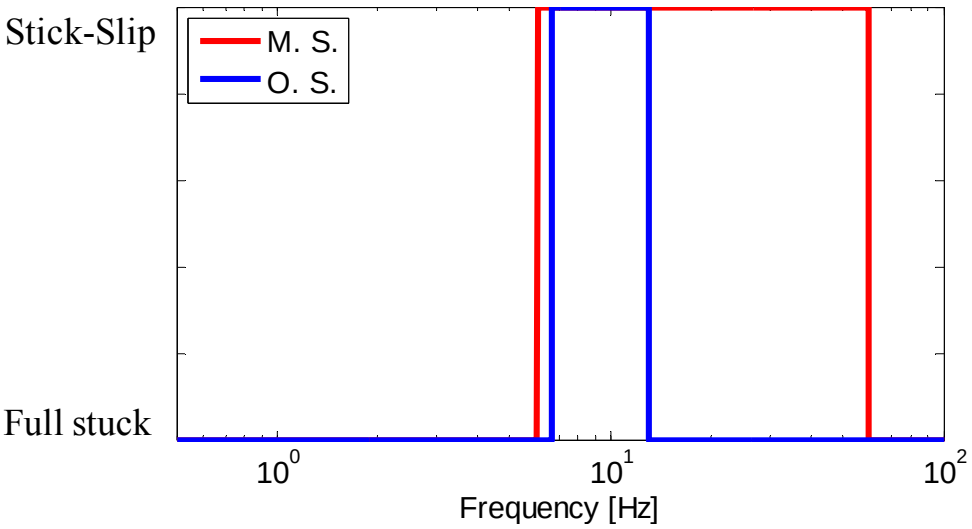

Figure 4.44. Comparison of states for original and modified system

This shows that, location, orientation, structural parameters and parameters regarding friction damping should be optimized in order to obtain the best results from engine mounting system with dry friction damping and prevent this type of undesired situations.

Investigating the results for original system with friction damping, it can be observed that displacements at x and z directions increased at high frequencies due to stiffening effect of friction. In order to solve this issue, stiffness of the mounts are reduced to 75% of the original value and results given in Figure 4.45 to Figure 4.50 are obtained.

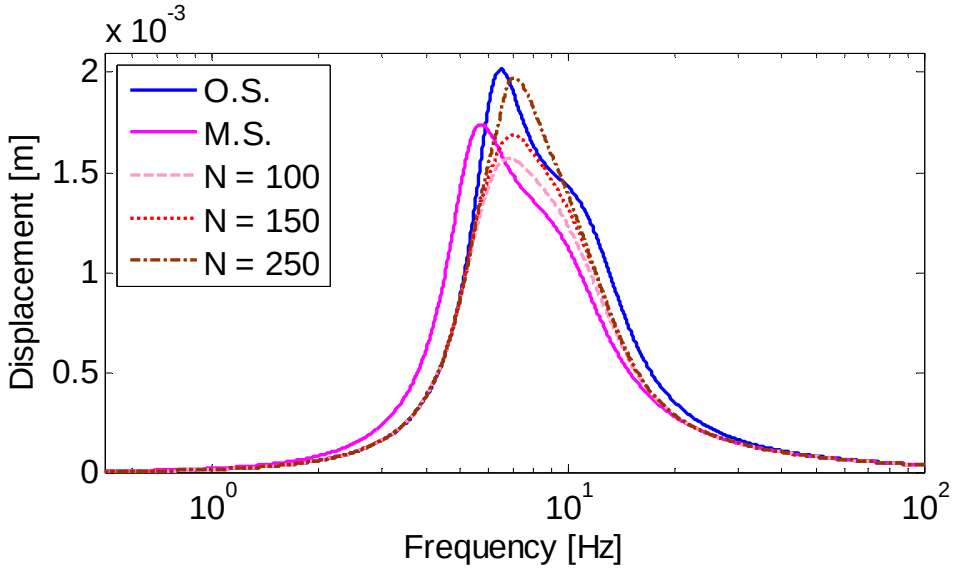

Figure 4.45. Displacement in x direction vs. frequency

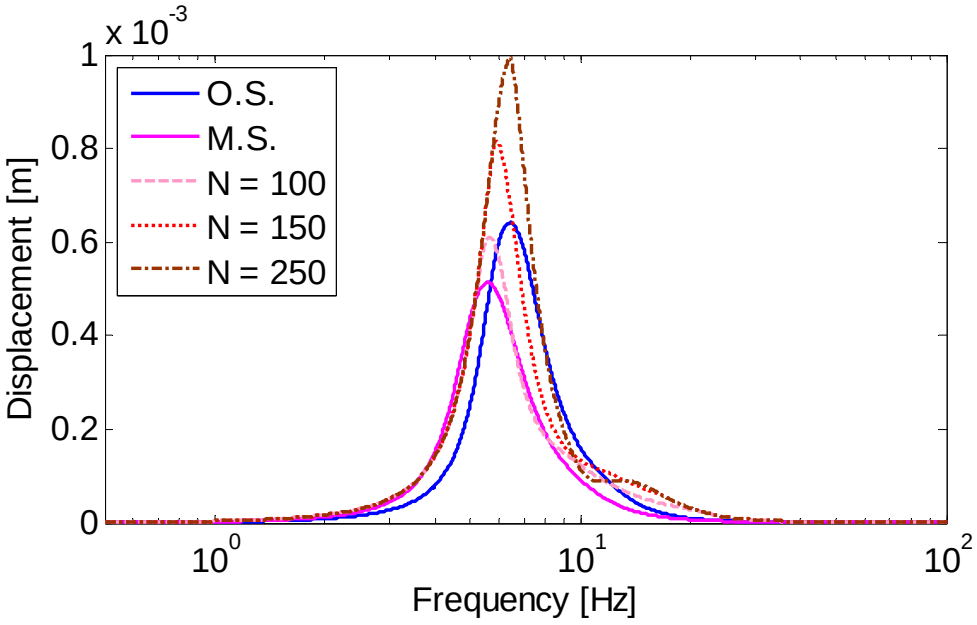

Figure 4.46. Displacement in y direction vs. frequency

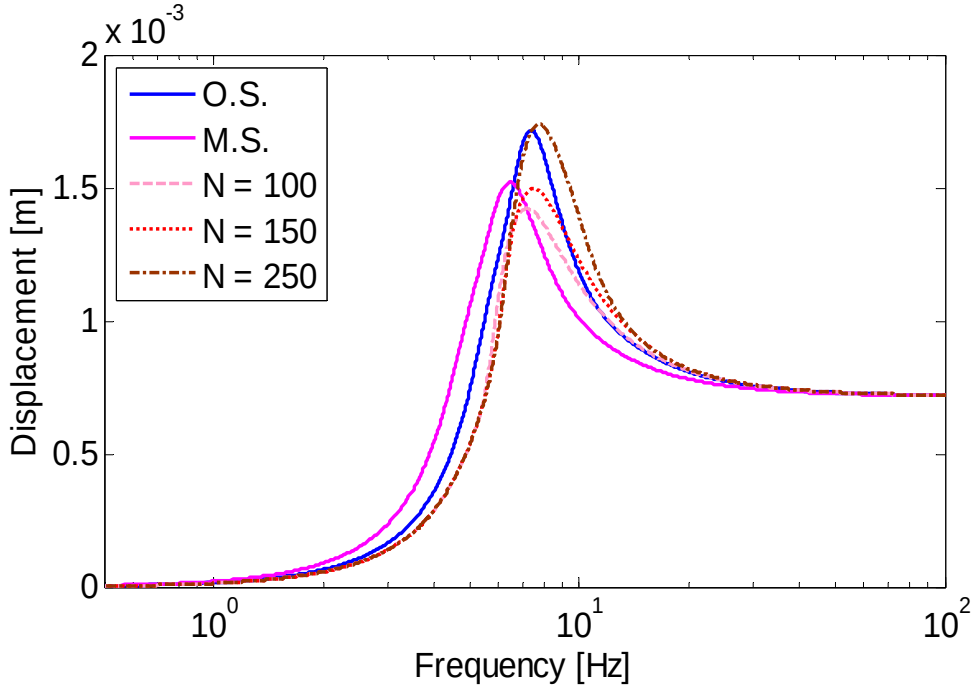

Figure 4.47. Displacement in z direction vs. frequency

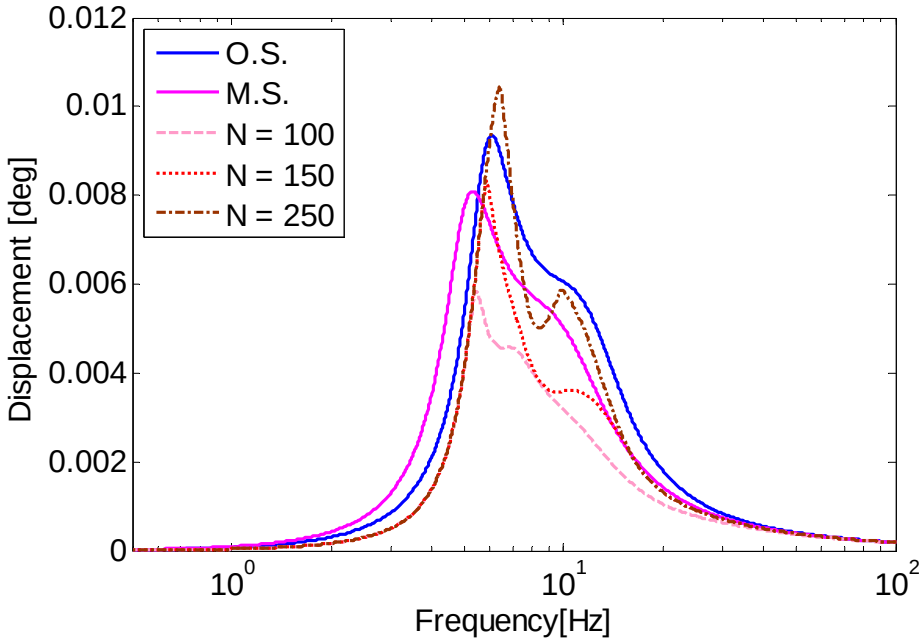

Figure 4.48. Rotation in α direction vs. frequency

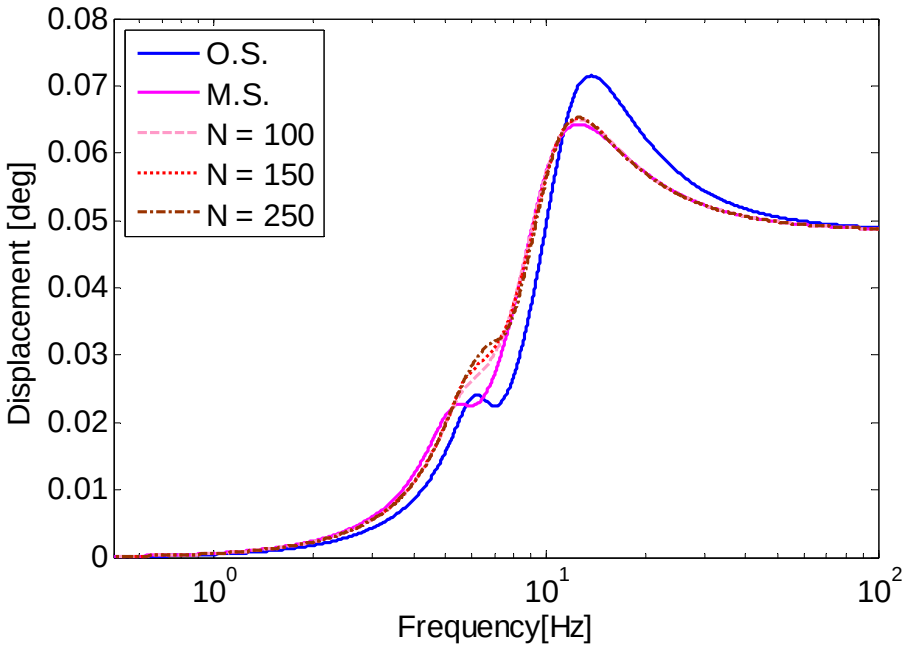

Figure 4.49. Rotation in β direction vs. frequency

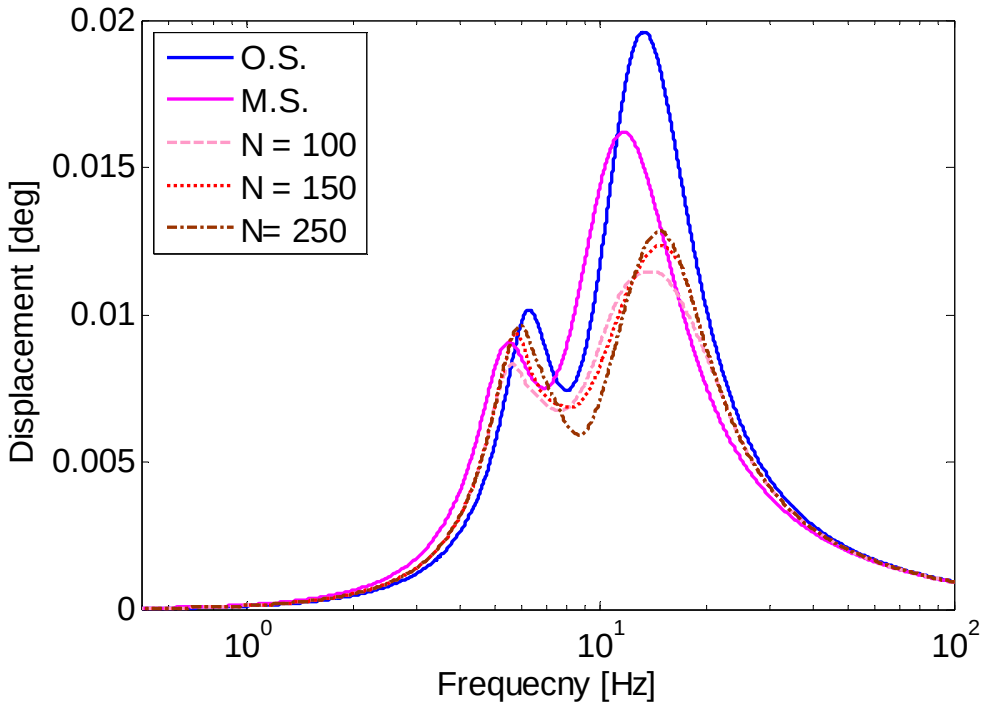

Figure 4.50. Rotation in γ direction vs. frequency

Results obtained show that the issue about displacement in x and z directions at high frequencies is solved with this modification; however, problems regarding displacement in y direction emerged. Looking at the magnitudes of displacement, displacement in y direction seems less critical than displacements in x and z directions; however, according to the available space in the vehicle this situation can change. To sum up, these results show that an optimization procedure with constraints that can be specified according to the design of the selected vehicle is required in order to get best results.

In order to study the affect of friction damping on another system, friction damping is added to the 6-DOF model used by Ma and Qi. In this model, 4 elastomeric engine mounts are used. A figure representing the model used is given in Figure 4.51.

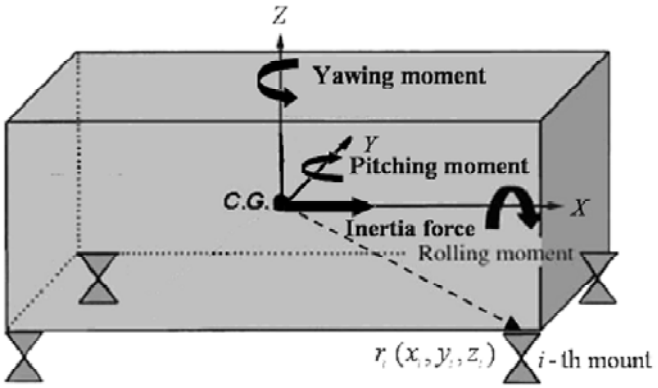

Figure 4.51. 6-DOF Engine Model [38]

In this system, friction damping is added to the three elastomeric mounts. Three friction surfaces are placed orthogonally. In order to get good results, an optimal value for normal forces in the friction surfaces should be obtained. In order to get these normal force values, each friction surface is added alone and effect of normal force to the displacements under engine force excitation is investigated. Finally results obtained separately are combined and the results of the modified system are compared with the original results in Figure 4.52 - Figure 4.57.

In these analyses, two sets of modified systems are used. At modified system 1, stiffness of the mounts in x direction is reduced by 50% and friction forces are added to the system in 3 directions. In modified system 2, stiffness of the mounts in x direction is reduced by 20% and friction forces are added in 3 directions. The values of the modification for both systems are given in Table 4.3 - Table 4.6.

Looking at the results given in Figure 4.52- Figure 4.57, we can conclude that dry friction damping can reduce the response of the system drastically however, a proper optimization of the normal force values, and modification of the stiffness values of the mounts should be conducted.

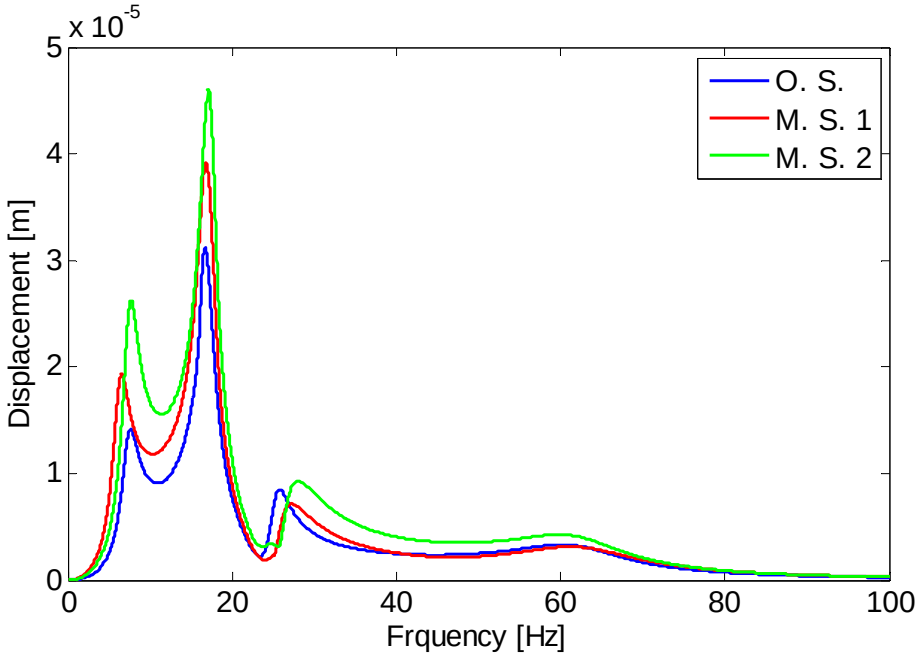

Figure 4.52. Displacement in x direction vs. frequency

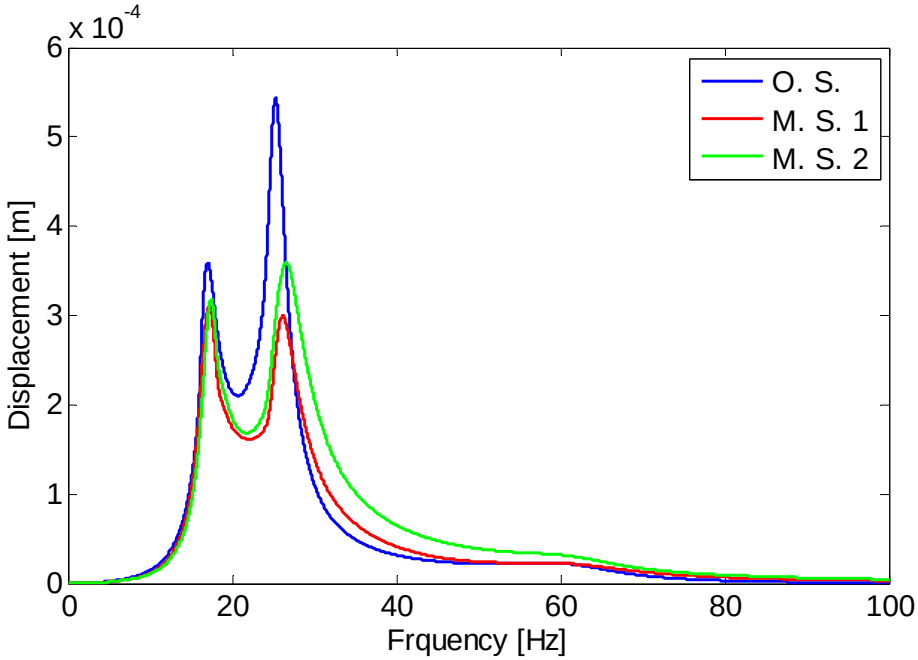

Figure 4.53. Displacement in y direction vs. frequency

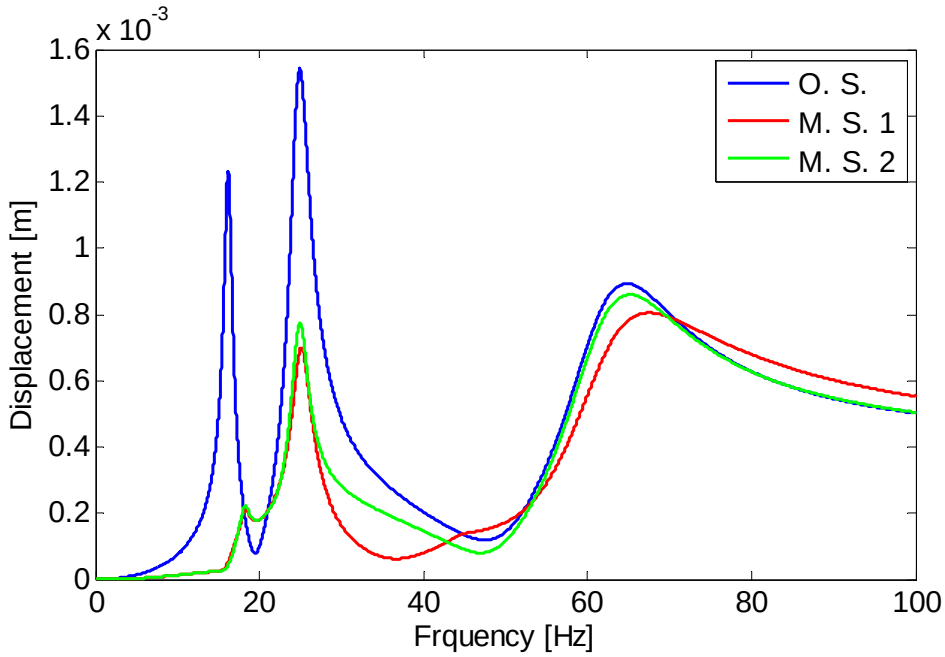

Figure 4.54. Displacement in z direction vs. frequency

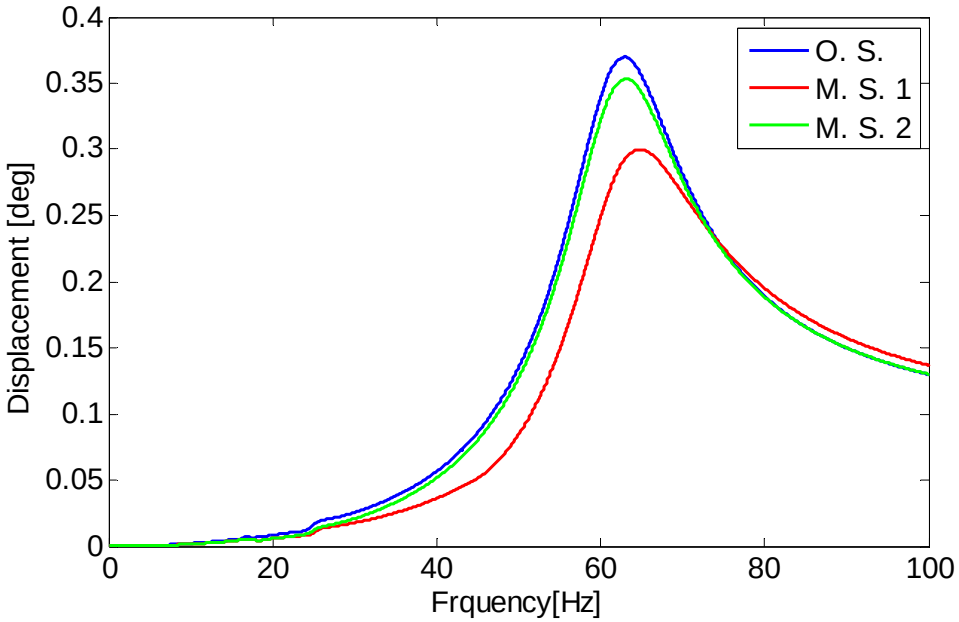

Figure 4.55. Rotation in α direction vs. frequency

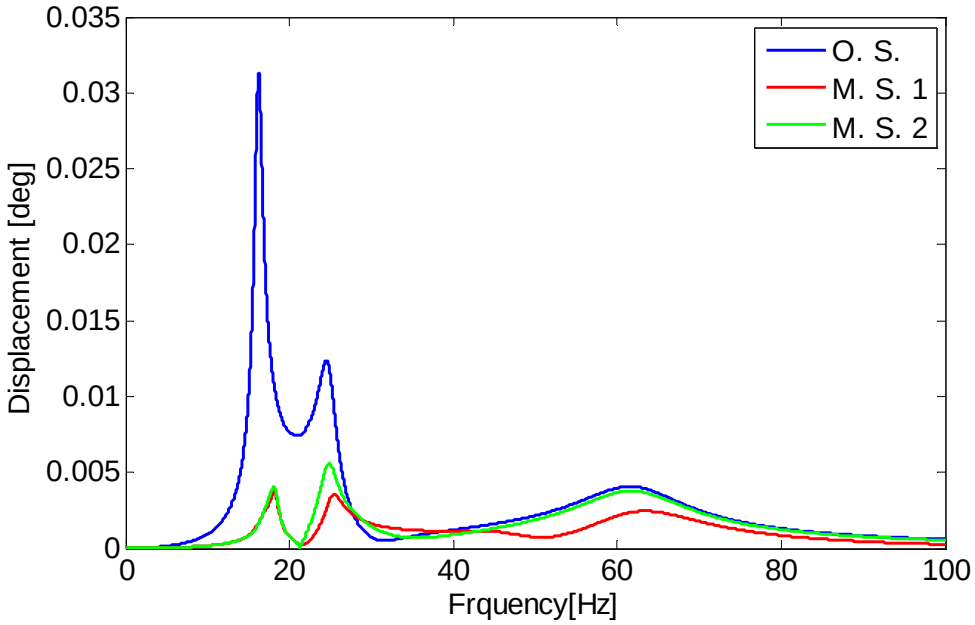

Figure 4.56. Rotation in β direction vs. frequency

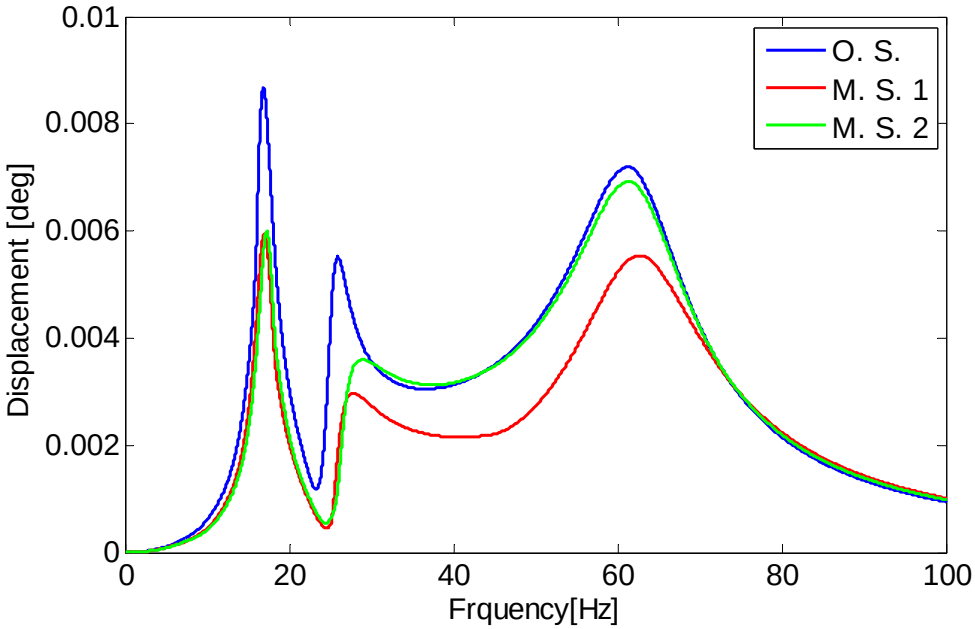

Figure 4.57. Rotation in γ direction vs. frequency

Table 4.3 Normal Force values used in system 1

Normal Force [N]	*x*	*y*	*z*
1st Mount	125	0	0
2nd Mount	0	300	0
3rd Mount	0	0	10000
4th Mount	0	0	0

Table 4.4 Reduction in stiffness of the system 1

Stiffness	*x*	*y*	*z*
Reduction	50%	0%	0%

Table 4.5 Normal Force values used in system 2

Normal Force [N]	*x*	*y*	*z*
1st Mount	250	0	0
2nd Mount	0	500	0
3rd Mount	0	0	1750
4th Mount	0	0	0

Table 4.6 Reduction in stiffness of the system 2

Stiffness	*x*	*y*	*z*
Reduction	20%	0%	0%

CHAPTER 5

ENGINE MOUNT DESIGN

Up to this section, effect of addition of friction damping to elastomeric engine mounts is investigated. At this section a physical design is proposed to achieve an appropriate design for real life applications.

Friction surfaces should be added to the system without changing the available mount design. In order to achieve this, friction elements are placed around the elastomeric mount. Other important issue was to use engine weight to ensure contact between contacting surfaces. Contacting surfaces might change due to wear and this might affect the performance of the engine mount. When engine weight is used to generate the normal force between the friction surfaces, wear does not affect engine mount performance significantly.

Another point is to generate structural parameters that can be optimized later. When engine weight is used to generate normal force between contacting bodies, other parameters are required to achieve desired conditions. In Figure 5.1, initial design proposed to TOFAŞ is given.

In Figure 5.1, the first friction surface is between the red and blue parts. There is a second friction surface which is between the blue part and the turquoise plate. Brown parts act like linear springs and ensure that the first friction surface is always in contact.

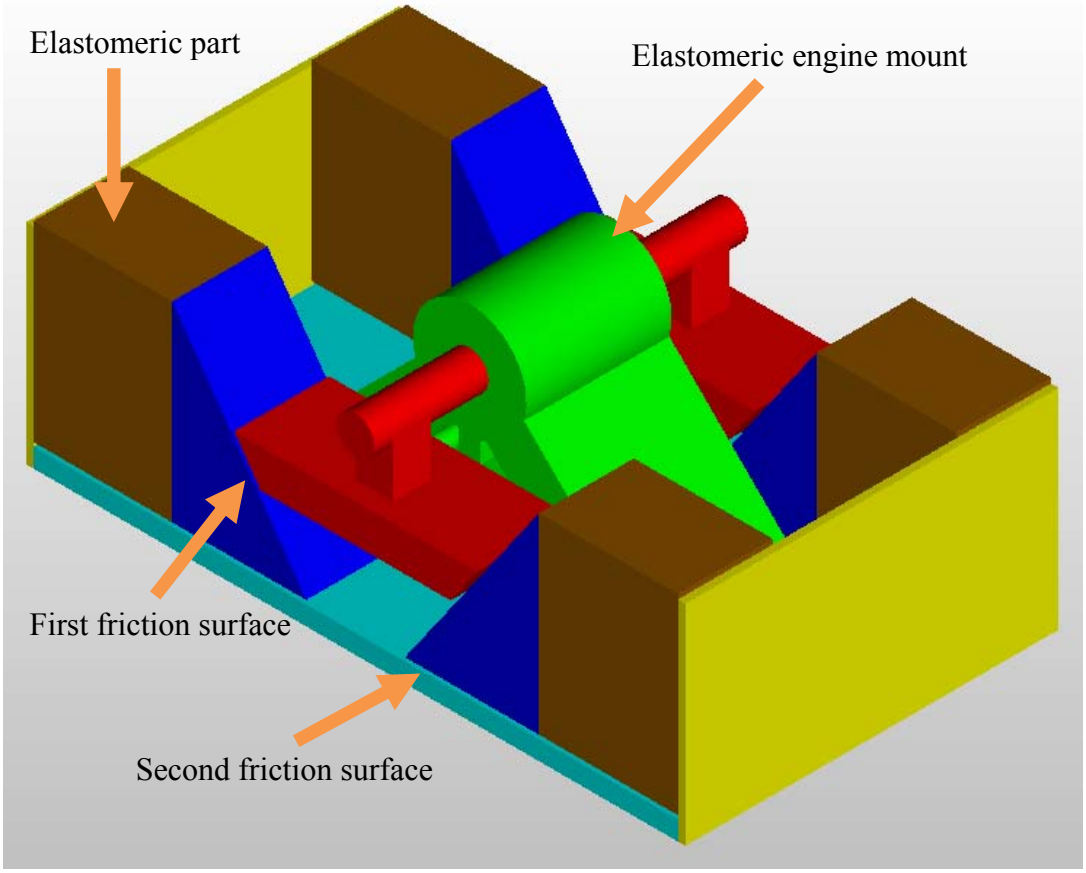

Figure 5.1. Initial design

In this design, angle of the first friction surface and stiffness of the brown parts (elastomeric rubber or springs) can be arranged to get the desired normal force between the blue and the red parts. Using two friction surfaces can be an advantage during optimization process. Since extra parameters are added to the system with addition of the second friction surface, better results can e obtained from the optimization.

Based on the initial design presented here TOFAŞ modified their available elastomeric mount which can be installed on a vehicle directly. In Figure 5.2, design made by TOFAŞ is shown for the 60° friction surface angle.

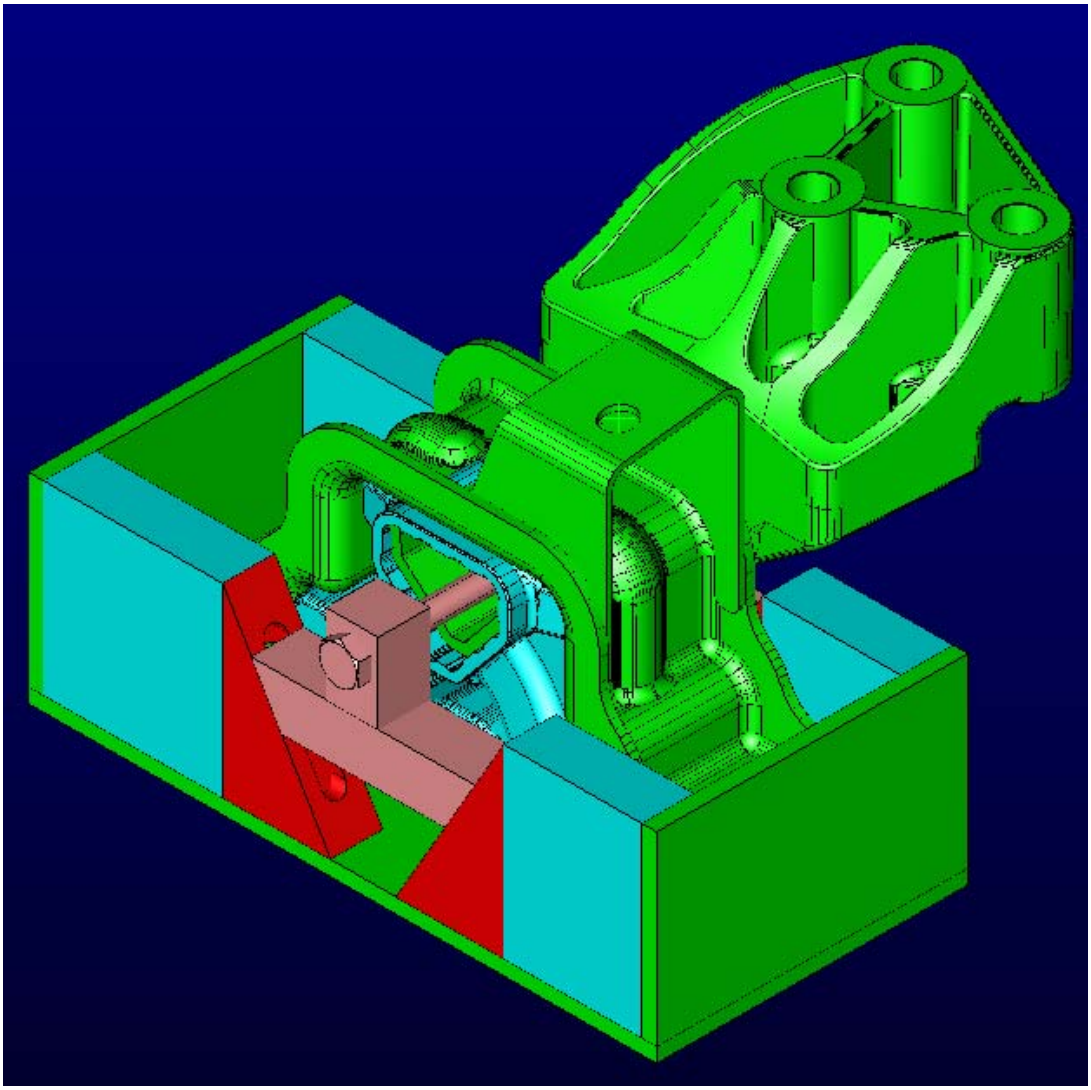

Figure 5.2. Design of TOFAŞ

Inclined friction surfaces used on this design make controlling normal force hard and require more complex friction models with variable normal force [33]. In order to compare results obtained in this thesis with experimental results, TOFAŞ made another design with 90° friction surface angle. Benefits of this design is to control normal force on the first friction surface easily by simply adjusting stiffness of the brown pieces and the preload on them. Therefore constant normal force is maintained at all cases. This design is given in Figure 5.3.

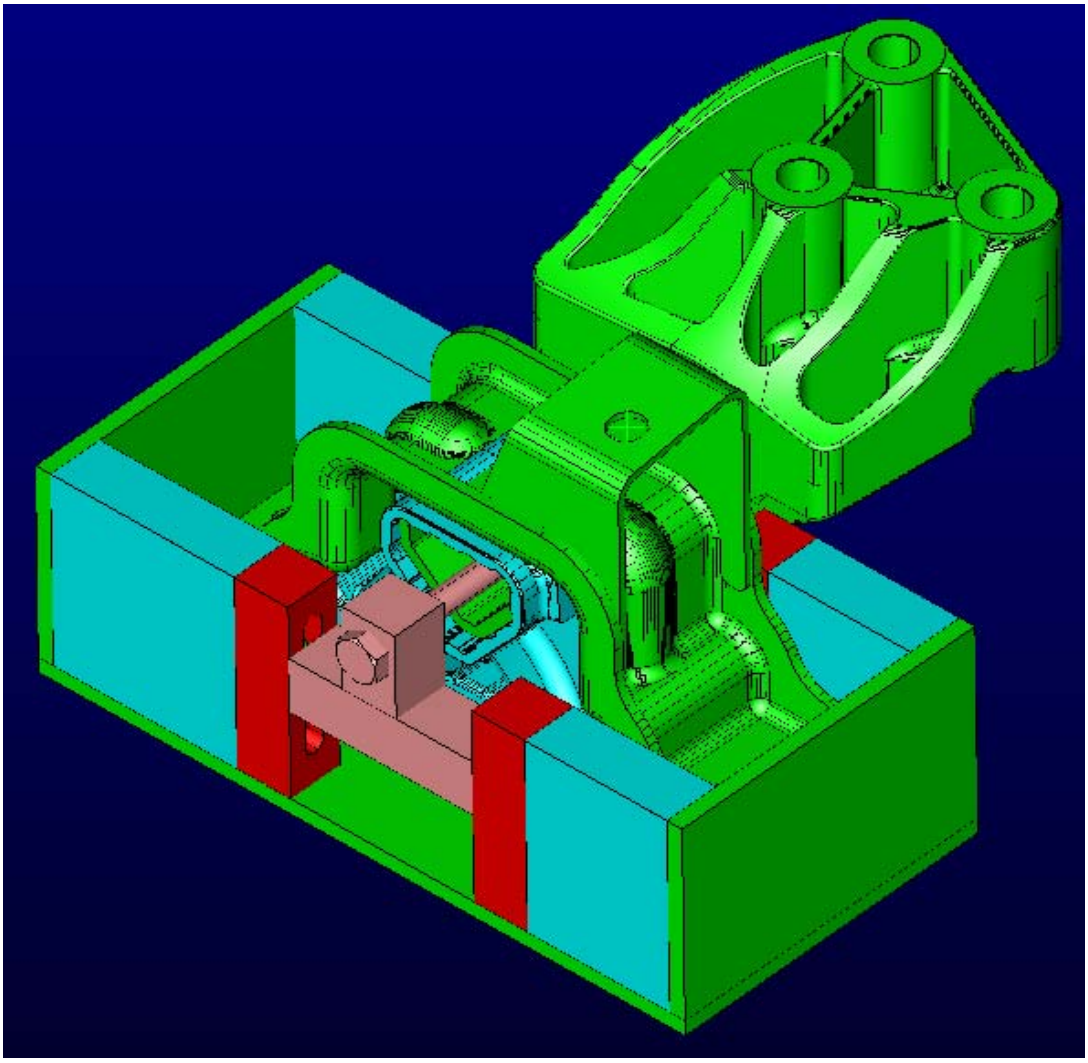

Figure 5.3. Design for comparing theoretical and experimental results

In order to calculate the normal forces between contacting surfaces, model given in Figure 5.4 is used. This model ignores inertia effects. This model represents the quarter of the friction surfaces due to the symmetry in the problem.

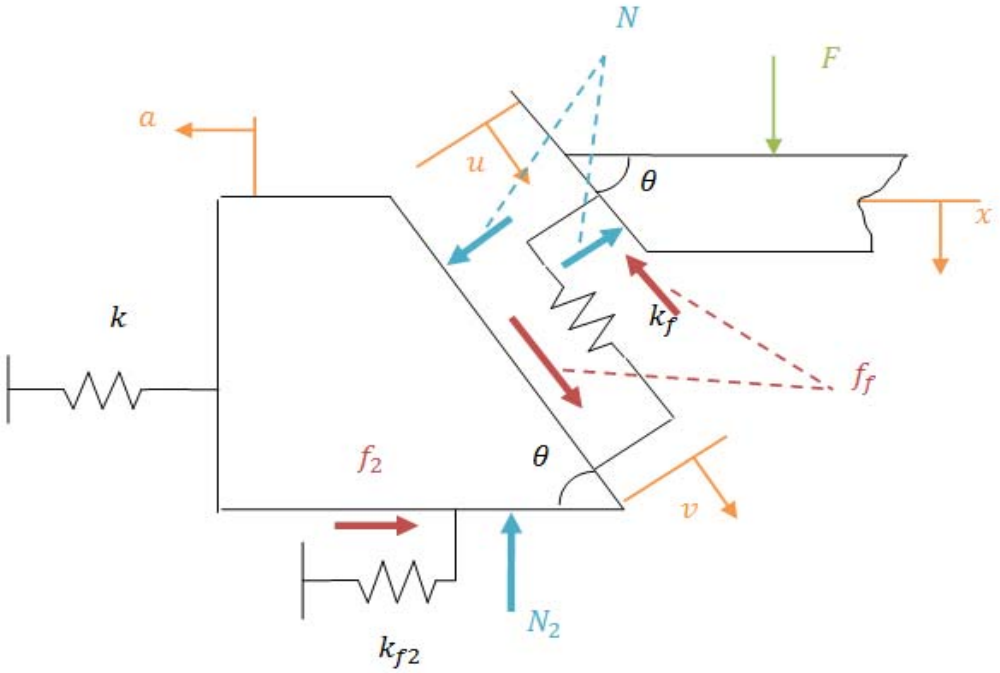

Figure 5.4. Model used to calculate dynamics of proposed mount design

Ignoring the inertia effects and assuming the slip has not started in any of the friction surfaces yet, the equations used in the kinematic analysis of the model are given as:

$$F = f_f \sin(\theta) + N\cos(\theta), \tag{5.1}$$

$$N_2 = f_f \sin(\theta) + N\cos(\theta), \tag{5.2}$$

$$f_2 + ka + f_f \cos(\theta) = N\sin(\theta), \tag{5.3}$$

$$a = \frac{x}{\tan(\theta)}, \tag{5.4}$$

$$u = \frac{x}{\sin(\theta)}, \tag{5.5}$$

$$v = -\frac{a}{\cos(\theta)}, \tag{5.6}$$

$$f_f = (u - v)k_f, \tag{5.7}$$

$$f_2 = ak_{f2}. \tag{5.8}$$

These equations change due to states of the friction surfaces. Assuming the first friction surface (inclined) is slipping, friction force on the first friction surface is given as:

$$f_f = \mu_1 N. \tag{5.9}$$

For the condition where the second friction surface is slipping, friction force on the second friction surface is given as:

$$f_2 = \mu_2 N_2. \tag{5.10}$$

Finally, assuming both friction surfaces slip, equations for both friction force is replaced by Equations (5.9) and (5.10).

These kinematic analyses are based on the design with inclined surfaces. Since constant normal force condition cannot be achieved with this design, 90° angle is used in this thesis.

CHAPTER 6

CONCLUSION AND FUTURE WORK

6.1. Conclusion

In this thesis, a new vibration isolation method is proposed in order to improve the performance of the elastomeric engine mounts. Dry friction damping is added to the elastomeric engine mounts. Macro-slip friction model is used to model the friction between the contacting surfaces. Engine is modeled as a single degree-of-freedom, a three-degree-of-freedom and six-degree-of-freedom system. Investigating addition of dry friction to the elastomeric mounts arise nonlinear equations which should be handled. Nonlinear forces are modeled periodically with Harmonic Balance Method. The equation of motion is solved using Newton's method with arc-length continuation. Arc-length continuation method make it possible to obtain the solution at the unsteady region.

Analysis with SDOF model revealed general characteristics about friction damping. Friction damping changes resonance frequency of the system while decreasing response of the system. An important parameter is the normal force between contacting surfaces. Effect of this parameter is investigated. Transmissibility of the system is calculated for various values of normal force. Results showed that increasing the normal force shifts resonance frequency to higher values. Transmissibility value at resonance decreases up to a certain normal force value than it starts to increase.

3-DOF system was used to investigate the response of the system excited by road input. Results showed that high normal forces are required to achieve improvement at low frequencies; whereas, low normal forces are required to obtain improvement at high frequencies. Therefore, an optimal value for normal force should be used with softened mount for the best results.

Finally 6-DOF system is used to study the performance of the mount with friction damping. Mounts used had stiffness at three directions and friction damping in their axial direction. Analysis with 6-DOF model revealed the requirement of optimization for best performance. Position and orientation of the mounts have significant effect on how dry friction damping affects the system.

To sum up, addition of dry friction damping to elastomeric engine mounts can increase performance of the mount significantly with optimal parameters.

6.2. Future Work

Dry friction damping is a complex concept. It is represented with the macro-slip friction model in this study. In order to get more realistic results, the micro-slip friction model with varying normal force can be used which represents friction between contacting bodies better than the macroslip model. With such models, investigation of the inclined friction surfaces, which results in varying normal force, is possible.

Another improvement which can be made is to use non-symmetrical friction surfaces. This will add many new parameters to the optimization problem; hence, better results might be obtained.

In real life applications three or more engine mounts carry the engine or the engine and the transmission. This system performs best with optimal values. An optimization procedure including mount stiffness values, normal force between

contacting surfaces, mount locations and orientations, constraints on angular and translational displacements and structural parameters regarding the designed engine mount with dry friction damping should be performed to get the best results for the elastomeric mount with friction damping.

The proposed model with many friction surfaces can be easily added to many other systems like lathes, machining centers, suspension systems of vehicles, and it can be used for protection of important electronic equipment in military vehicles and planes. The simple construction of the friction surfaces makes it a cheap and easy to apply solution to many problems regarding undesired vibration amplitudes.

There is also great potential in controlling the normal force on the friction surfaces. Active systems that adjust the normal force exerted on the friction surface might combine benefits of applying low normal load at high frequencies and applying high normal force at low frequencies. A semi-active system might also be used to control the normal force which will be used for the same purpose mentioned above.

REFERENCES

[1] S. R. Johnson, J. W. Subhedar, "Computer optimization of engine mounting systems", *SAE* Paper #790974.

[2] Y. Yu, S. M. Peelamedu, N. G. Naganathan, R. V. Dukkipati "Autmotive vehicle engine mounting systems: a survey" *Journal of Dynamic Systems, Measurement and Control*, Vol. 123 Issue 2, pp. 186-194, 2001.

[3] Y. Yu, N. G. Naganathan, R. V. Dukkipati, "A literature review of automotive vehicle engine mounting systems", *Mechanism and Machine Theory* 36 123-142, 2001.

[4] Ruian Cop. Auto Parts Co. Ltd, http://balljoint.en.made-in-china.com, last visited date 29/07/2010.

[5] M. J. Mashayekhi, N. Vahdati "Application of tuned vibration absorbers in fluid mounts" *Shock and Vibration*, Vol. 16, Issue 6, pp. 565-580, 2009

[6] R. Wang, "A study of vibration isolation of engine mount system", A thesis in the department of Mechanical and Industrial Engineering, Concordia University, Montreal, Quebec, Canada, 2005.

[7] J. J. Kim, H. Y. Kim, "Shape design of a engine mount by a method of parametric shape optimization", IMechE, *Journal of Automobile Engineering*, Part D, Vol.211, pp.155-159, 1997.

[8] J. Christopherson, G. Nakhaie Jazar, "Dynamic behavior comparison of passive hydraulic engine mounts. Part 1: Mathematical analysis", *Journal of Sound and Vibration* 290 1040-1070, 2006.

[9] M. M. Haque, "Evaluation of a class of hydraulic dampers for isolation of vibration and shock", PhD Dissertation, Concordia University, Montreal, Canada, 1996.

[10] B. Paul, “Kinematics and Dynamics of Planar Machinery”, Englewood Cliffs, NJ: Prentice-Hall, Second Edition, 1979.

[11] J. C. Tao, G.R. Liu, and K.Y. Lam, “Design optimization of marine engine mount system”, *Journal of Sound and Vibration*, Vol.235, No.3, pp.477-494, 2000.

[12] S. Kaul, “Modelling techniques for vibration isolation in motorcycles”, Thesis at the University of Wisconsin, May 2006.

[13] S. Kaul, and A. K. Dhingra, ”Engine mount optimization for vibration isolation in motorcycles” ,*Vehicle System Dynamics*, 47:4, 419 - 436, 2009

[14] T. Arai T. Kubozuka, S.D. Gray, “Development of an engine mount optimization method using modal parameters”, *SAE* Paper #932898

[15] Y.S. Ünlüsoy. H. Bilal, K. Çalışkan, “Motor destek takozlarının optimizasyonu”, OTEKON’10 5. *Otomotiv Teknolojileri Kongresi, Kongre Kitabı*, s. 145-156, Haziran 2010, Bursa.

[16] J. Y. Park, R. Singh, “Analysis of powertrain motions given a combination of active and passive isolators”, *Noise and Control Engineering Journal*, Vol. 57, Issue 3, pp. 232-243, May 2009.

[17] J. S. Lee, S. C. Kim, “Optimal design of engine mount rubber considering stiffness and fatigue strength”, *Proceedings of the institution of mechanical engineers part D-Journal of Automobile Engineering*, Vol. 221, Issue D7, pp. 823-835, July 2007.

[18] H. Olsson, K.J. Åström, C. Canudas de Wit, M. Gäfvert, P. Lischinsky, “Friction models and friction compensation”, J. Eur. Control, 4, pp. 176-195, 1998.

[19] D. A. Haessig and B. Friedland. On the modelling and simulation of friction. *Journal of Dynamic Systems Measurement and Control Transactions of ASME*, 113H3I:354–362, September 1991.

[20] C. Iurian, F. Ikhouane, J.Rodellar, R.Griñó, “Identification of a system with dry friction” Inst. d'Org. i Control de Sistemes Ind., Univ. Politècnica de Catalunya, Barcelona, Spain, Tech. Rep., 2005.

[21] E.Ciğeroğlu, H. N. Özguven, "Nonlinear vibration analysis of bladed disks with dry friction dampers", *Journal of Sound and Vibration* 295, pp. 1028–1043, 2006.

[22] C. M. Firrone, S. Zucca, "Underplatform dampers for turbine blades: The effect of damper static balance on the blade dynamics", *Mechanics Research Communications* Vol: 36, issue: 4, pp.515-522, 2009.

[23] K. Y. Şanlıtürk, D. J. Ewins, A. B. Stanbridge, "Underplatform dampers for turbine blades: theoretical modelling, analysis and comparison with experimental data" *Journal of Engineering for Gas Turbines and Power*, Vol. 132, pp. 919-929, 2001.

[24] E. Ciğeroğlu, W. Lu, C. H. Menq, "One-dimensional dynamic microslip friction model. *Journal of Sound and Vibration* 292, 881–898, 2006.

[25] R. G. Parker, "Influence of tensioner dry friction on the vibration of belt drives with belt bending stiffness", *Journal of Vibration and Acoustics*, Vol. 130, 011002, 2008.

[26] F. Ricciardeli, B. J. Vickery, "Tuned vibration absorbers with dry friction damping", *Earthquake Engineering and Structural Dynamics*, 28, 707-723, 1999.

[27] M. Wang, T. Zan, Y. Yang, R. Fei, "Design and implementation of nonlinear tmd for chatter suppression: an application in turning process " *International Journal of Machine Tools and Manufacture*, Vol. 50, Issue 5, pp. 474-479, 2010.

[28] M. Lorenz, B. Heimann, J. Tschimmel, V. Hartel, "Applying semi-active friction damping to elastic supports for automobile applications", *IEEE* 2003.

[29] C. W. Stammers, T. Sireteanu, "Semi-active seat control for vehicle driver protection", *Proceedings of Romanian Academy* - Series *A*, 2, 1-2, pp.27-31, 2001.

[30] L. Gaul, H. Albrecht, J. Wirnitzer, "Semi-active friction damping of large space truss structures" *Shock and Vibration*, Vol. 11, Issue 3-4, pp. 173-186, 2004.

[31] C. M. Harris, A. G. Piersol, "Harris' Shock and Vibration Handbook", 5th Ed., McGraw-Hill Companies, Inc., New York, 2002.

[32] E. Ciğeroğlu, N. An, C. H. Menq, "Forced response prediction of constrained and unconstrained structures coupled through frictional contacts", *Journal of engineering for Gas Turbines and Power*, 131(2), 2009.

[33] E. Cigeroglu, N. An, C. H. Menq, "A microslip friction model with normal load variation induced by normal motion" *Nonlinear Dynnamics,* 50:609–626, 2007.

[34] G. Orbay, H. N. Özgüven, "Non-linear periodic response analysis of mistuned bladed disk assemblies in modal domain", *Proceedigs of 9th International Conference on Vibrations in Rotating Machinery*, v. 1 pp. 159-170, IMechE, University of Exeter, UK, September 8-10, 2008.

[35] E. Yümer, E. Ciğeroğlu, H. N. Özgüven, "Non-Linear forced response analysis of mistuned bladed disk assemblies", *ASME Turbo Expo 2010*, June 14-18 2010, Glascow, Scotland (Accepted for Publication)

[36] G. Orbay, "Nonlinear vibration of mistuned bladed disk assemblies", MS Thesis Middle East Technical University, 2008.

[37] M. A. Crisfield, "A Fast incremental/iterative solution procedure that handles "snap-through"," *Computers and Structures*, vol. 13 55-62, 1981.

[38] Z. D. Ma, C. Qi, "Multidisciplinary design optimization of elastomeric mounting systems in automotive vehicles" *International Journal of Product Development*, vol. 1, Nos. 3/4, pp. 365-382, 2005.